

Table 3.1.3: Table of  $f_2$  values

$a/c$	$a/t$	$c/W = 0.0$		$c/W = 0.1$		$c/W = 0.2$		$c/W = 0.5$		$c/W = 0.8$		$c/W = 1.0$	
		$a\text{-tip}$	$c\text{-tip}$										
0.0	0.0	0.997	1.904	0.958	1.162	0.934	1.027	0.861	-0.390	0.765	-1.705	0.727	-2.582
	0.1	1.061	1.930	1.029	1.371	1.002	1.082	0.947	-0.235	0.871	-1.507	0.826	-2.355
	0.2	1.191	1.986	1.144	1.553	1.114	1.159	1.085	-0.087	1.004	-1.328	0.938	-2.155
	0.5	1.764	2.843	1.706	2.300	1.652	1.832	1.598	0.332	1.479	-1.156	1.419	-2.133
	0.8	2.521	4.436	2.458	4.117	2.457	3.814	2.564	2.400	2.582	0.421	2.723	-1.210
	1.0	3.150	5.951	3.087	6.411	3.191	6.273	3.480	4.114	4.004	1.609	4.383	-0.654
0.2	0.0	1.037	1.280	1.006	1.054	0.976	0.822	0.900	0.138	0.800	-0.566	0.740	-1.033
	0.1	1.078	1.311	1.050	1.080	1.020	0.848	0.955	0.150	0.866	-0.550	0.805	-1.018
	0.2	1.157	1.374	1.119	1.123	1.090	0.896	1.039	0.190	0.952	-0.522	0.885	-0.996
	0.5	1.515	1.752	1.469	1.492	1.440	1.259	1.400	0.530	1.313	-0.276	1.250	-0.814
	0.8	2.031	2.498	1.997	2.282	2.009	2.081	2.124	1.447	2.200	0.614	2.300	0.058
	1.0	2.475	3.286	2.470	3.085	2.558	2.967	2.873	2.536	3.320	1.821	3.700	1.347
0.4	0.0	1.070	1.175	1.050	1.000	1.010	0.796	0.940	0.215	0.845	-0.335	0.769	-0.714
	0.1	1.095	1.198	1.070	1.015	1.037	0.812	0.970	0.242	0.875	-0.324	0.806	-0.700
	0.2	1.131	1.241	1.100	1.039	1.074	0.852	1.010	0.276	0.922	-0.284	0.859	-0.658
	0.5	1.317	1.488	1.281	1.288	1.271	1.112	1.250	0.563	1.196	-0.045	1.150	-0.419
	0.8	1.630	1.985	1.629	1.798	1.652	1.635	1.772	1.199	1.912	0.649	1.998	0.282
	1.0	1.941	2.504	1.970	2.318	2.044	2.167	2.376	1.861	2.778	1.548	3.177	1.194
0.5	0.0	1.086	1.158	1.055	0.989	1.020	0.789	0.942	0.244	0.854	-0.269	0.792	-0.625
	0.1	1.102	1.179	1.074	1.000	1.040	0.809	0.968	0.272	0.884	-0.255	0.825	-0.603
	0.2	1.130	1.211	1.100	1.025	1.070	0.846	1.004	0.310	0.930	-0.212	0.878	-0.561
	0.5	1.272	1.414	1.241	1.230	1.234	1.067	1.216	0.566	1.187	0.025	1.157	-0.311
	0.8	1.546	1.827	1.538	1.649	1.560	1.502	1.701	1.123	1.851	0.652	1.938	0.362
	1.0	1.801	2.260	1.851	2.075	1.926	1.939	2.271	1.685	2.680	1.435	3.068	1.132
1.0	0.0	1.138	1.138	1.087	0.965	1.047	0.785	0.962	0.345	0.961	-0.070	0.964	-0.352
	0.1	1.141	1.142	1.097	0.977	1.060	0.810	1.000	0.375	0.983	-0.043	0.990	-0.323
	0.2	1.144	1.145	1.111	0.993	1.080	0.838	1.033	0.419	1.031	-0.006	1.043	-0.279
	0.5	1.192	1.236	1.176	1.094	1.167	0.980	1.194	0.590	1.280	0.228	1.407	-0.005
	0.8	1.343	1.416	1.348	1.288	1.368	1.180	1.574	0.942	1.831	0.698	2.028	0.637
	1.0	1.523	1.601	1.573	1.488	1.650	1.408	2.012	1.270	2.551	1.189	2.992	1.154

### 3.2 CC08 – Quarter Elliptical Corner Crack(s) at Hole (Offset) in a Plate – Univariant WF

#### 3.2.1 Overview

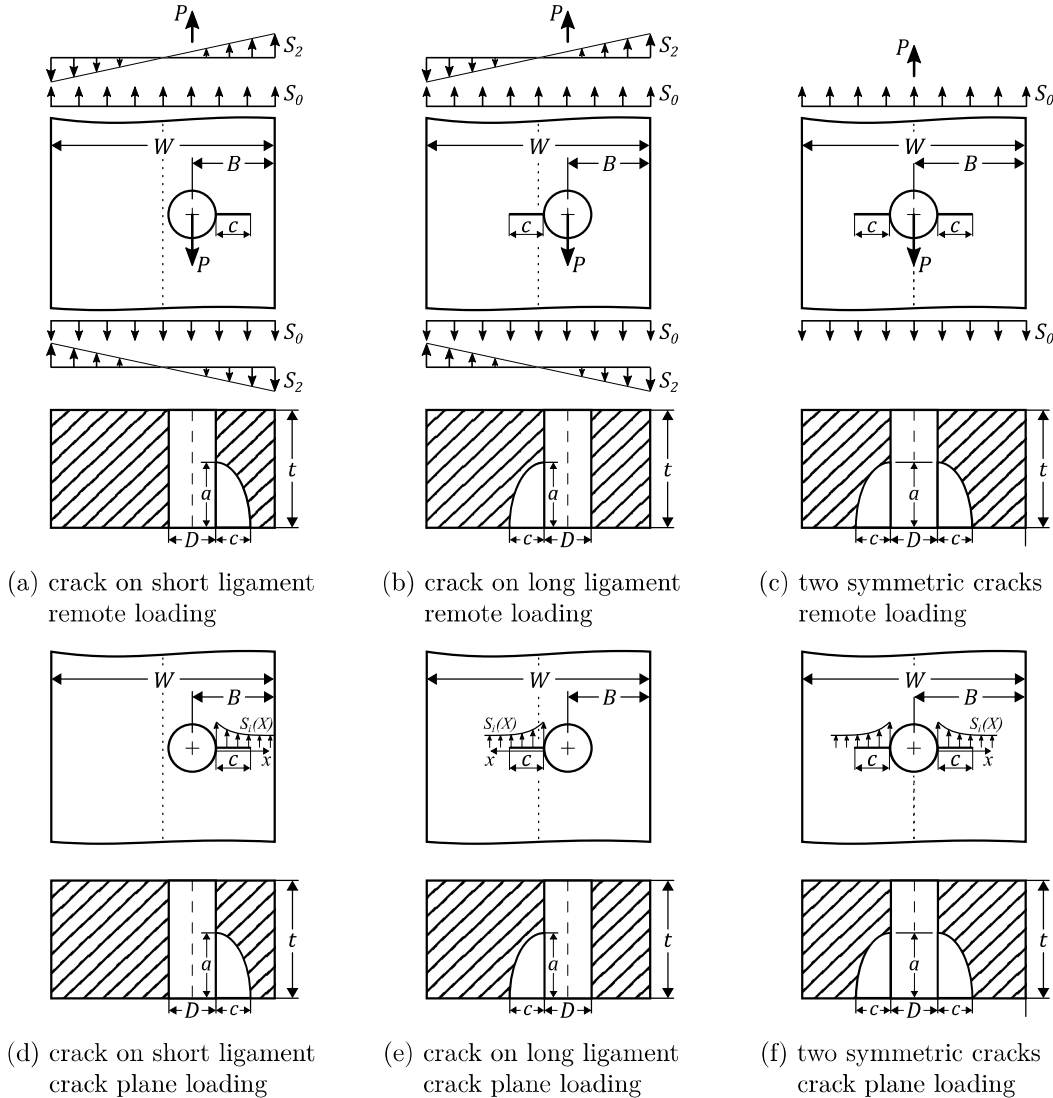


Figure 3.2.1: Configuration of the crack case CC08

Crack case CC08 is a weight function solution for the corner crack at an off-center hole in a finite width plate with a general nonlinear stress distribution. It is nominally the same geometry as CC02. The difference between CC02 and CC08 is that CC02 is defined in terms of remote loads and moments and pin loads, while CC08 is a weight function solution defined in terms of general nonlinear stress distributions on the crack plane in the corresponding uncracked body. CC08 also allows convenient specification of remote tension, in-plane bend and pin-load stresses.

Following subconfigurations are available for this case:

1. The crack on the short ligament side of the offset hole (Figs. 3.2.1a and 3.2.1d)

2. The crack on the long ligament side of the offset hole (Figs. 3.2.1b and 3.2.1e)
3. Two symmetric cracks from the centered hole under symmetric stressing (Figs. 3.2.1c and 3.2.1f)

The Fig. 3.2.1a is the default configuration in the GUIs of NASFLA, NASSIF and NASCCS. The other two configurations can be activated by checking the radio box next to “Two symmetric cracks” or “Crack in long ligament” options.

### 3.2.2 Geometry

The model geometry is defined by size input parameters listed below (refer to Fig. 3.2.1):

- $W$  : plate full width
- $t$  : plate thickness
- $D$  : hole diameter
- $B$  : distance from the hole center to the right edge of the plate
- $a$  : crack size in the thickness direction
- $a/c$ : aspect ratio of the corner crack

Note that  $2B = D$  must hold true for the symmetric cracks from the centered hole option.

For the cracks located on the short ligament of the hole and for twin cracks from the centered hole, the geometry and crack size validity ranges of the model are as follows:

$$\begin{aligned} 0.02 &\leq D/B \leq 1.8 \\ 0.1 &\leq D/(2t) \leq 10.0 \\ 0.1 &\leq 2B/W \leq 1.0 \\ 0 &\leq a/t \leq 0.95 \\ 0 &\leq \frac{c}{B - D/2} \leq 0.9 \\ 0 &\leq c/a \leq 10.0 \end{aligned}$$

For cracks located on the long ligament of the hole, the ranges are same as above except:

$$\begin{aligned} 0.2 &\leq 2B/W \leq 1.0 \\ 0 &\leq \frac{c}{W - B - D/2} \leq 0.9 \end{aligned}$$

If the crack continues to propagate until  $a/t$  reaches the limit given above, then it will self-transition to a case TC13. Refer to Appendix D of the NASGRO manual for more details about the case transitions of CC08.

### 3.2.3 Loading

Crack case CC08 provides consistent stress intensity factor solutions for stresses in two different input forms:

1. The fundamental weight function solution permits direct input of the principal normal stresses on the crack plane as pairs of  $[X_i, S_i]$ . Here, the  $X$ -axis is the normalized coordinate system that originates from the hole edge and extends along the width of the plate as depicted in

Figs. 3.2.1d to 3.2.1f. Depending on the crack location, the  $X$ -axis is defined as follows:

$$X = \begin{cases} \frac{x}{B - D/2} & \text{for a single crack on short ligament or double symmetric cracks} \\ \frac{x}{W - B - D/2} & \text{for a crack on long ligament} \end{cases}$$

The range of  $X$  for stress definition must be:  $0 \leq X \leq 1$ .

Up to four separate tabular stress distributions ( $S_0$  to  $S_3$ ) can be defined.

2. The user can alternatively input a uniform remote tension stress ( $S_0$ ), remote bending stress ( $S_2$ ), and pin-load induced stress ( $S_3$ ) on the plate. The code internally calculates the local stresses along the crack plane in the corresponding uncracked body, including the effects of the off-center hole, and then invokes the same weight function solution as above.

The pin-loading induced stress is defined as:

$$S_3 = \frac{P}{Dt} \quad (3.2.1)$$

where,  $P$  is the applied pin-load.

The user is given two options on treatment of the negative pin-load: (a) Compression clipping, (b) Full range. Refer to Section 13 of this Appendix for more details about each option.

### 3.2.4 Optional Features

This case allows incorporation of a static residual stress field along the crack plane. See Section 11.6 for more details on how the residual stresses are accounted for in NASFLA.

The cyclic stress shakedown option is available to account for local plasticity. Refer to Appendix M of the manual for more details.

### 3.2.5 Development History

Crack case CC08 (from NASGRO 6.0 onwards) includes a symmetric geometry (with twin cracks) loaded symmetrically. From NASGRO 8.1 CC08 supports pin loading, has greatly expanded geometric limits, and enables cracks located on the long ligament side of the hole. NASGRO 9.2 expands the hole offset limits for cracks on the short ligament side of the hole.

### 3.2.6 Theory

The new CC08 solution is based on a completely independent set of reference solutions derived using the boundary element computer program FADD-3D [25, 26] and the finite element analysis program Abaqus. CC08 has no relationship to the original CC02 solution. The new solution provides some improvements in solution accuracy, although a complete comparison of CC02 vs. CC08 has not yet been completed. The previous CC02 solution has been left unchanged for legacy purposes.

The CC08 solution uses the approximate weight function proposed by Glinka [23, 24].

The weight function at the  $c$ -tip (the tip on the plate surface) is

$$W_c = \frac{2}{\sqrt{2\pi(c-x)}} \left[ 1 + M_{1c} \sqrt{\frac{c-x}{c}} + M_{2c} \frac{c-x}{c} + M_{3c} \left( \frac{c-x}{c} \right)^{3/2} \right] \quad (3.2.2)$$

The weight function at the  $a$ -tip (the crack tip in the bore of the hole) is

$$W_a = \frac{2}{\sqrt{\pi x}} \left[ 1 + M_{1a} \sqrt{\frac{x}{c}} + M_{2a} \frac{x}{c} + M_{3a} \left( \frac{x}{c} \right)^{3/2} \right] \quad (3.2.3)$$

The variable  $x$  is the distance normal to the hole axis measured from the location where the crack emanates (the root of the hole). The parameters  $M_{1c}, M_{2c}, \dots$ , etc. depend on the geometrical parameters and are defined by reference solutions.

At the  $c$ -tip,  $M_{1c}$ ,  $M_{2c}$ , and  $M_{3c}$  are defined by

$$\begin{aligned} M_{1c} &= \frac{\pi}{\sqrt{2Q}} (4Y_0 - 6Y_1) - \frac{24}{5} \\ M_{2c} &= 3 \\ M_{3c} &= 2 \left( \frac{\pi}{\sqrt{2Q}} Y_0 - M_{1c} - 4 \right) \end{aligned} \quad (3.2.4)$$

and at the  $a$ -tip,  $M_{1a}$ ,  $M_{2a}$ , and  $M_{3a}$  are given by

$$\begin{aligned} M_{1a} &= \frac{\pi}{\sqrt{4Q}} (30F_1 - 18F_0) - 8 \\ M_{2a} &= \frac{\pi}{\sqrt{4Q}} (60F_0 - 90F_1) + 15 \\ M_{3a} &= -(1 + M_{1a} + M_{2a}) \end{aligned} \quad (3.2.5)$$

$Q$  is the shape factor for an elliptical crack approximated by

$$Q = \begin{cases} 1 + 1.464(a/c)^{1.65} & \text{for } (a/c) \leq 1 \\ 1 + 1.464(a/c)^{-1.65} & \text{for } (a/c) > 1 \end{cases} \quad (3.2.6)$$

and  $F_0$ ,  $F_1$ ,  $Y_0$  and  $Y_1$  are normalized SIFs or the reference solutions.  $F_0$ ,  $F_1$  are obtained at the  $a$ -tip, and  $Y_0$  and  $Y_1$  are at the  $c$ -tip. The subscripts identify the two associated reference loads on the crack surfaces: 0 denotes uniform tension, and 1 denotes a linearly decreasing bending stress  $\sigma_r(x) = -x/c + 1$ .

The stress intensity factors at the  $a$ - and  $c$ -tips,  $K_{a,c}$ , can thus be determined by direct integration as

$$K_{a,c} = \int_0^c W_{a,c} \sigma(x) dx \quad (3.2.7)$$

where  $\sigma(x)$  is the univariant stress applied on the crack surface, and the integration is carried out from  $x = 0$  to  $x = c$ .

The reference solutions along the crack perimeter near the two intersections of the corner crack with the surface generally exhibited increasing values approaching the surface and then decreased sharply immediately at the surface. The reference solutions assigned to the surface value (the  $c$ -tip or the

$a$ -tip) were selected at the maximum value of  $K$  near the corresponding surface, which typically occurred about three degrees inside the surface.

The effects of near-surface constraint on the growth of fatigue cracks is accounted for by multiplying these near-surface  $\Delta K$  values by the crack closure factor,  $\beta_R$ . Refer to Section 15 for more details about the  $\beta_R$  factor.

References: [23, 24, 25, 26]

### 3.3 CC09 – Quarter Elliptical Corner Crack in a Plate – Bivariant WF

#### 3.3.1 Overview

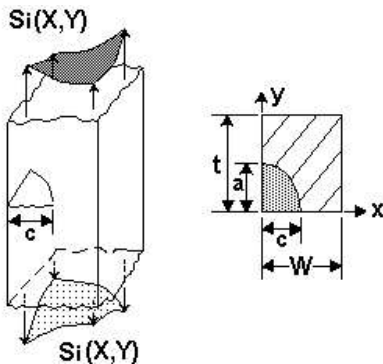


Figure 3.3.1: Configuration of CC09 – a corner crack in a plate – bivariant WF

The crack case CC09 is a weight function solution for the corner crack in a finite plate, which is nominally the same geometry as CC01 and CC05. The difference between CC01 and CC09 is that CC01 is defined in terms of remote tension and bending stresses, while CC09 is a weight function solution defined in terms of general nonlinear bivariant stress distributions on the crack plane in the corresponding uncracked body. CC05 and CC09 have nominally the same capabilities, but CC05 was a first-generation bivariant solution with some accuracy limitations, and CC09 is a second-generation bivariant solution with improved accuracy.

The CC09 solution is based on a new weight function formulation and an independent set of reference solutions derived using the boundary element computer program FADD-3D [25, 26], and has no relationship to the previous CC01 or CC05 solutions. The CC09 solution provides improvements in solution accuracy in comparison to both CC01 and CC05. Crack case CC01 has been left unchanged for legacy purposes; CC05 has been moved under *Superseded Solutions*.

#### 3.3.2 Geometry

This model requires four geometric input parameters:

- $W$  : plate width
- $t$  : plate thickness
- $a$  : crack size in the thickness direction
- $a/c$ : aspect ratio of the corner crack

The current geometry and crack size validity ranges for CC09 solutions are as follows:

$$0.025 \leq a/c \leq 40$$

$$0 \leq a/t \leq 0.95$$

$$0 \leq c/W \leq 0.95$$

When one of the crack sizes reaches the limit (i.e. if  $a/t = 0.95$  or  $c/W = 0.95$ ) in NASFLA, the corner crack will transition to either TC12 or TC28, depending on the user selection in the Geometry tab of the GUI.

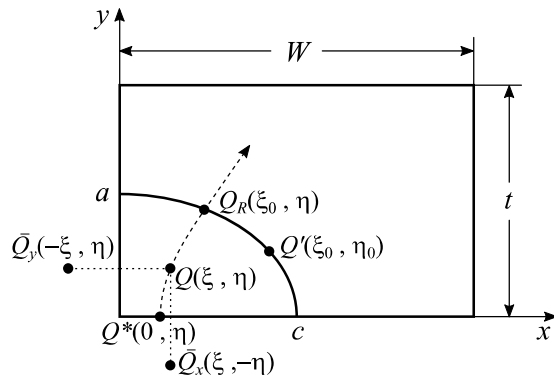


Figure 3.3.2: Geometry configuration and nomenclature for corner crack in plate.

### 3.3.3 Loading

The stresses on the plane of crack in an uncracked body are input via a text file that contains the coordinates and stress values. Details of the available file formats for bivariant stresses are described later in Section 11.1, Stress Gradient Input Formats.

### 3.3.4 Optional Features

CC09 allows incorporation of a static residual stress field along the crack plane. See Section 11.6 for more details on how the residual stresses are accounted for in NASFLA.

The cyclic stress shakedown option is available to account for local plasticity. Refer to Appendix M of the NASGRO manual for more details.

NASFLA allows separate definitions of tension/compression or t1/t2 stress gradients. Refer to Sections 11.2 and 11.3 for further details about these features.

### 3.3.5 Theory

The CC09 solution uses a bivariant weight function formulation derived by Lee [47]. The corner crack in a rectangular plate of finite width and thickness is assumed to have a quarter-elliptical shape that can be characterized by two degrees of freedom, the crack dimensions  $c$  and  $a$  in the width and thickness directions, respectively (Fig. 3.3.2).

Due to its simplicity and accuracy, the PWF proposed by Orynyak [48, 49] for an elliptical crack in an infinite body was used as the basic weight function. This form can be written as

$$W_{QQ'} = \frac{\sqrt{R^2 - r^2}}{\pi l_{QQ'}^2 \sqrt{\pi R}} \quad (3.3.1)$$

The equation represents the weighting effects on any point  $Q'$  along the crack front contributed by a point unit load applied at  $Q$  on the elliptical crack surface. Here,  $R$  is the distance between  $Q^*$  and  $Q_R$ ,  $r$  – the distance between  $Q$  and  $Q^*$ , and  $l_{QQ'}$  – the distance between  $Q$  and  $Q'$ . The definitions for  $Q$ ,  $Q'$ ,  $Q_R$ , and  $Q^*$  are more concise using elliptical coordinate notation. Respectively, they are given by  $Q = (\xi, \eta)$ ,  $Q' = (\xi_0, \eta_0)$ ,  $Q_R = (\xi_0, \eta)$  and  $Q^* = (0, \eta)$  where  $\xi$  and  $\eta$  are the parameters

in the elliptical coordinate system to identify a point along the crack plane with its origin at the center of the crack. It can be seen that  $Q$ ,  $Q_R$ , and  $Q^*$  are defined along the same elliptical angle  $\eta$ .  $\xi_0$  is the “elliptical radius” defining the elliptical crack front. This PWF equation is similar to the one for circular cracks derived by Kassir and Sih [50] as well as Shah and Kobayashi [51] except for different definitions for the length parameters.

To account for the free boundary correction for a quarter-elliptical corner crack in a quarter-infinite body, Eq. (3.3.1) was modified to include two additional length parameters. Now the basic point weight function applicable at  $Q'$  for a point unit load applied at  $Q$  is given by

$$W_{QQ'} = \frac{\sqrt{R^2 - r^2}}{\pi l_{QQ'}^2 \sqrt{\pi R}} \left( 1 + \frac{l_{QQ'}^2}{l_{Q_x Q'}^2} + \frac{l_{QQ'}^2}{l_{Q_y Q'}^2} \right) \quad (3.3.2)$$

The additional length parameters  $l_{Q_x, Q'}$  and  $l_{Q_y, Q'}$  correct the free surface effects for a corner crack by assuming a symmetrical stress distribution for an imaginary prolonged crack extending into the other three quadrants. In reference to the Fig. 3.3.2,  $l_{Q_x, Q'}$  is the distance between  $\bar{Q}_x$  and  $Q'$ , and  $l_{Q_y, Q'}$  the distance between  $\bar{Q}_y$  and  $Q'$ . The locations,  $\bar{Q}_x$  and  $\bar{Q}_y$ , are points symmetrical to the location of point load  $Q$  with respect to the  $x$ - and  $y$ -axes.

Additional correction terms are required to account for finite width and thickness effects. Following several exploratory investigations, a formulation was identified with reasonable numerical accuracy and stable convergent approach. The point weight function at  $Q'$  for a point unit load applied at  $Q$  for a quarter elliptical crack in a finite plate is thus provided by

$$W_{QQ'} = \frac{\sqrt{R^2 - r^2}}{\pi l_{QQ'}^2 \sqrt{\pi R}} \left( 1 + \frac{l_{QQ'}^2}{l_{Q_x Q'}^2} + \frac{l_{QQ'}^2}{l_{Q_y Q'}^2} \right) \times \left[ 1 + \Pi_1 \sqrt{1 - \frac{r}{R}} + \Pi_2 \left( 1 - \frac{y}{y'} \right) + \Pi_3 \left( 1 - \frac{x}{x'} \right) \right] \quad (3.3.3)$$

where  $x$  and  $y$  define the Cartesian coordinates of  $Q$ , and  $x' = c\sqrt{1 - x^2/a^2}$  and  $y' = a\sqrt{1 - x^2/a^2}$ .

The SIF can therefore be evaluated by performing surface integration across the crack area. For a given stress distribution  $\sigma(x, y)$  applied on the crack plane obtained from an uncracked body subjected to remote loadings, the stress intensity factor is written as

$$K = \int_0^a \int_0^{c\sqrt{1-y^2/a^2}} \sigma(x, y) W_{QQ'} dx dy \quad (3.3.4)$$

The parameters  $\Pi_1$ ,  $\Pi_2$ , and  $\Pi_3$  are calibrated by reference solutions at both  $a$ - and  $c$ -tips to characterize the finite boundary effects. Accordingly, in this approach, three reference stress solutions are required at each tip, and the stress intensity factor at  $a$ - and  $c$ -tips can be determined by

$$K^{a,c} = \int_0^a \int_0^{c\sqrt{1-y^2/a^2}} \sigma(x, y) \frac{\sqrt{R^2 - r^2}}{\pi l_{QQ^{a,c}}^2 \sqrt{\pi R}} \left( 1 + \frac{l_{QQ^{a,c}}^2}{l_{Q_x Q^{a,c}}^2} + \frac{l_{QQ^{a,c}}^2}{l_{Q_y Q^{a,c}}^2} \right) \times \left[ 1 + \Pi_1^{a,c} \sqrt{1 - \frac{r}{R}} + \Pi_2^{a,c} \left( 1 - \frac{y}{y'} \right) + \Pi_3^{a,c} \left( 1 - \frac{x}{x'} \right) \right] dx dy \quad (3.3.5)$$

where, the superscripts  $a$  and  $c$  denote parameters associated with  $a$ - and  $c$ -tips, respectively.

To facilitate the computation, Eq. (3.3.5) is preferably written in terms of elliptical coordinate parameters instead of Cartesian. For  $\alpha = a/c \leq 1$ , the relationships between Cartesian and elliptical coordinates ( $\xi, \eta$ ) are as follows:

$$\begin{aligned} x &= b \cosh \xi \cos \eta \\ y &= b \sinh \xi \sin \eta \\ b &= \sqrt{c^2 - a^2} \end{aligned} \quad (3.3.6)$$

For any point along the crack front, the “elliptical radius” in elliptical coordinate system is the same and is given by

$$\xi_0 = \frac{1}{2} \ln \left( \frac{1+\alpha}{1-\alpha} \right) \quad (3.3.7)$$

The above equation is derived by eliminating the dependency on the elliptical angle  $\eta$  among coordinate transformation equations. The Cartesian coordinates for  $Q, Q_R, Q^*, Q'$ ,  $\bar{Q}_x$ , and  $\bar{Q}_y$  in terms of elliptical coordinate parameters, are as follows:

$$Q = (b \cosh \xi \cos \eta, b \sinh \xi \sin \eta) \quad (3.3.8)$$

$$Q_R = (b \cosh \xi_0 \cos \eta, b \sinh \xi_0 \sin \eta) \quad (3.3.9)$$

$$Q^* = (b \cosh \eta, 0) \quad (3.3.10)$$

$$Q' = (b \cosh \xi_0 \cos \eta, b \sinh \xi_0 \sin \eta) \quad (3.3.11)$$

$$\bar{Q}_x = (-b \cosh \xi \cos \eta, b \sinh \xi \sin \eta) \quad (3.3.12)$$

$$\bar{Q}_y = (b \cosh \xi \cos \eta, -b \sinh \xi \sin \eta) \quad (3.3.13)$$

and the infinitesimal area becomes

$$dxdy = b^2 (\sinh^2 \xi + \sin^2 \eta) d\eta d\xi \quad (3.3.14)$$

Furthermore, the integration limits are converted from  $y : 0 \rightarrow a\sqrt{1-x^2/c^2}$  and  $x : 0 \rightarrow c$  to  $\xi : 0 \rightarrow \xi_0$  and  $\eta : 0 \rightarrow \pi/2$ . The integration sequence is now interchangeable.

The effects of near-surface constraint on the growth of corner fatigue cracks in plates using this solution are not yet fully understood. At the present time, in order to be conservative, fatigue crack growth calculations in NASGRO do not multiply these near-surface  $\Delta K$  values by the crack closure factor,  $\beta_R$ .

### Reference Solutions

The weight function method requires an accurate set of reference solutions for a matrix of crack geometries. These reference solutions were numerically generated using the FADD3D fracture mechanics software, a general boundary element code for three-dimensional linear elastic fracture analysis [25, 26]. Reference solutions were generated at 150 different combinations of geometrical aspect ratios:  $a/c = 0.1, 0.2, 0.4, 0.6, 0.8, 1.0$ ;  $c/W = 0.1, 0.2, 0.5, 0.8, 0.9$ ; and  $a/t = 0.1, 0.2, 0.5, 0.8, 0.9$ . For  $a/c$  and  $a/t$  less than 0.1 and approaching zero, reference stress solutions for edge cracks were generated and used [22]. For  $a/c$  larger than 1, the reference solutions were obtained from the corresponding  $c/a$  ratios by reversing the stress field and the associated geometry dimensions. As a result, the expanded reference solution matrix constitutes a discrete database covering a complete range of aspect ratio combinations; i.e.,  $a/c$  from 0 to  $\infty$ ,  $a/t$  from 0 to 0.9 and  $c/W$  from 0 to 0.9. For any arbitrary combination of aspect ratios, the reference solutions are determined from the

matrix of specific solutions through Hermite interpolation. Three sets of reference solutions were determined for each crack geometry. These are denoted as solutions for unit tension, unit bending along the  $x$ -axis, and unit bending along the  $y$ -axis. The solutions were generated by applying the reference stresses on the crack plane in the corresponding uncracked body. The three reference stresses are given by  $\sigma_0 = 1$ ,  $\sigma_1 = -y/a + 1$ , and  $\sigma_2 = -x/c + 1$ .

The reference solutions along the crack perimeter near the two intersections of the corner crack with the surface generally exhibit increasing values approaching the surface and then decrease sharply immediately at the surface. The reference solutions assigned to the surface value (the  $c$ -tip or the  $a$ -tip) were selected at the maximum value of  $K$  near the corresponding surface, which typically occurred about three degrees inside the surface.

### 3.3.6 Verification

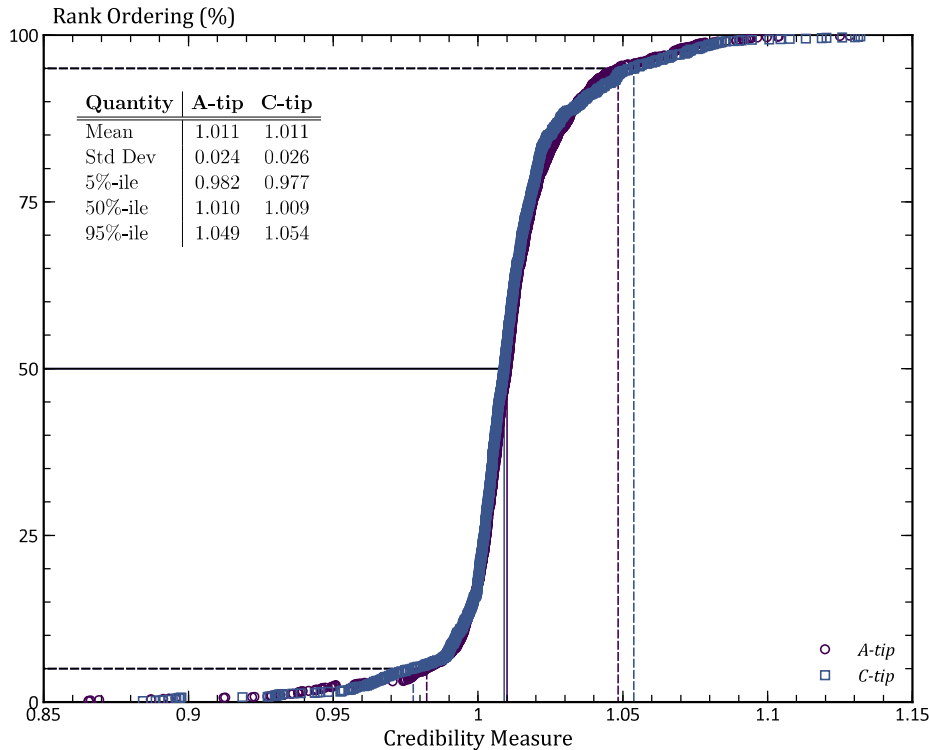


Figure 3.3.3: Verification plot for CC09 showing the cumulative distribution of discrepancies. The credibility measure is the ratio of the NASGRO SIF solution to the FEA SIF solution. This figure rank orders the credibility matrix and provides statistical quantity measures.

Verification of CC09 follows the verification procedure outlined in [52]. Full details of the verification effort can be found in that document. Fig. 3.3.3 presents the key verification plot for CC09. These results employ 172 geometries semi-randomly generated by Latin Hypercube methods. These geometries are independent on the calibration matrix. For this bivariant solution, Fig. 3.3.3 employs

7 stress gradients. The credibility measure is the ratio of the NASGRO SIF solution to the FEA SIF solution for the same solution.

As shown in Fig. 3.3.3, most ( $> 90\%$ ) of the SIF's values computed by NASGRO are within 5% of the value computed by high-fidelity FEA. Large discrepancies in the SIF solution tend to indicate extreme geometries.

### 3.4 CC10 – Quarter Elliptical Corner Crack at Hole (Offset) in Plate – Bivariant WF

#### 3.4.1 Overview

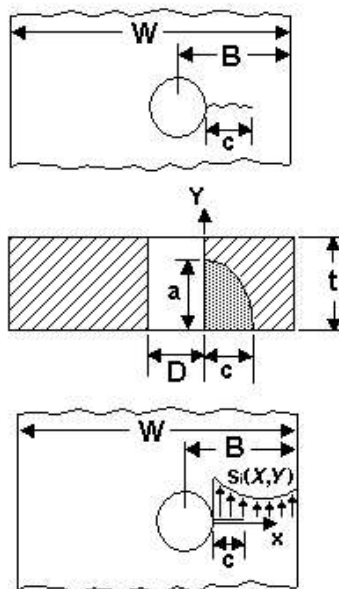


Figure 3.4.1: Configuration of crack case CC10.

Crack case CC10 is a weight function solution for a corner crack at an off-center hole in a finite-width plate with a general bivariant stress distribution on the crack plane.

#### 3.4.2 Geometry

The key input geometric parameters of CC10 are:

- $t$  : plate thickness
- $W$  : plate width
- $D$  : hole diameter
- $B$  : distance from the hole center to the right edge of the plate
- $a$  : crack size in thickness direction
- $a/c$ : aspect ratio of the corner crack

The current geometry, crack size/aspect ratio validity ranges for CC10 are as follows:

$$\begin{array}{lll} 0.5 \leq D/t \leq 4 & D/2 < B \leq W/2 & 0 \leq (W - 2B)/W \leq 0.8 \\ 0 \leq a/t \leq 0.9 & 0.5 \leq a/c \leq 5 & \end{array}$$

When the  $a$ -tip of the crack exceeds the limit during propagation, i.e.  $a/t > 0.9$ , the case transition from CC10 to TC13 is invoked. The transition assumes immediate change from a deep corner crack at the bore to a straight through-thickness crack of the same crack length “ $c$ ”. See Appendix D of the NASGRO manual for additional details regarding the case transition.

### 3.4.3 Loading

The bivariant stress distributions on the plane of crack in an uncracked body are defined in a tabular form and stored in a text file format. The GUI is then used to specify the file locations and names for analysis. The stress file format is of generic NASGRO format for bivariant stresses used by bivariant WF solution modules. For more details on the file format, refer to Section 11.1 – Stress Gradient Input Formats of this appendix.

### 3.4.4 Optional Features

This case allows incorporation of a static residual stress field along the crack plane. See Section 11.6 for more details on how the residual stresses are accounted for in NASFLA.

The cyclic stress shakedown option is available to account for local plasticity. Refer to Appendix M of the manual for more details.

### 3.4.5 Development History

This SIF solution was introduced to NASGRO in v5.0.

### 3.4.6 Theory

The derivation of the weight function methodology used for this crack case is outlined in the Theory section of CC09.

### 3.5 CC11 – Quarter Elliptical Corner Crack in a Plate – Univariant WF

#### 3.5.1 Overview

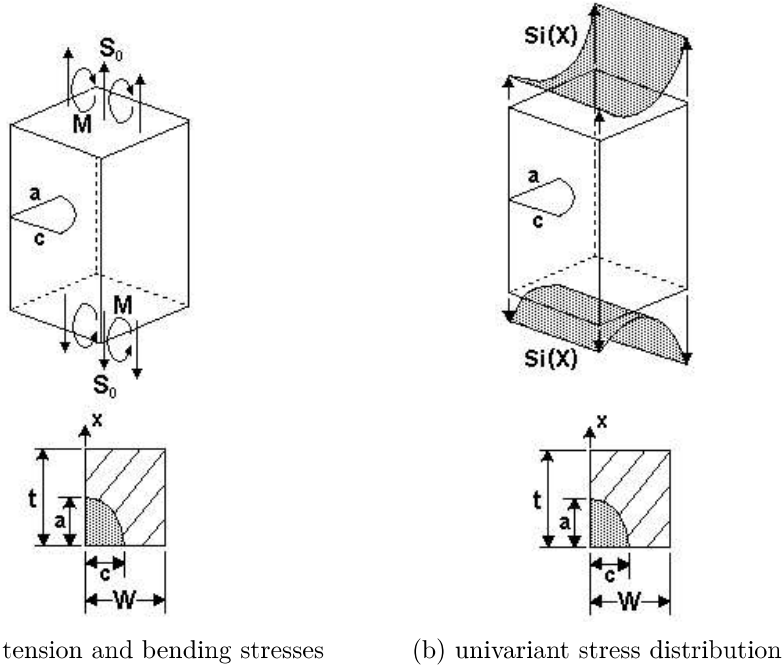


Figure 3.5.1: Configuration of CC11 – a corner crack in a plate – univariant WF

CC11 represents a corner crack in a finite width plate under univariant stress distribution as depicted in Fig. 3.5.1b. It also allows convenient specifications of remote tension and bending stresses (Fig. 3.5.1a).

CC11 is a weight function solution for a corner crack in a plate subjected to a user defined crack plane stress distribution. It is based on the same reference solutions as CC09 (Corner Crack in a Plate with Bivariant Stress Gradient) and gives consistent answers with CC09 when a univariant stress distribution is applied.

#### 3.5.2 Geometry

This model requires four input parameters to define the cracked plate geometry:

- $W$  : plate width
- $t$  : plate thickness
- $a$  : crack size in the thickness direction
- $a/c$ : aspect ratio of the corner crack

The current geometry and crack size validity ranges for CC09 solutions are as follows:

$$0.025 \leq a/c \leq 40$$

$$0 \leq a/t \leq 0.95$$

$$0 \leq c/W \leq 0.95$$

When one of the crack sizes reaches the limit in NASFLA (i.e. if  $a/t = 0.95$  or  $c/W = 0.95$ ), the corner crack will transition to either TC12 or TC28, depending on the user selection in the Geometry tab of the GUI.

### 3.5.3 Loading

Stress loading can be defined in three different ways:

1. The user can apply a uniform tension ( $S_0$ ) and/or bending ( $S_1$ ) stresses at the remote ends of the plate. This is the default option in the GUI. The bending stress  $S_1$  is related to the applied moment  $M$  as:

$$S_1 = \frac{6M}{Wt^2} \quad (3.5.1)$$

2. The stress gradients can be defined via sixth-order polynomials along the normalized  $x$ -direction:

$$X = x/t \quad (3.5.2)$$

Where  $x$  is axis in the through-thickness direction. Up to four polynomials may be entered ( $S_0$  through  $S_3$ ).

3. The weight function solution permits direct input of the principal normal stresses on the crack plane as pairs of  $(X_i, S_i)$ . Here, the  $X$ -axis is the normalized coordinate defined in Eq. (3.5.2). The range of  $X$  for stress definition must be:  $0 \leq X \leq 1$ . Up to four separate tabular stress distributions ( $S_0$  to  $S_3$ ) can be defined by direct input in Geometry tab or via an external text file. Details of the available file formats for univariant stresses are described later in Section 11.1, Stress Gradient Input Formats.

### 3.5.4 Optional Features

This case allows incorporation of a static residual stress field along the crack plane. See Section 11.6 for more details on how the residual stresses are accounted for in NASFLA.

The cyclic stress shakedown option is available to account for local plasticity. Refer to Appendix M of the manual for more details.

NASFLA allows separate definitions of tension/compression or  $t_1/t_2$  stress gradients when entered via tabular input. Refer to Sections 11.2 and 11.3 for further details about this capability.

### 3.5.5 Development History

This SIF model was introduced to NASGRO in v5.2. It previously only permitted input of stresses on the crack plane in tabular or polynomial formats. Starting from NASGRO v8.2, the capability was added to enable users to provide tension and bending remote loadings. Formal verification of CC11 was performed in 2016 using FAA funding for DARWIN.

### 3.5.6 Theory

The approximate weight function approach proposed by Glinka was utilized. The weight function is based on a three-term expansion near the crack tip singularity. The formulation defines the weight function at the *c*-tip or the crack tip at the front surface of the plate as

$$W_c(a : x) = \frac{2}{\sqrt{\pi x}} \left[ 1 + M_{1c} \sqrt{\frac{x}{a}} + M_{2c} \frac{x}{a} + M_{3c} \left( \frac{x}{a} \right)^{3/2} \right] \quad (3.5.3)$$

The weight function at the *a*-tip or the crack tip along the thickness direction is given by

$$W_a(a : x) = \frac{2}{\sqrt{2\pi(a-x)}} \left[ 1 + M_{1a} \sqrt{1 - \frac{x}{a}} + M_{2a} \left( 1 - \frac{x}{a} \right) + M_{3a} \left( 1 - \frac{x}{a} \right)^{3/2} \right] \quad (3.5.4)$$

The variation of stress gradient is along the thickness direction and designates its origin at the front surface of the plate. The coefficients in the above weight functions; i.e.,  $M_{1c}$ ,  $M_{1a}$ , etc., are determined using the reference solutions. Respectively, the coefficients are given by:

- Coefficients with *c*-tip

$$\begin{aligned} M_{1c} &= -8 + \frac{3\pi}{\sqrt{Q}} (2F_1 - 5F_2) \\ M_{2c} &= 15 + \frac{15\pi}{\sqrt{Q}} (-F_1 + 3F_2) \\ M_{3c} &= -(1 + M_{1c} + M_{2c}) \end{aligned} \quad (3.5.5)$$

- Coefficients with *a*-tip

$$\begin{aligned} M_{1a} &= -\frac{24}{5} + \frac{\pi}{\sqrt{2Q}} (-2Y_1 + 6Y_2) \\ M_{2a} &= 3 \\ M_{3a} &= \frac{8}{5} + \frac{6\pi}{\sqrt{2Q}} (Y_1 - 2Y_2) \end{aligned} \quad (3.5.6)$$

The shape factor  $Q$  is a function of the crack shape aspect ratio  $a/c$  and its definition can be found in other 2D crack models. The reference solutions  $F_1$ ,  $F_2$ ,  $Y_1$ , and  $Y_2$ , are normalized SIFs with respect to the crack depth  $a$  in connection to two reference stresses:  $\sigma_1 = 1$  and  $\sigma_2 = x/a$ , applied on the crack surfaces.  $Y_1$  and  $Y_2$  are with  $\sigma_1$  and  $\sigma_2$  at *a*-tip respectively, and  $F_1$  and  $F_2$  are solutions with *c*-tip.

The weight function is used as a Green's function in the following equation for the determination of stress intensity factor.

$$K_{a,c} = \int_0^a W_{a,c}(a : \xi) \sigma(\xi) d\xi \quad (3.5.7)$$

where  $\sigma(\xi)$  is the stress component normal to the crack plane and its variation is along the thickness. The integration is carried out numerically to circumvent the singularity at  $\xi = a$ . The internal routines in NASGRO deploy a pre-integration approach to evaluate the integral in accordance with the user-specified interpolation option among data points.

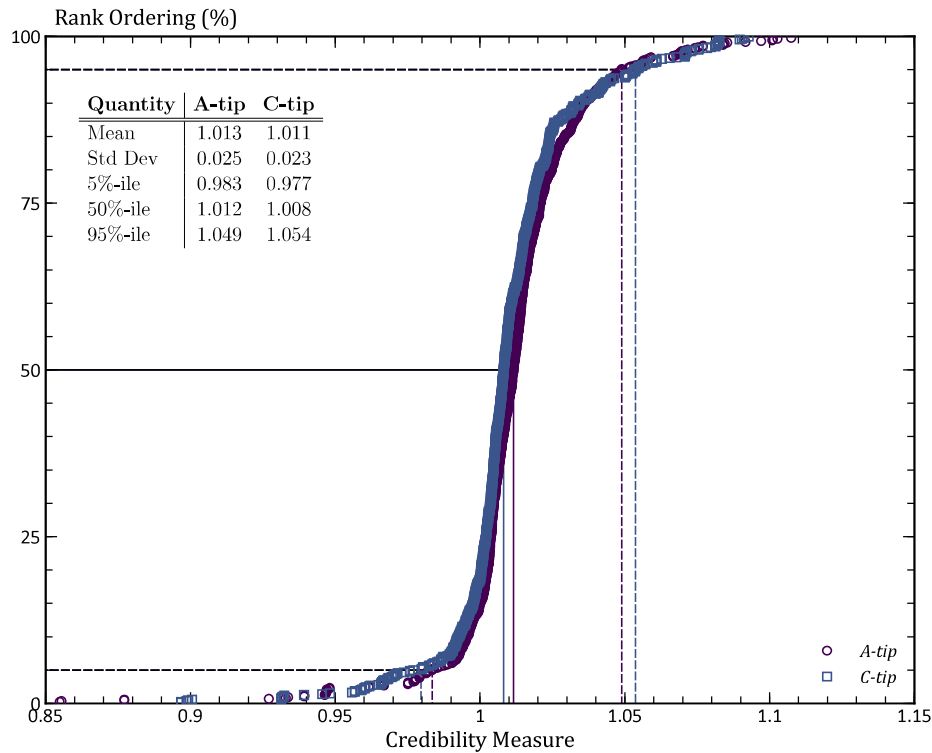


Figure 3.5.2: Verification plot for CC11 showing the cumulative distribution of discrepancies. The credibility measure is the ratio of the NASGRO SIF solution to the FEA SIF solution. This figure rank orders the credibility matrix and provides statistical quantity measures.

### 3.5.7 Verification

Verification of CC11 follows the verification procedure outlined in [52]. Full details of the verification effort can be found in that document. Fig. 3.5.2 presents the key verification plot for CC11. These results employ 172 geometries semi-randomly generated by Latin Hypercube methods. These geometries are independent on the calibration matrix. For this univariant solution, Fig. 3.5.2 employs 4 stress gradients. The credibility measure is the ratio of the NASGRO SIF solution to the FEA SIF solution for the same solution.

As shown in Fig. 3.5.2, most ( $> 90\%$ ) of the SIF's values computed by NASGRO are within 5% of the value computed by high-fidelity FEA. Large discrepancies in the SIF solution tend to indicate extreme geometries.

### 3.6 CC12 – Quarter-Elliptical Corner Crack at Chamfer in Plate – Bivariant WF

#### 3.6.1 Overview

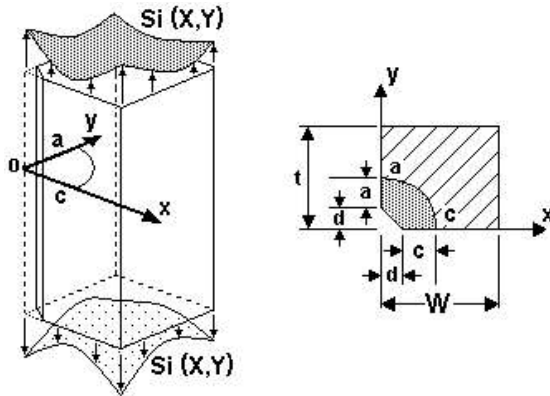


Figure 3.6.1: Configuration of crack case CC12

CC12 is a quarter-elliptic corner crack model at a chamfered corner of a finite plate. The two chamfer legs must be equal. The corner crack must completely span the chamfer. Loading is specified by general bivariant stress distributions on a crack plane in an uncracked plate.

#### 3.6.2 Geometry

The crack model is illustrated in Fig. 3.6.1. It takes following geometric inputs:

- $t$  : plate thickness
- $W$  : plate width
- $d$  : chamfer depth
- $a$  : initial flaw size in the thickness direction
- $a/c$  : aspect ratio of the corner crack

The current geometry validity ranges for CC12 are as follows:

$$\begin{aligned} 10 &\leq \min(W, t)/d \\ 0 &\leq (a + d)/t \leq 0.9 \\ 0 &\leq (c + d)/W \leq 0.9 \end{aligned}$$

#### 3.6.3 Loading

The bivariant stresses on the plane of crack in an uncracked body are input via a text file that contains the coordinates and stress values. Details of the available file formats for bivariant stresses are described later in Section 11.1, Stress Gradient Input Formats.

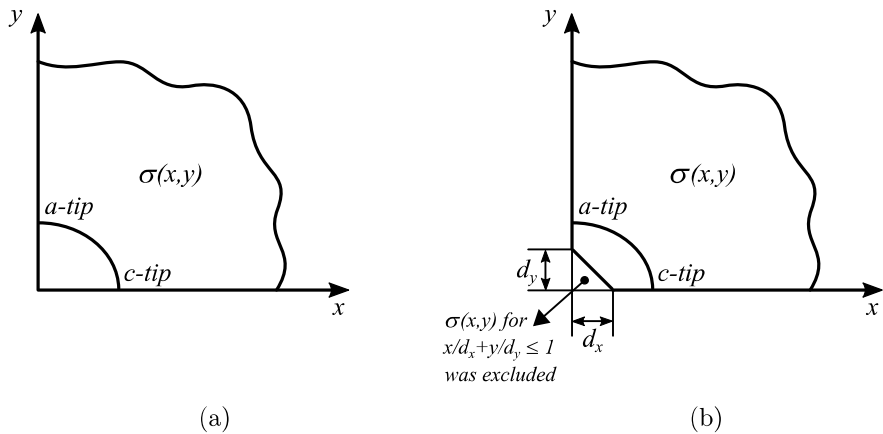


Figure 3.6.2: The ratio of two different corner crack solutions was used for determining the stress intensity factors for chamfered corner: (a) the integration for weight function solution over the quarterly elliptical corner crack surface, and (b) the integration over the domain confined by the corner crack perimeter and the chamfer.

### 3.6.4 Optional Features

CC12 allows incorporation of a static residual stress field along the crack plane. See Section 11.6 for more details on how the residual stresses are accounted for in NASFLA.

NASFLA allows separate definitions of tension/compression or t1/t2 stress gradients. Refer to Sections 11.2 and 11.3 for further details about these features.

### 3.6.5 Development History

This SIF solution was introduced to NASGRO in v6.0.

### 3.6.6 Theory

The stress intensity factor for a corner crack at a chamfered corner is based on the weight function solutions implemented for the crack case CC09. Note that the corner crack must completely span the chamfer, as shown in Fig. 3.6.2b. The two chamfer legs  $d_y$  and  $d_x$  in Fig. 3.6.2b must be equal.

To account for the effect of reduction in corner crack area due to chamfering, a multiplication factor was applied to the determined CC09 solutions. This correction factor is based on the ratio of two quarterly infinite domain solutions, as illustrated in Fig. 3.6.2. One is the bivariant corner crack solution by integrating the weight function over the quarterly elliptical crack surface as shown in Fig. 3.6.2a, and the second one is the bivariant corner crack solution by integrating the weight function over the domain confined by the corner crack perimeter and the chamfer as illustrated in Fig. 3.6.2b. The weight function in both cases was for the corner crack in a quarterly infinite domain. By designating the first corner crack solution by  $K_{corner}^{\infty}$  and the second one by  $K_{chamfer}^{\infty}$ , the stress intensity factor for the cracks at the chamfered corner is defined by

$$K^{CC12} = K_{chaper} = \frac{K_{chamfer}^{\infty}}{K_{corner}^{\infty}} K^{CC09} = C.F. \times K^{CC09} \quad (3.6.1)$$

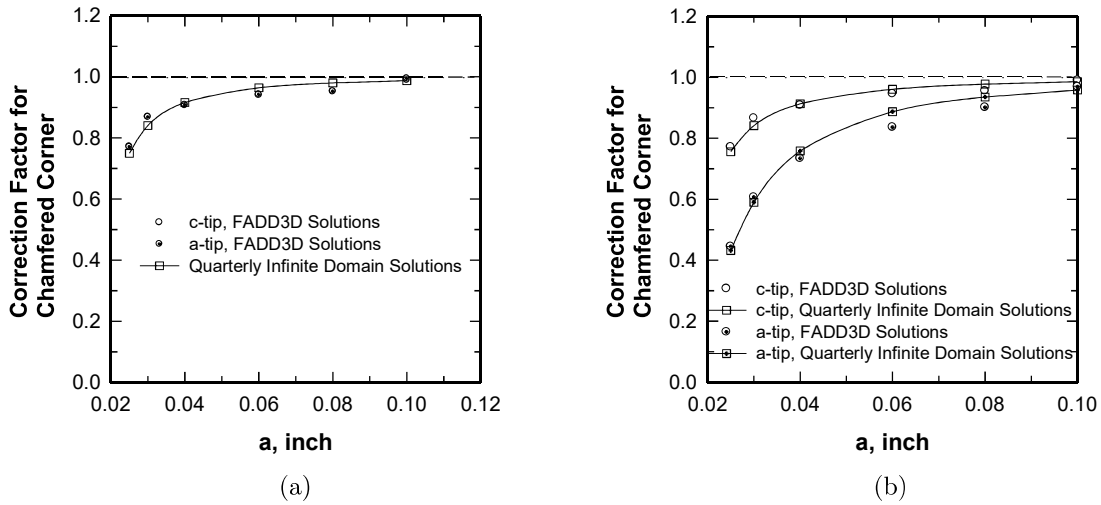


Figure 3.6.3: Comparison of correction factors due to chamfering between FADD3D results for finite plate dimensions and weight function solutions for quarterly infinite domain: (a) unit tension and (b) unit bending

where  $K^{CC09}$  is the stress intensity factor computed using the CC09 module for finite dimensions. The correction factor (C.F.) is thus dependent on the stress variation besides the crack tip location and needs to apply to both crack tips separately.

Note that in NASSIF correction factor outputs, the normalization factor for CC12 is in reference to a pseudo crack depth ( $a + d$ ) instead of  $a$ ; e.g.,  $\sqrt{\pi(a + d)}$ .

### 3.6.7 Verification

To verify the approach described in the Theory section above, two sets of stress intensity solutions were determined numerically using the three-dimensional (3D) fracture mechanics program FADD3D. One is for the corner crack in the rectangular plate, and the other is for the corner crack in the chamfered rectangular plate. Two stress variations were applied for validation: one is unit tension  $\sigma = 1$ , and the other is unit bending where  $\sigma = 1 - y/a$  and  $a$  is the crack depth along the plate thickness direction  $y$ .

The ratios of the solutions based on these two cracked configurations are corresponding to  $K_{chamfer}/K^{CC09}$  and they are used to compare with the above-defined correction factors  $K_{chamfer}^\infty/K_{corner}^\infty$ . Notice the former is for a finite domain, while the later is for a quarterly infinite domain. The comparison of these factors for both crack tips is displayed in Fig. 3.6.3a for unit tension and in Fig. 3.6.3b for unit bending. The excellent agreement shown in these two figures validates the approach for multiplying the CC09 solution by the correction factor to account for the effect of reduction in crack area due to chamfering.

### 3.7 CC13 – Quarter-Elliptical Corner Crack at Edge Notch in Plate

#### 3.7.1 Overview

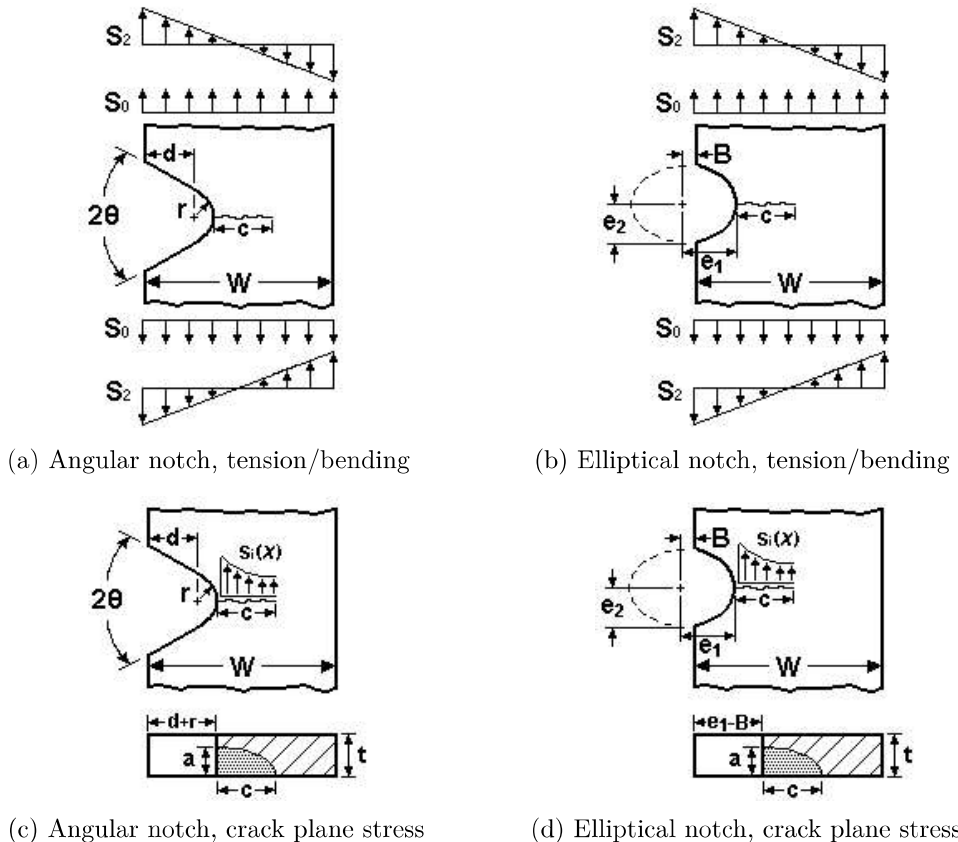


Figure 3.7.1: Configuration of the crack case CC13

CC13 is a model of a quarter-elliptical corner crack at the tip of an edge notch in a finite-width plate. Two different notch types are supported as described in the Geometry section below. The model can be loaded by remote tension/bending stress or by general univariant stress distribution defined on the crack plane.

#### 3.7.2 Geometry

CC13 supports two common notch types:

- angular straight-edge notch as shown in Figs. 3.7.1a and 3.7.1c
- elliptical notch as shown in Figs. 3.7.1b and 3.7.1d

The angular notch is characterized by two straight edges with an enclosed angle  $\theta$  resulting in a nominal notch depth  $d$  and a local root radius  $r$  at the notch tip. In contrast, the elliptical notch is fully described by an ellipse of  $e_1$  as the long axis and  $e_2$  as the short axis with an additional offset  $B$ . The validity limits of the SIF solutions thus depend on the user-selectable notch shape and are listed in the following. Note the crack length  $a$  denotes the crack depth along the root of the notch

and the crack length  $c$  denotes the crack depth measured on the front surface of the plate and along the plate width direction.

### Angular straight-edge notch

The geometric input parameters for the plate with the angular straight-edge notch are as follows:

- $t$  : plate thickness
- $W$  : plate full width
- $d$  : nominal notch depth measured from the left edge of the plate to the center of the notch root radius
- $r$  : notch root radius of curvature
- $c$  : initial flaw size along the notch root
- $a/c$  : initial aspect ratio

The validity ranges for the angular straight-edge notched crack model are listed below.

$$0 \leq \theta \leq 75^\circ$$

$$0 < \frac{d+r}{W} \leq 0.75$$

$$0 \leq \frac{d/r}{c} \leq 24$$

$$\frac{c}{W-d-r} \leq 0.95$$

$$a/t \leq 0.95$$

where,  $\theta$  is the angle enclosed by the straight edges of the notch. Similar to TC17, the angle  $\theta$  has no effect on the stress gradients over the specified range, and thus its input is not required.

### Elliptical notch

The geometric input parameters for the plate with the elliptical notch are as follows:

- $t$  : plate thickness
- $W$  : plate full width
- $e_1$  : semimajor axis of ellipse
- $e_2$  : semiminor axis of ellipse
- $B$  : offset of elliplse away from the plate edge surface
- $a$  : initial flaw size along the notch root
- $a/c$  : initial aspect ratio

The validity ranges for the elliptical notched crack model are listed below.

$$0.2 \leq e_1/e_2 \leq 5$$

$$0 < \frac{e_1 - B}{W} \leq 0.75$$

$$0 \leq B \leq e_1$$

$$\frac{c}{W + B - e_1} \leq 0.95$$

$$a/t \leq 0.95$$

Note the offset of the ellipse  $B$  is always assumed away from the edge surface of the plate instead of into the plate.

Regardless of the notch type, when the crack depth along the root of the notch exceeds 95% of the plate thickness in NASFLA (i.e.  $a/t \geq 0.95$ ) the corner crack will self-transition to a through crack

TC17. The crack length along the width direction becomes the depth of the through crack, and all stress definitions remain the same. Refer to the Appendix D of the NASGRO documentation for additional details about crack transitions.

### 3.7.3 Loading

Three types of stress definition can be specified as listed below.

- The simplest one is to apply tension stress  $S_0$  and in-plane bending stress  $S_2$  at the remote ends (in contrast to applying stresses on the crack surface).
- The second and the third options for stress definition are provided for users to specify crack opening stress distributions along the crack plane. The second kind describes the stress variation by polynomial functions of up to the sixth power expressed in terms of normalized coordinate. The normalized coordinate as the independent variable is with respect to the net section width. The polynomial function is given by

$$\sigma(x) = \sum_{i=0}^6 C_i \left( \frac{x}{W_{net}} \right)^i \quad (3.7.1)$$

where the “effective” sectional width  $W_{net}$  is given by  $W - (d + r)$  for angular notch or by  $W - (e_1 - B)$  for elliptical notch. The coefficients  $C_i$  are provided by the user. The coordinate  $x$  is measured from the notch tip and across the net section.

- The third kind represents the stress variation in tabulated format consisting of stress pairs  $[X_i, S_i]$ , where  $X = x/W_{net}$  is the normalized axis along the width of the plate. All stress pairs are listed row by row according to coordinates in ascending order. By this definition, the normalized coordinates cannot be less than zero or larger than 1, i.e.  $0 \leq X \leq 1$ .

### 3.7.4 Optional Features

Tabular stress input option of this case allows incorporation of a static residual stress field along the crack plane. See Section 11.6 for more details on how the residual stresses are accounted for in NASFLA.

The tabular stress gradients can be defined separately for tension/compression or t1/t2 time instants. Refer to Sections 11.2 and 11.3 of this document for additional details.

The cyclic stress shakedown option is available for remote tension/bend and tabular stress input options to account for stress relief near the notch tip due to local plasticity. Refer to Appendix M of the manual for more details.

### 3.7.5 Development History

This SIF model was introduced to NASGRO in v7.0.

### 3.7.6 Theory

The SIF solution for this crack model is based on the same weight function formulation for univariant stresses as that used by CC11. The univariant distribution of crack opening stress along the crack

growth direction is used along with the weight functions to determine the stress intensity factors at two surface tip locations. For remotely applied stress definition, the CC13 fracture mechanics module internally computes resulting crack opening stress variation by interpolating among an array of net section stress variations extracted from finite element results at discrete geometric aspect ratios.

### 3.8 CC14 – Quarter-Elliptical Corner Crack at Offset Embedded Slot or Elliptical Hole in Plate

#### 3.8.1 Overview

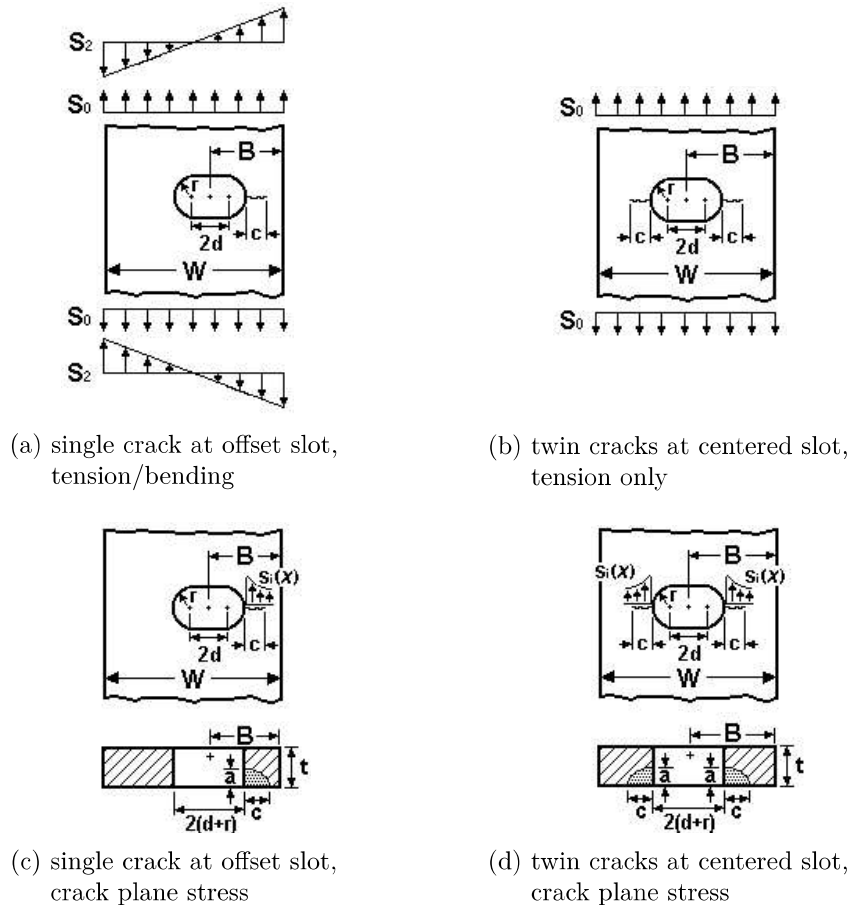


Figure 3.8.1: Configuration of the crack case CC14 with a straight-edge slot

CC14 is a crack case of a quarter-elliptical corner crack (or two symmetrical corner cracks) at the notch tip(s) of an (offset) embedded slot or elliptical hole in a plate. The model supports remote application of tension/bending stress as well as general nonlinear crack plane stressing.

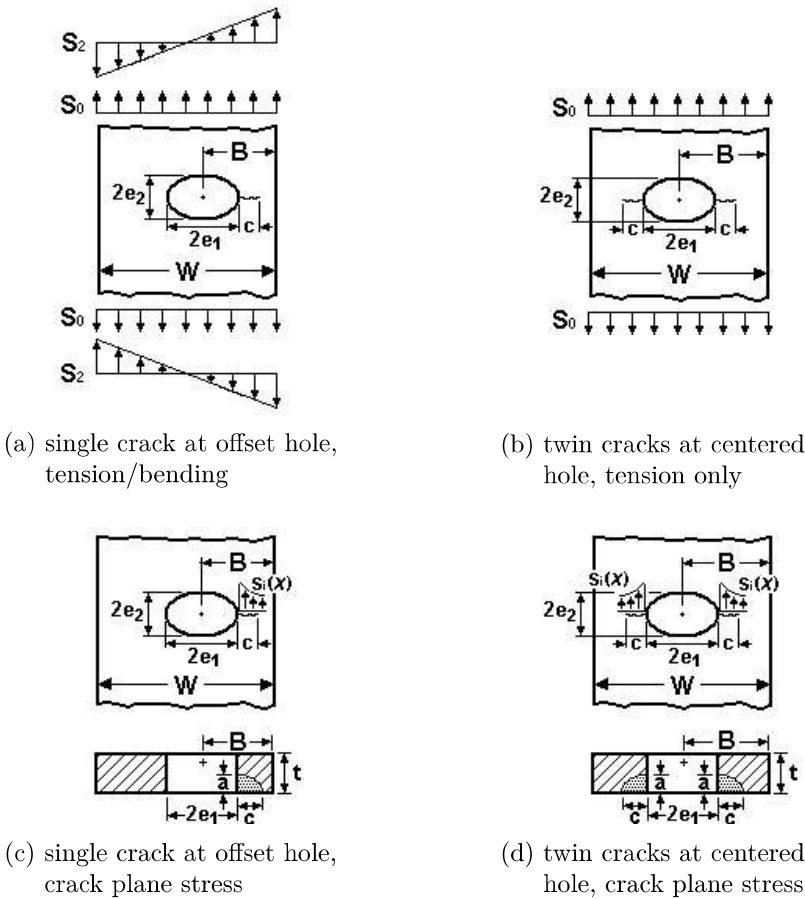


Figure 3.8.2: Configuration of the crack case CC14 with an elliptical hole

### 3.8.2 Geometry

This model supports two types of slots. The first and default notch option in the GUI is the straight-edge slot as shown in Fig. 3.8.1. The second notch type is the elliptical hole as depicted in Fig. 3.8.2.

#### Straight-edge slot

The straight-edge slot is characterized by two parallel straight edges and two semi-circular notch ends. The following are model input parameters when this notch type is selected:

- $t$  : plate thickness
- $W$  : plate full width
- $d$  : one-half nominal slot length
- $r$  : notch root radius of curvature
- $B$  : slot offset distance from plate edge surface to slot center
- $a$  : initial flaw size along the bore of the hole
- $a/c$ : initial flaw aspect ratio

Note the crack depth along the bore is denoted by  $a$ , and the surface crack length along the plate width direction and on the front plate surface is denoted by  $c$ .

The nominal length  $2d$  defines the distance from one center of root radius to the other center, and

thus  $2(d + r)$  is the distance between two notch tips.

For the centered slot configuration with symmetric twin cracks as shown in Figs. 3.8.1b and 3.8.1d, the slot offset parameter must be set to one half the plate width, i.e.  $B = W/2$ .

Below are the model validity ranges for the straight-edge slot:

$$0.05 \leq (d + r)/B \leq 0.75$$

$$0.1 \leq (d + r)/t \leq 10$$

$$0 \leq d/r \leq 24$$

$$0.2 \leq 2B/W \leq 1$$

$$0 \leq \frac{c}{B - d - r} \leq 0.8$$

$$0.5 \leq a/c$$

$$0 \leq a/t \leq 0.9$$

### Elliptical slot

The elliptical hole is described by an ellipse of  $e_1$  as the long axis and  $e_2$  as the short axis. The offset of the slot or hole from the right side of the plate defines the offset  $B$ . The following are all required input parameters to define the crack geometry with elliptical slot:

- $t$  : plate thickness
- $W$  : plate full width
- $e_1$  : semimajor axis of ellipse
- $e_2$  : semiminor axis of ellipse
- $B$  : hole offset distance from the plate edge surface to the ellipse center
- $a$  : initial flaw size along the bore of the hole
- $a/c$ : initial flaw aspect ratio

Note the crack depth along the bore is denoted by  $a$ , and the surface crack length along the plate width direction and on the front plate surface is denoted by  $c$ .

For the centered hole configuration with symmetric twin cracks as shown in Figs. 3.8.2b and 3.8.2d, the hole offset parameter must be set to half the plate width, i.e.  $B = W/2$ .

The validity limits of SIF solutions for elliptical slots are listed as follows.

$$0.05 \leq e_1/B \leq 0.75$$

$$0.1 \leq e_1/t \leq 10$$

$$0.2 \leq e_1/e_2 \leq 5$$

$$0.2 \leq 2B/W \leq 1$$

$$0 \leq \frac{c}{B - e_1} \leq 0.8$$

$$0.5 \leq a/c$$

$$0 \leq a/t \leq 0.9$$

Regardless of the notch type, when the crack depth along the bore reaches the limit  $a/t = 0.9$ , the corner crack in NASFLA will self-transition to a through crack TC18. The crack length along the width direction becomes the depth of the through crack, and all stress definitions remain the same. Refer to the Appendix D of the NASGRO documentation for additional details about crack transitions.

### 3.8.3 Loading

This crack case supports the same two options of stressing that are available in related cases TC18 and SC27. The simplest one is to apply tension stress  $S_0$  and in-plane bending stress  $S_2$  at remote ends.

The second loading option is to define univariant stress gradient on the crack plane in an uncracked geometry. NASGRO allows tabular input, which can be entered directly in the Geometry tab of the GUI. The discretized stress pairs  $[X_i, S_i]$  are provided by the user. Here,  $X$  is the normalized coordinate system defined as follows:

$$\begin{aligned} X &= x/(B - d - r) && \text{for the straight-edge slot} \\ X &= x/(B - e_1) && \text{for the elliptical hole} \end{aligned} \quad (3.8.1)$$

The coordinate  $x$  is measured from the notch tip across the net section along which the crack growth path is assumed. By this definition, the variation of the normalized coordinate is  $0 \leq X \leq 1$ . The entries  $X_i$  must be sorted in an ascending order. Up to four tabular stress distributions may be entered directly via GUI.

The univariant stress gradient tables can also be provided via an external text file. Details of the available file formats for univariant stresses are described in Section 11.1.

### 3.8.4 Optional Features

Tabular stress input option of this case allows incorporation of a static residual stress field along the crack plane. See Section 11.6 for more details on how the residual stresses are accounted for in NASFLA.

The tabular stress gradients can be defined separately for tension/compression or t1/t2 time instants. Refer to Sections 11.2 and 11.3 of this document for additional details.

The cyclic stress shakedown option is available for remote tension/bend and tabular stress input options to account for stress relief near the notch tip due to local plasticity. Refer to Appendix M of the manual for more details.

### 3.8.5 Development History

This SIF model was introduced to NASGRO in v7.0. Starting from v8.2, the geometry limits of the model were extended to better handle thin sheets.

### 3.8.6 Theory

The univariant distribution of crack opening stress along the crack growth direction is used along with the weight functions to determine the stress intensity factors at two surface tip locations. For remote stressing option, the CC14 fracture mechanics module internally computes resulting crack opening stress variation by interpolating among an array of net section stresses extracted from finite element results at discrete geometric parameters.

Most of the CC14 SIF solutions are based on the same weight function approach for CC08 where the radius of the hole characterizing CC08 crack model is replaced by the “effective” notch depth

in CC14 crack model. The definition of this “effective” notch depth depends of the type of the slot. For elliptical holes, it is the long axis  $e_1$  while for straight-edge slots, it is the straight edge plus the root radius,  $d + r$ . For elliptical holes with  $e_2/e_1 > 1$ , the following interpolation between the SIF results from CC08 and CC11 weight function solutions is used.

$$K^{CC14} = (K^{CC08} - K^{CC11}) \left( \frac{e_1^2}{e_2^2} \right)^{0.2} + K^{CC11} \quad (3.8.2)$$

The interpolation ensures when the ratio of short axis to long axis  $e_2/e_1$  equals to 1.0, the SIF solution for CC14 crack model is solely based on the weight function approach used by CC08 crack model; i.e.,  $K^{CC14} = K^{CC08}$ , while when  $e_2/e_1 \rightarrow 8$  or  $e_1/e_2 \rightarrow 0$ , the SIF solution retreats to the one for CC11 crack model. The interpolative relationship is empirically determined based on finite element results.

### 3.9 CC15 – Quarter-Elliptical Corner Crack at Offset Hole in Plate with Broken Ligament

#### 3.9.1 Overview

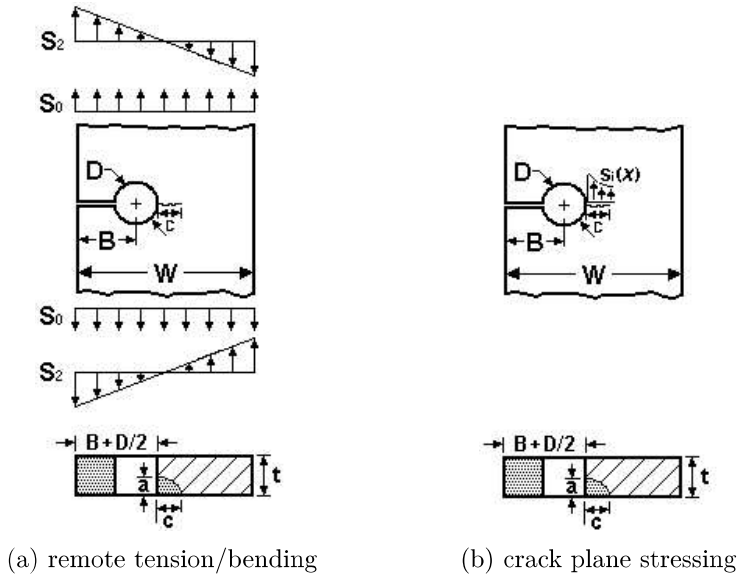


Figure 3.9.1: Configuration of the crack case CC15

The crack case CC15 is for a corner crack at a hole in a plate with one of the net sections completely broken through as depicted in Fig. 3.9.1. The crack should be at the exact opposite side of the hole with respect to the broken ligament. This crack case can be used to describe the continuous damage scenario after the smaller net section in TC13 crack case is broken through and a corner crack initiates at the opposite side of the hole. The broken ligament is represented by two parallel edge surfaces with an infinitesimal gap.

#### 3.9.2 Geometry

The crack geometry is defined by specifying the following input parameters:

- $t$  : plate thickness
- $W$  : plate full width
- $B$  : hole center offset from the left edge of the plate
- $D$  : hole diameter
- $a$  : initial flaw size along the bore surface
- $a/c$  : initial flaw aspect ratio, where  $c$  is the surface flaw size on the plate front face

The solution validity limits for this case are listed below.

$$0 \leq 2B/D \leq 24$$

$$0 \leq \frac{B + D/2}{W} \leq 0.75$$

$$\frac{c}{W - B - D/2} \leq 0.9$$

$$a/t \leq 0.95$$

When the crack depth along the bore reaches the limit  $a/t = 0.95$ , the corner crack in NASFLA will self-transition to a through crack TC19. The crack length along the width direction becomes the depth of the through crack with a single tip, and all stress definitions remain the same. Refer to the Appendix D of the NASGRO documentation for additional details about crack transitions.

### 3.9.3 Loading

Three options are provided to specify stress definition as described below.

1. The plate can be loaded by remote tension stress  $S_1$  and remote in-plane bending stress  $S_2$
2. Users can define univariant crack opening stress distributions on the crack plane by providing the coefficients  $C_i$  of the polynomial stress functions of up to sixth order, given by:

$$\sigma(x) = \sum_{i=0}^6 C_i(X)^i \quad (3.9.1)$$

where  $X = x/W_{net}$  is the coordinate axis normalized by the “effective” sectional width given by  $W_{net} = W - (B + D/2)$ . The axis  $x$  starts from the bore surface on the crack plane and runs parallel to the growth direction of  $a$ -tip toward the plate right edge.

3. Tabulated stressing option allows definition of univariant crack opening stress variations by stress pairs consisting of normalized coordinates and associated stress values  $[X_i, S_i]$ . The same normalized axis  $X$  is used as defined above for polynomial inputs. Refer to Section 11.1 for additional details about NASGRO convention for tabular stress definition. The fracture mechanics module interpolates the intermediate stress values when evaluating the integration for weight function solutions.

### 3.9.4 Optional Features

Remote tension/bend and tabular stress input options of this crack case allow incorporation of a static residual stress field along the crack plane. See Section 11.6 for more details on how the residual stresses are accounted for in NASFLA.

The tabular stress gradients can be defined separately for tension/compression or t1/t2 time instants. Refer to Sections 11.2 and 11.3 of this document for additional details.

The cyclic stress shakedown option is available for remote tension/bend and tabular stress input options to account for stress relief near the notch tip due to local plasticity. Refer to Appendix M of the manual for more details.

### 3.9.5 Development History

This SIF model was introduced to NASGRO in v7.0.

### 3.9.6 Theory

The weight function approach for this crack case is identical to the one used by CC11. The univariant distribution of crack opening stress along the net section is used to determine the SIFs at two surface tips; one along the bore and the other on the front surface of the plate. If the load is defined by remote tension/bending stress, NASGRO internally determines resulting crack opening stress distribution by interpolating a discrete set of crack plane stress solutions obtained from finite element models with no crack.

To employ the weight function formulation for CC11 crack model, the following transformations are used: (1) the “effective” sectional width  $W_{net}$  of this crack model replaces the “thickness” used by CC11, (2) the surface crack length  $c$  along the plate width direction of this crack model replaces the “crack depth”  $a$  used by CC11, and (3) the surface crack length  $a$  along the bore of this crack model replaces the “surface crack length”  $c$  used by CC11.

## 3.10 CC16 – Corner Crack(s) at a Hole Based on Fawaz-Andersson Solution

### 3.10.1 Overview

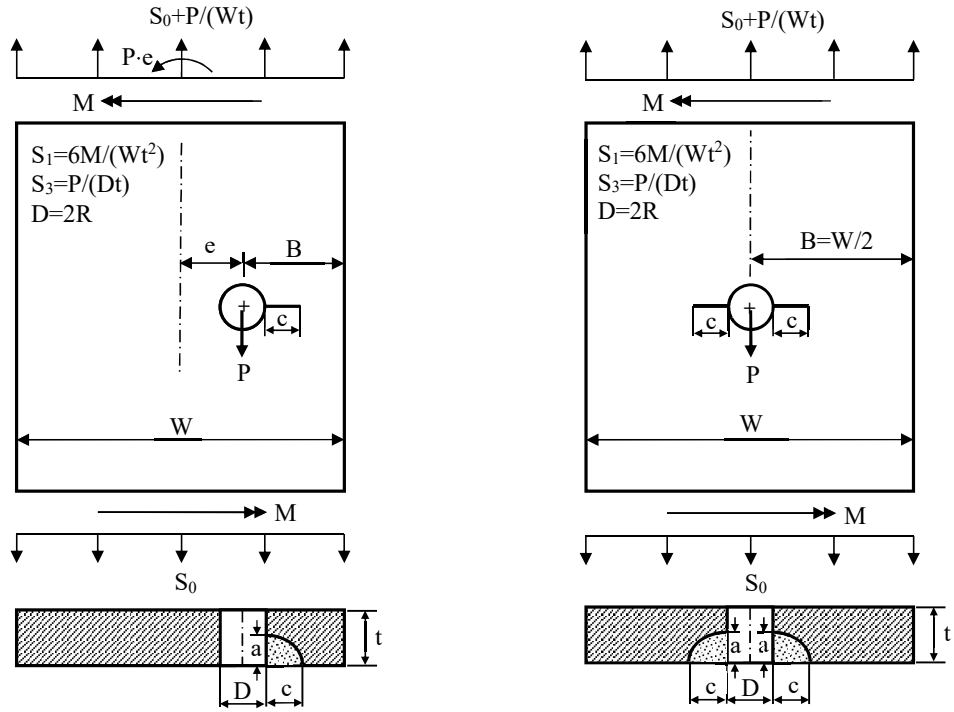
CC16 is a corner-crack-at-hole solution based on Fawaz-Andersson solution for one corner crack at a hole [53] and the modified Newman finite width correction equations [54]. The crack case deals with a single corner crack at an offset hole or two symmetric corner cracks at a central hole in a finite plate subjected to remote tension ( $S_0$ ), out-of-plane bending ( $S_1$ ), and pin load ( $S_3$ ), as shown in Figure 3.10.1, where  $B$  can be larger or less than or equal to  $W/2$ .

### 3.10.2 Geometry

The key input geometric parameters of CC16 are  $t$ ,  $W$ ,  $D$ ,  $B$ ,  $a$  and  $a/c$ .

- $t$ : Plate thickness;
- $W$ : Plate width;
- $D$ : Hole diameter;
- $B$ : Distance between the hole center and the right edge of the plate;
- $a$ : Crack size in thickness direction;
- $a/c$ : Crack aspect ratio of the corner crack.

Solution limits of CC16:



(a) Single corner crack at an offset hole      (b) Two symmetric corner cracks at a central hole

Figure 3.10.1: Configuration of crack case CC16

- For single corner crack,

If  $B < W/2$  :

$$B/D \geq 1, \quad 0.2 \leq D/t \leq 20, \quad 0.1 \leq a/c \leq 10, \quad 0 \leq a/t \leq 0.99, \quad (D+c)/(2B-c) \leq 0.7$$

If  $B \geq W/2$  :

$$B/D \geq 1, \quad 0.2 \leq D/t \leq 20, \quad 0.1 \leq a/c \leq 10, \quad 0 \leq a/t \leq 0.99, \quad (D/2+c)/B \leq 0.9$$

- For two symmetric corner cracks,

$$B/D \geq 1, \quad 0.2 \leq D/t \leq 20, \quad 0.1 \leq a/c \leq 10, \quad 0 \leq a/t \leq 0.99, \quad (D/2+c)/B \leq 0.9$$

### 3.10.3 Loading

Crack case CC16 supports remote tension ( $S_0$ ), out-of-plane bending ( $S_1$ ), and pin load ( $S_3$ ).

### 3.10.4 Development History

CC16 was first implemented in NASGRO version 7.1. It was discovered during the v8.0 development cycle that CC16 results for pin-loaded holes (and only pin-loaded holes) in narrow plates could be excessively non-conservative. Therefore, a modified finite-width correction factor for pin-loaded CC16 was developed based on the CC08 solution, which had been modified to accommodate pin-loading and to widen the geometry range significantly. Further study of this revised solution

indicated that, while accurate for narrow plates with centered holes, these values could be over-conservative for narrow plates with holes highly offset from the centerline. Therefore, a second CC16 revision focusing on the hole-offset correction factor was developed, verified, and implemented in v8.1a. Once again, the revised CC16 solution only changed K-values under pin-loading – solutions for tension and out-of-plane bending have been unaffected. These solutions were applied to CC17 starting in 8.01 and 8.1f.

Even further study revealed non-physical oscillations – “peaks” and “troughs” – in the solution introduced by the interpolation process. These “peaks” and “troughs” only influenced relatively small cracks ( $a/t \leq 0.2$ ) at small holes ( $D/\min(2B, 2(W-B)) \leq 0.5$ ). The oscillations themselves tend to reduce the overall effect on fatigue lives. Some portions of the fatigue crack growth curve will give crack growth rates that are too low due to low stress intensity factor values. Other portions of the fatigue crack growth curve will give rates that are too high due to high stress intensity factor values. It is unclear exactly how these changes will impact fatigue crack growth lives overall, but the errors may effectively cancel out in some cases.

Several attempts were made to eliminate the non-physical oscillations in the solution. Adding more points to the solution matrix shifted the oscillations to other parts of the solution space, even if the solution matrix tripled in size. NASGRO 8.2b changed the solution space in only the small crack regime and left the remainder of the solution space untouched. Unfortunately, this modification introduced a discontinuity in the stress intensity factor solution at the boundary ( $a/t = 0.2$ ). This discontinuity was triggered by fundamental differences in the two interpolation schemes. This approach has been abandoned.

NASGRO 8.2f takes the radical step of changing the entire parameterization for pin-loaded CC16 to eliminate the non-physical oscillations. This approach eliminates the non-physical oscillations and improves the solution quantity. It does not introduce any discontinuities into the solution. The new parameterization scheme interpolates over the relative hole size rather than over the relative crack depth. Consequently, stress intensity factors in NASGRO 8.2f will differ from stress intensity factors in earlier versions of NASGRO. These changes only affect cracks under pin-loading. Again, it is unclear exactly how these changes will impact fatigue crack growth lives overall, but the differences may effectively cancel out in some cases. Preliminary investigations with these new pin-loaded geometry correction factors have revealed lower lives for: 1) cracks on the long ligament side of highly offset holes as  $0.5D/(W-B) > 0.5$  and 2) cracks in very thick plates where  $D/(2t) \rightarrow 0.2$ . In this second case, additional studies suggest that both the old and new geometry correction factors are systematically conservative.

### 3.10.5 Theory

#### 3.10.5.1 The fundamental stress intensity factors of single corner crack

The fundamental stress intensity factors (beta factors) of single corner crack at a hole in an infinite plate, developed by Fawaz and Andersson using the finite element method, are given on a grid of  $25 \times 11 \times 26$ , i.e., twenty five  $a/c$  values, eleven  $a/t$  values, and twenty six  $R/t$  values.

- The 25  $a/c$  values : 0.1, 0.1111, 0.125, 0.1428, 0.1667, 0.2, 0.25, 0.333, 0.5, 0.667, 0.75, 0.8, 1.0, 1.25, 1.333, 1.5, 2, 3, 4, 5, 6, 7, 8, 9, 10
- The 11  $a/t$  values : 0.1, 0.2, 0.3, 0.4, 0.5, 0.6, 0.7, 0.8, 0.9, 0.95, 0.99
- The 26  $R/t$  values : 0.1, 0.1111, 0.125, 0.1428, 0.1666, 0.2, 0.25, 0.333, 0.5, 0.6666, 0.75, 0.8, 1.0, 1.25, 1.333, 1.5, 1.6666, 2, 3, 4, 5, 6, 7, 8, 9, 10

The beta factors are available at multiple points along the whole crack front, but only the data at the vertices (*a*-tip and *c*-tip) are needed. The beta factors at the vertices are actually the local maximum beta factors near or at *a*-tip and *c*-tip.

The original database of the beta factors has the following problems based on our analysis:

- The database for remote tension ( $S_0$ ):
  - A number of beta factors are missing near the boundary of the domain.
- The database for out-of-plane bending ( $S_1$ ):
  - A number of beta factors are missing near the boundary of the domain.
  - The beta factors for  $R/t=4, 5, 6, 7$  and  $10$ , as well as the beta factors at  $a/c=8$  and  $9$ ,  $a/t=0.2\sim0.99$  and  $R/t=0.1428$  do not make sense.
- The database for pin load ( $S_3$ ):
  - A number of beta factors are missing near the boundary of the domain.
  - The beta factors for  $R/t=8$  and  $9$  are incorrect. A few beta factors under pin load are negative.

Based on our observation, the beta factors are not very sensitive to the change of  $R/t$ , especially when  $R/t$  reaches a certain higher value. The beta factors under bending do not change much for  $R/t > 3$ . For a case with the specific values of  $a/c$  and  $a/t$ , the questionable beta factors (missing betas or incorrect betas) are reconstructed using the betas at the adjacent valid  $R/t$  values as shown in Figure 3.10.2.

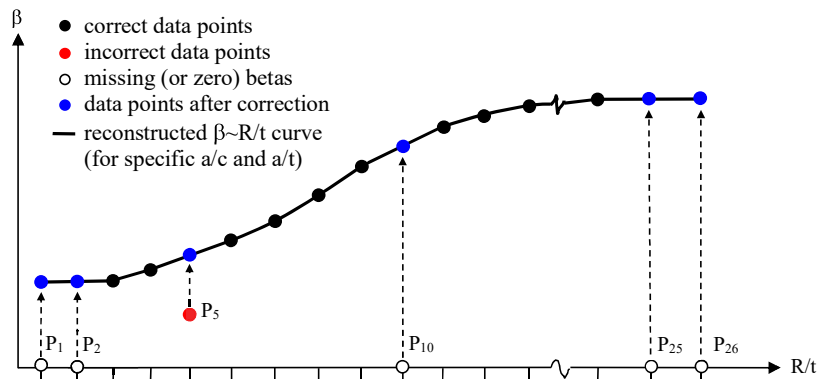


Figure 3.10.2: Schematic diagram for reconstructing the F-A database for a specific crack profile

- If a questionable beta is at the end, such as  $P_1$ ,  $P_2$ ,  $P_{25}$  or  $P_{26}$ , it is assigned to the valid beta at the boundary.
- If a questionable beta is in the middle, like  $P_5$  or  $P_{10}$ , it is replaced by the beta value obtained by linear interpolation from the beta values at its adjacent points.

There are  $25 \times 11 \beta \sim R/t$  curves for each crack tip under each load condition (tension, bending, or pin load). Each of the  $\beta \sim R/t$  curves is reconstructed that way.

The database of beta factors are extended down from  $a/t = 0.1$  to  $a/t = 0$ , with the betas at  $a/t = 0$  determined by the  $K_t$ -based method proposed by Yi-Der Lee,

$$\beta = F_{Kt} \cdot \frac{F_{ca}}{E_k} \quad (3.10.1)$$

where  $F_{Kt} = 1.122K_t$  for tension ( $S_0$ ) and bending ( $S_1$ ), and  $F_{Kt} = 0.98175$  for pin load ( $S_3$ ).  $K_t$  is

the stress concentration factor at the corner of the vanishing crack.  $F_{ca} = c/a$  for  $a$ -tip and  $F_{ca} = 1$  for  $c$ -tip.  $E_k$  is a function of crack aspect ratio,

$$E_k = \begin{cases} \sqrt{1 + 1.464 \left(\frac{c}{a}\right)^{1.65}} & \text{if } \frac{c}{a} \leq 1 \\ \frac{c}{a} \sqrt{1 + 1.464 \left(\frac{a}{c}\right)^{1.65}} & \text{if } \frac{c}{a} > 1 \end{cases} \quad (3.10.2)$$

In summary, the questionable beta factors in the original F-A database have been corrected and the solution has been extended down from  $a/t=0.1$  to  $a/t=0$ . Note that the reconstructed F-A solution is for infinite plate only.

### 3.10.5.2 Calculation of stress intensity factors for single corner crack

The total stress intensity factor for a given crack size “ $a$ ” and crack aspect ratio “ $a/c$ ” in a finite plate is calculated by

$$K = \sum_i F_i S_i \sqrt{\pi a} = \sum_i (\beta_i F_{H,i}) S_i \sqrt{\pi a} = \sum_i (\beta_i F_{W,i} F_{off,i}) S_i \sqrt{\pi a} \quad (3.10.3)$$

where  $i$  is the stress quantity index ( $i = 0$  for tension, 1 for bending, and 3 for pin load).  $\beta_i$  is the primary beta factor, i.e., the beta factor of the corresponding infinite plate.  $F_{H,i}$  is the general finite width correction factor. It equals the product of the finite width correction factor ( $F_{W,i}$ ) and the hole offset correction factor ( $F_{off,i}$ ), i.e.,  $F_{H,i} = F_{W,i} \cdot F_{off,i}$ .

#### Calculation of the primary geometry factor ( $\beta_i$ )

The primary geometry factor ( $\beta_i$ ) during crack propagation is obtained by interpolating off the reconstructed F-A database. Since the beta factors in the database are given on a pretty dense grid, linear interpolation is employed.

For a specific problem, the  $R/t$  value is fixed. So the first step is to construct the beta tables as a function of  $a/c$  and  $a/t$  for the specific  $R/t$  value before crack propagation analysis. For each  $a/c$  and  $a/t$  in the F-A database, the beta factor under the specific  $R/t$  is obtained by linear interpolation.

During crack propagation,  $a/c$  and  $a/t$  are changing. If  $a/t \geq 0.1$ , the stress intensity factor for the given  $a/c$  and  $a/t$  values is obtained by 2-D linear interpolation based on the beta tables constructed for the specific  $R/t$  value in the above step. If  $a/t < 0.1$ , Hermite interpolation is employed.

#### Finite width correction factor ( $F_{i,W}$ ) for tension and bending

The Newman finite width correction factor [55] for a corner crack at a central hole in the plate of width  $2B$  is defined as

$$F_W = \sqrt{\sec\left(\frac{\pi R}{2B}\right) \sec\left[\frac{(2R+nc)\pi}{4(B-c)+2nc} \sqrt{\frac{a}{t}}\right]} \quad (3.10.4)$$

where  $R(=D/2)$  is the radius of the hole.  $n$  is the number of cracks ( $n=1$  for single corner crack and  $n=2$  for two cracks). Note that the same finite width correction equation is used for both  $c$ - and  $a$ -tip.

Evaluation [54] on the Newman finite width correction by comparing it with the CC08 solution reveals that:

The original Newman finite width correction equation works well at *c*-tip for  $(R + c)/B$  up to 0.9, but it does a poor job at *a*-tip. It does not work well for narrow plates (with small  $B/R$  values) either.

The following equations are then developed by Guo [54] for remote tension based on the original Newman finite width correction equation:

$$\bar{F}_W(\text{a-tip}) = G_1 G_2 F_W = G_1 G_2 \sqrt{\sec\left(\frac{\pi R}{2B}\right) \sec\left[\frac{(2R + nc)\pi}{4(B - c) + 2nc} \sqrt{\frac{a}{t}}\right]} \quad (3.10.5)$$

$$\bar{F}_W(\text{c-tip}) = G_1 F_W = G_1 \sqrt{\sec\left(\frac{\pi R}{2B}\right) \sec\left[\frac{(2R + nc)\pi}{4(B - c) + 2nc} \sqrt{\frac{a}{t}}\right]} \quad (3.10.6)$$

where  $G_1$  is used to fine-tune the correction for narrow plates, and  $G_2$  is used to characterize the different effects at *a*-tip.

$$G_1 = 1 + \left(\frac{R}{B}\right)^{n_1} \left[ \left(1 - \frac{a}{t}\right) \frac{R}{R + c} \right]^{n_2} \quad (3.10.7)$$

$$G_2 = \frac{1 + \left(\frac{R}{B}\right)^{n_3}}{1 + \left(\frac{a}{t}\right)^{n_4} \left(\frac{R + c}{B}\right)^{n_5}} \quad (3.10.8)$$

The exponents  $n_1 \sim n_5$  are obtained by calibrating the solution with the results obtained from CC08 and FEA.

### Hole offset correction factor ( $F_{i,off}$ ) for tension and bending

NASGRO borrows the hole offset correction equations from AFGROW [6].

- If  $B < W/2$  :

$$F_{off} = \frac{\sin\left(\sqrt{\frac{a}{t}} \cdot \frac{D+c}{B-c/2} \cdot \frac{W-2B}{W}\right)}{\sqrt{\frac{a}{t}} \cdot \frac{D+c}{B-c/2} \cdot \frac{W-2B}{W}} F_C \quad (3.10.9)$$

where  $F_C = \min\{1 - (0.45F_G - 0.021)[c/(B - D/2)]^{16}, 1.0\}$  and  $F_G = \min\{\frac{2B}{W} + \frac{D}{2B}, 0.7\}$ .

The above equation is valid for  $(D + c)/(2B - c) \leq 0.7$ , i.e.,  $(R + c)/B \leq 0.824 - 0.176R/B$ .

Evaluation [54] on the AFGROW hole offset correction equation for  $B < W/2$  [Eq. (3.10.9)] by comparing it with CC08 solution reveals that:

- The hole offset effect becomes significant only if the hole is very close to the edge in a wide plate, like  $B/R < 2 \sim 2.5$  and  $W/B > 5 \sim 10$ .
- The agreement between the AFGROW hole offset correction and the CC08 results is not bad within the solution limits of CC08, especially at *c*-tip. The errors are usually less than 5% at *c*-tip and 10% at *a*-tip.
- If  $B = W/2$ ,  $F_{off} = 1$ .
- If  $B > W/2$ , the following hole offset correction equation is used in AFGROW:

$$F_{off} = F_A \cdot F_B \quad (3.10.10)$$

where

$$F_A = 1 + \frac{\sqrt{\sec\left[\frac{\pi D}{4B}\left(\frac{4}{7} \cdot \frac{B}{W-B} + \frac{3}{7}\right)\right]} - 1}{1 + 0.21 \sin\{8 \arctan[(2B/W - 1)^{0.9}]\}}$$

and

$$\begin{aligned} F_B &= 1 + F_c \sin(\pi \tanh[2\delta^{1.1} + (1.18\delta)^7]) \\ F_c &= \frac{0.5}{\exp(10\gamma + 4.2\gamma^2 + (3\gamma)^{14})} \quad \text{and} \quad \gamma = 1 - B/W \\ \delta &= \frac{D+c}{2B-c} \sqrt{\frac{a}{t}} \end{aligned}$$

The above AFGROW hole offset correction equation for  $B > W/2$  gives  $F_{off} = \sqrt{\sec \frac{\pi D}{4B}}$  when  $B \rightarrow W/2$  (a central hole), which does not make sense. In order to have  $F_{off}=1$  for a central hole, the following corrected equation is employed in NASGRO:

$$\bar{F}_{off} = F_A \cdot F_B \cdot \sqrt{\cos\left(\frac{\pi D}{4B}\right)} \quad (3.10.11)$$

NASGRO team did not perform further evaluation on the AFGROW hole offset correction equation for  $B > W/2$ , i.e., Eq. (3.10.11).

Note that the same general finite width correction factor ( $F_{H,i}$ ) is used for remote tension and out-of-plane bending.

### Correction factors for pin loading

When crack case CC16 was first implemented in NASGRO (starting with v7.1), a new finite width correction factor was derived for remote tension loading, and this same factor was also used for pin loading. Work to develop new (future) pin loading capabilities for weight function crack case CC08 (first implemented in v8.1) demonstrated that the CC16 finite width correction factors for tension loading could be non-conservative when used for pin loading. Therefore, an improved CC16 finite width correction factor for pin loading was developed from the enhanced CC08 solution. This pin-loaded correction factor was first implemented in v8.0 (beginning with the production release) and was also backported to the bug-fix release v7.12.

Further study of this revised solution indicated that, while accurate for narrow plates with centered holes, these values could be over-conservative for narrow plates with holes highly offset from the centerline. Therefore, a second CC16 revision focusing on the hole-offset correction factor was developed, verified, and implemented in v8.1a. Once again, the revised CC16 solution only changed K-values under pin-loading – solutions for tension and out-of-plane bending have been unaffected. These solutions were applied to CC17 starting in 8.01 and 8.1f.

Even further study revealed non-physical oscillations – “peaks” and “troughs” – in the solution introduced by the interpolation process. These “peaks” and “troughs” only influenced relatively small cracks ( $a/t \leq 0.2$ ) at small holes ( $D/\min(2B, 2 \times (W-B)) \leq 0.5$ ). These “peaks” and “troughs” were visible in the stress intensity factors computed with increasing crack depth ( $a/t$ ). These oscillations were due to the interpolation scheme. In these routines, the pin-loaded correction factor interpolated over the non-dimensional crack length  $c/(B^* - D/2)$ , where  $B^* = \min(B, W - B)$ . Varying

this parameter has the unintentional consequence of simultaneously varying the relative hole size,  $D/2B^*$ , which largely controls the geometry correction factor for pin-loaded holes. Consequently, the interpolation process sampled from various ratios of  $D/2B^*$  as crack growth progressed and lead to the observed “peaks” and “troughs”.

Several attempts were made to eliminate the non-physical oscillations in the solution. Adding more points to the solution matrix shifted the oscillations to other parts of the solution space, even if the solution matrix tripled in size. Changing the solution space in only the small crack regime ( $a/t \leq 0.2$ ) introduced a discontinuity at the boundary,  $a/t = 0.2$ . This discontinuity was triggered by differences in the interpolation schemes.

NASGRO 8.2f takes the radical step of changing the entire parameterization for pin-loaded CC16 to eliminate the non-physical oscillations. This approach eliminates the non-physical oscillations and improves the solution quantity. It does not introduce any discontinuities into the solution. The new parameterization scheme interpolates over the relative hole size rather than over the relative crack depth. Consequently, stress intensity factors in NASGRO 8.2f will differ from stress intensity factors in earlier versions of NASGRO. These changes only affect cracks under pin-loading. Again, it is unclear exactly how these changes will impact fatigue crack growth lives overall, but the differences may effectively cancel out in some cases.

Preliminary investigations with these new pin-loaded geometry correction factors have revealed lower lives for: (1) cracks on the long ligament side of highly offset holes as  $0.5 \times D/(W - B) > 0.5$  and (2) cracks in thick plates where  $D/2t \rightarrow 0.1$ . In this second case, additional studies suggest that both the old and new geometry correction factors are systematically conservative.

In the new parameterization, NASGRO defines the plate by the non-dimensional parameters  $D/2B^*$ ,  $D/2t$ , and  $1 - 2B^*/W$ . (This last parameter is symmetric for cracks on the short and large ligaments.) The crack can be defined by two of the following three parameters: crack depth ( $a/t$ ), crack shape ( $a/c$ ), and crack length ( $c/(B^* - D/2)$ ). NASGRO uses the  $a/t$  and  $a/c$ . In CC16, allowable combinations of  $a/t$  and  $a/c$  lead to non-physical cracks, i.e., cracks that are longer than the plate. For example, a deep crack ( $a/t = 0.95$ ) breaks through most plates if the crack has a very low aspect ratio ( $a/c = 0.1$ ). The solution matrix must accommodate this case, even though it is rare in practice. The crack length can be confined to the plate by restricting  $a/t$  and  $a/c$ . Specifically, if  $0 \leq c/(B^* - D/2) \leq 0.9$ , then:

$$\begin{aligned} \left(\frac{a}{c}\right)_{lower} &= \max\left(0.1, \frac{10}{9} \times \frac{a}{t} \times \frac{2t}{D} \times \left(\frac{\frac{D}{2B^*}}{1 - \frac{D}{2B^*}}\right)\right) \leq \frac{a}{c} \leq 10 = \left(\frac{a}{c}\right)_{upper} \\ \left(\frac{a}{t}\right)_{lower} &= 0 \leq \frac{a}{t} \leq \max\left(0.95, 9 \times \frac{D}{2t} \times \left(\frac{1 - \frac{D}{2B^*}}{\frac{D}{2B^*}}\right)\right) = \left(\frac{a}{t}\right)_{upper} \end{aligned}$$

These limits only come into effect in certain geometries – usually, the crack is confined by the more restrictive limits of CC08 that have been bolded in the previous equations. The new routines sample and interpolate over the non-dimensional parameters  $P_{a/t}$  and  $P_{a/c}$  defined over the available range. That is,  $P_{a/t} \in [0, 1]$  and  $P_{a/c} \in [0.1, 10]$ . For a given geometry, we map  $a/t$  to  $P_{a/t}$  by first determining the upper bound and then dividing  $a/t$  by it. That is,  $P_{a/t} = (a/t)/(a/t)_{upper}$ . We apply a similar mapping between  $a/c$  and  $P_{a/c}$ .

The improved geometry correction factors for pin-loaded holes employ a look-up table of the appropriate correction factor based on CC08 and have discrete values for the following non-dimensional

geometric ratios:

$$\begin{aligned} \frac{D}{2B^*} &= 0.01, 0.05, 0.1, 0.2, 0.3, 0.4, 0.5, 0.6, 0.7, 0.8, 0.9 \\ \log_{10} \left( \frac{D}{2t} \right) &= -1, -0.6, -0.3, 0, +0.3, +0.6, +1 \\ \log_{10}(P_{a/t}) &= -2, -1.6, -1.3, -1., -0.4, -0.1, 0 \\ \log_{10}(P_{a/c}) &= -1, -0.6, -0.3, 0, +0.3, +0.6, +1 \\ 1 - (2B^*)/W &= 0, 0.5, 0.7, 0.8 \end{aligned}$$

The final parameter defines the offset of the hole in the plate. NASGRO distinguishes between the cracks on the short and long ligament of the plate. The total solution matrix contains 52,822 entries. Interpolation with cubic Hermite splines provides correction factors for non-dimensional ratios between known ratios in the look-up table (e.g.,  $D/2B^* = 0.15$  which is between  $D/2B^* = 0.1$  and  $D/2B^* = 0.2$ ). The ratios  $D/2t$ ,  $P_{(a/c)}$ , and  $P_{(a/t)}$  are interpolated over log-10 space to minimize oscillations, whereas the other ratios are interpolated in real space. When the input non-dimensional ratio is outside of these limits (e.g.,  $a/t = 0.99$ ), the resulting correction factor is set equal to the value at the closest non-dimensional ratio found in the solution matrix (e.g.,  $a/t = 0.95$ ). NASGRO 8.2 now outputs a warning message when the crack tip exceeds the bounds of  $a/t > 0.95$  and  $c/(B^* - 0.5D)$ . The geometry correction factor extrapolates for parametric crack depths  $P_{a/c} < 0.01$ .

The geometry correction factor (for a given set of non-dimensional ratios in this table) equals the ratio of  $K_I^{ND}/K_I^{D=0.01W}$ , where both values of  $K_I$  have been computed using the CC08 weight function solution and the appropriate stress variation along the crack plane. Here,  $K_I^{ND}$  reflects  $K_I$  for the input non-dimensional ratios, and  $K_I^{D=0.01W}$  represents  $K_I$  with the same geometric dimensions as  $K_I^{ND}$  but with a plate width equal to 100 times the hole diameter.

### 3.10.5.3 Calculation of stress intensity factors for two symmetric corner crack

The stress intensity factors of two symmetric corner cracks at a central hole are obtained from the stress intensity factors of the corresponding single corner crack solution and the Shah correction factor ( $F_{Shah}$ ), i.e.,

$$K_{2\text{cracks}} = \frac{K_{1\text{crack}}}{F_{Shah}} \cdot \frac{\bar{F}_W(n=2)}{\bar{F}_W(n=1)} \quad (3.10.12)$$

where  $\bar{F}_W(n=1)$  and  $\bar{F}_W(n=2)$  are the finite width correction factors of one corner crack and two corner cracks (see Equations (3.10.5) and (3.10.6)), respectively.  $F_{Shah}$  is the Shah correction factor [38],

$$F_{Shah} = \sqrt{\frac{D + \frac{\pi ac}{4t}}{D + \frac{\pi ac}{2t}}} \quad (3.10.13)$$

### 3.10.5.4 Solution Limits

The solution limits are controlled by the domain of the reconstructed F-A database and the valid ranges of the finite width correction and the hole offset correction equations.

- Domain of the reconstructed F-A database (the fundamental beta factors):

$$0.1 \leq R/t \leq 10, \quad 0.1 \leq a/c \leq 10, \quad 0 \leq a/t \leq 0.99$$

- Valid range of the improved finite width correction:

$$B/D \geq 1, \quad 0.1 \leq R/t \leq 10, \quad 0.1 \leq a/c \leq 10, \quad (R+c)/B \leq 0.9$$

- Valid range of the AFGROW hole offset correction:

If  $B < W/2$ :  $(D+c)/(2B-c) \leq 0.7$ , i.e  $(R+c)/B \leq 0.824 - 0.176R/B$

If  $B = W/2$ : no need to perform hole offset correction

If  $B > W/2$ : no valid range is mentioned in AFGROW user's manual

Combining the above three conditions leads to the solutions limits given under the Geometry section of this crack case (Section 3.10.2).

### 3.10.6 Verification

#### 3.10.6.1 Verification of the finite width correction factors for tension and bending

The improved finite width correction factors (Equations (3.10.5) and (3.10.6)) have been verified extensively with 198 cases, where 160 cases are within the geometry limits of CC08, and 38 cases are outside the limits. The benchmark results of finite width correction factors for the 160 cases are obtained from CC08 while the benchmark results for the 38 cases outside the geometry limits of CC08 are obtained from the p-version FEA software StressCheck. The improved finite width correction equations, along with the original Newman equation, are compared with the benchmark results in Figure 3.10.3.

The top one in Figure 3.10.3 shows that the original Newman equation and the improved equation give almost identical results at  $c$ -tip except for the narrow plates with small  $W/D$  values, where the modified equation gives better results. For  $a$ -tip, most of the results given by the modified equation have errors less than 5%. A few data have errors larger than 5% but less than 10%. However, the original Newman equation gives results with much bigger errors, which can be either on the over-conservative or non-conservative side.

As shown in Figure 3.10.3, the improved finite width correction equations are verified valid within the following ranges:

$$W/D \geq 2, \quad 0.1 \leq R/t \leq 10, \quad 0.1 \leq a/c \leq 10, \quad (R+c)/B \leq 0.9$$

#### 3.10.6.2 Verification of the correction factors for pin-loading

The pin-loaded correction factor was verified against independent correction factors. The verification matrix sampled 2500 geometries (combinations of  $D/2t$ ,  $a/c$ , etc...) over the full parametric space using Latin Hypercube Sampling with reduced correlation. These geometries are separate from the geometries that define the solution matrix except by accident. For all geometries, a new correction factor was computed using CC08 and the geometry correction factor was predicted using the new routines. Figure 3.10.4 shows the rank ordering (i.e., the cumulative distribution function) of the results. The horizontal axis shows the ratio of the predicted geometry correction factor vs. independent correction factor. Ratios of one imply that the prediction exactly matches the

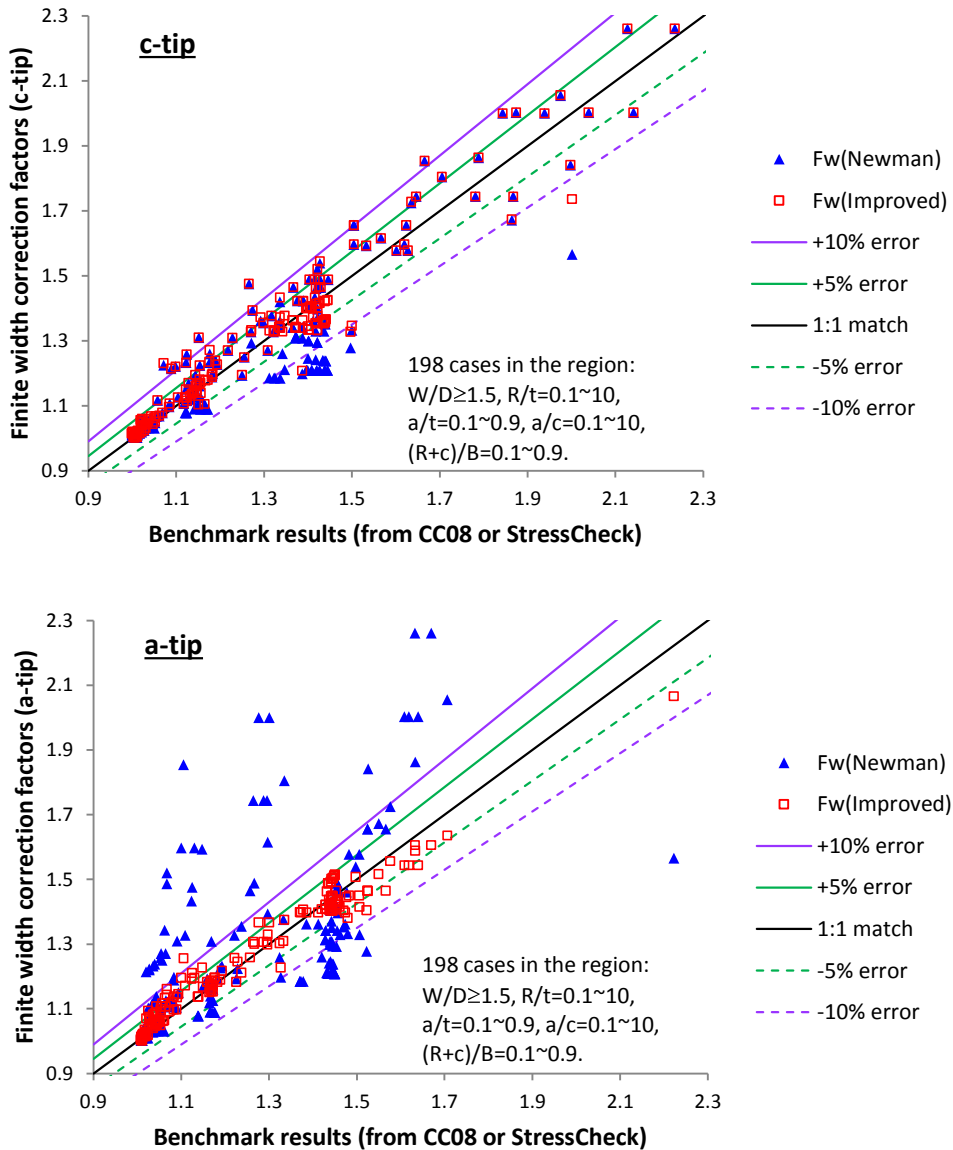


Figure 3.10.3: Verification of the modified finite width correction equations under remote tension

independent correction factor; ratios above one imply that the predictions are conservative; and ratios below one imply non-conservatism vs. CC08. For a given ratio, the vertical axis provides the percentage of solutions lower than that ratio. The results in this figure suggest good agreement between geometry correction factors computed directly using CC08 and the new parametric factor routines. The *a*-tip and *c*-tip both have a median value near unity. There is more scatter in the *c*-tip solution than in the *a*-tip solution.

The new solution was also examined for oscillations over the parameter space – that is, the “peaks” and “troughs” in the previous correction factor. To do this, the solution was plotted as it varied with each variable over the solution range – e.g.,  $a/t$  as it varied from  $\sim 0.001$  to its maximum value while  $D/2B^*$ ,  $D/2t$ ,  $1 - 2B^*/W$ , and  $a/c$  were held constant. These plots were prepared for all 2500 geometries from the LHS described earlier. These plots do not show the earlier non-physical

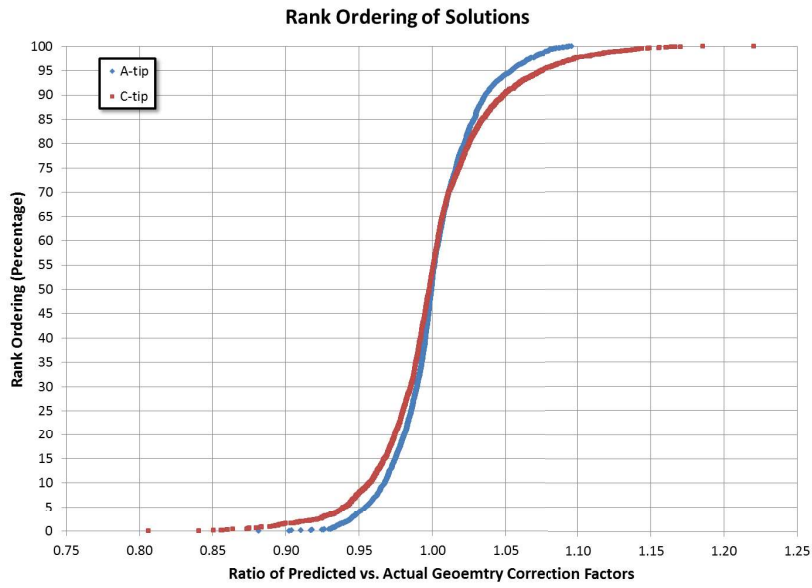


Figure 3.10.4: Verification of geometry correction factors for pin-loaded holes against CC08.

oscillations in the  $a$ -tip solutions with respect to  $a/t$ . There is a limited set of geometries where the  $c$ -tip solution show some non-physical curvature with respect to  $a/t$ . These oscillations are confined to thin plates ( $D/2t \rightarrow 10$ ) and to cracks with low aspect ratios ( $a/c \rightarrow 0.1$ ). This configuration is likely not stable – cracks should grow into a more stable shape where the interpolation is better behaved.

The pin-loaded correction factors were independently verified by comparing them with 162 stress intensity factor solutions calculated using finite element methods (Abaqus) for models containing cracks at pin-loaded holes. Comparisons of the FE verification results against the new CC16 correction factors for pin-loaded holes are shown in Figure 3.10.5. This comparison provides verification for both the new CC16 factor as well as the underlying CC08 model. In general, the geometry correction factor in NASGRO 8.2 is very similar to the geometry correction factor in NASGRO 8.1.

References: [6, 38, 53, 54, 55]

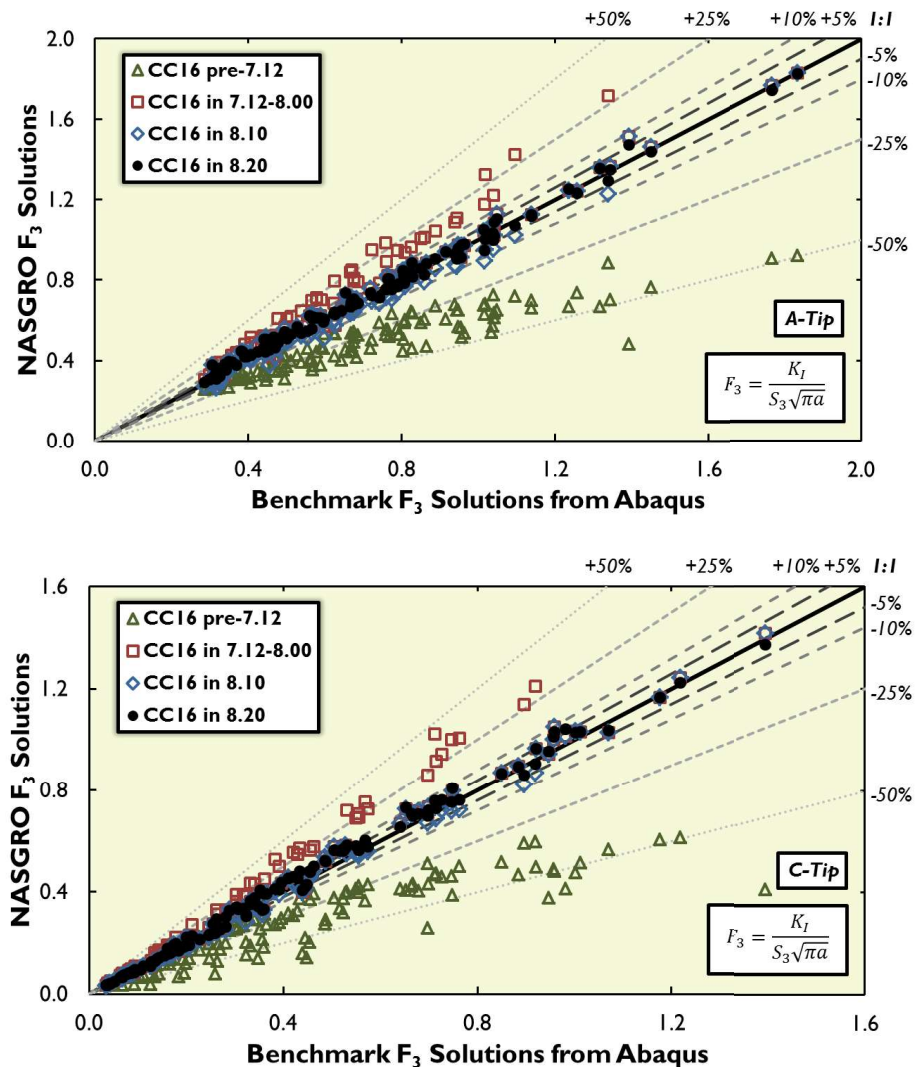


Figure 3.10.5: Verification of finite width correction factors for pin-loaded holes. Points shown in these figures have holes centered in the plate (i.e., no offset correction factors).

### 3.11 CC17 – Two Unequal Corner Cracks at a Hole in a Finite Plate

#### 3.11.1 Overview

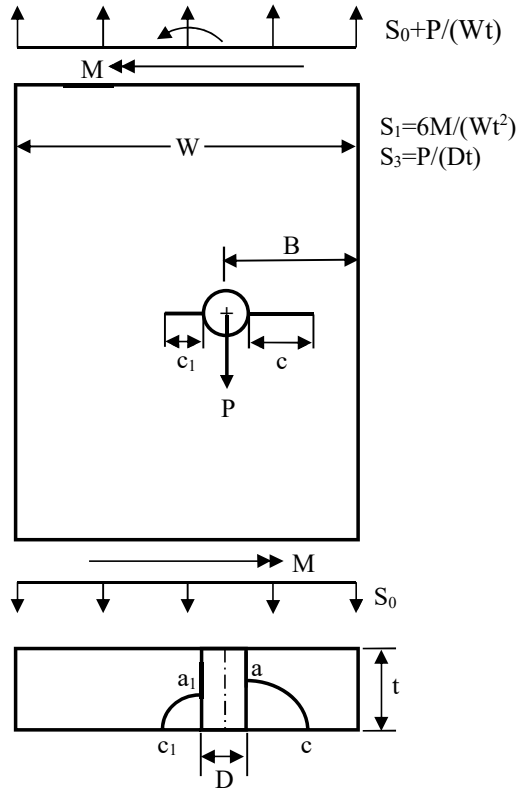


Figure 3.11.1: Configuration of crack case CC17

CC17 is a solution of two unequal corner cracks at a hole in a finite plate subjected to remote tension ( $S_0$ ), out-of-plane bending ( $S_1$ ) and pin load ( $S_3$ ), as shown in Figure 3.11.1. The solution is based on:

- the reconstructed Fawaz-Andersson (F-A) database of stress intensity factors for two unequal corner cracks at a hole in an infinite plate [8], and
- the equivalent hole method (EHM) for finite width correction [56].

#### 3.11.2 Geometry

The key input geometric parameters of CC17 are  $t$ ,  $W$ ,  $D$ ,  $B$ ,  $a$ ,  $a/c$ ,  $a_1$  and  $a_1/c_1$ .

- $t$ : Plate thickness;
- $W$ : Plate width;
- $D$ : Hole diameter;
- $B$ : Distance between the hole center and the right edge of the plate;
- $a$ : Crack size in thickness direction of the corner crack in the “ $B$ ” region;
- $a/c$ : Crack aspect ratio of the corner crack in the “ $B$ ” region.
- $a_1$ : Crack size in thickness direction of the other corner crack;

- $a_1/c_1$ : Crack aspect ratio of the other corner crack.

Solution limits of CC17:

$$\begin{aligned} B/R &\geq 2, \\ (W - B)/R &\geq 2, \\ 0.25 \leq D/t &\leq 20, \\ 0.2 \leq a/c &\leq 5, \\ 0.2 \leq a_1/c_1 &\leq 5, \\ 0 \leq a/t &\leq 0.95, \\ 0 \leq a_1/t &\leq 0.95, \\ \frac{D+c}{2B-c} &\leq 0.7, \\ \frac{D+c_1}{2(W-B)-c_1} &\leq 0.7 \end{aligned}$$

### 3.11.3 Loading

Crack case CC17 supports remote tension ( $S_0$ ), out-of-plane bending ( $S_1$ ), and pin load ( $S_3$ ).

### 3.11.4 Development History

This SIF model was implemented in NASGRO v7.1.

### 3.11.5 Theory

#### 3.11.5.1 The beta factors for an infinite plate

##### The original Fawaz-Andersson (F-A) database of beta factors

The beta factors in the original F-A database are given on a grid of  $25 \times 11 \times 25 \times 11 \times 26$ , i.e., 25  $a/c$  values, 11  $a/t$  values, 25  $a_1/c_1$  values, 11  $a_1/t$  values and 26  $R/t$  values.

- The 25  $a/c$  values : 0.1, 0.111, 0.125, 0.1428, 0.1667, 0.2, 0.25, 0.333, 0.5, 0.667  
0.75, 0.8, 1.0, 1.25, 1.333, 1.5, 2, 3, 4, 5, 6, 7, 8, 9, 10
- The 11  $a/t$  values : 0.1, 0.2, 0.3, 0.4, 0.5, 0.6, 0.7, 0.8, 0.9, 0.95, 0.99
- The 25  $a_1/c_1$  values : 0.1, 0.111, 0.125, 0.1428, 0.1667, 0.2, 0.25, 0.333, 0.5, 0.667  
0.75, 0.8, 1.0, 1.25, 1.333, 1.5, 2, 3, 4, 5, 6, 7, 8, 9, 10
- The 11  $a_1/t$  values : 0.1, 0.2, 0.3, 0.4, 0.5, 0.6, 0.7, 0.8, 0.9, 0.95, 0.99
- The 26  $R/t$  values : 0.1, 0.1111, 0.125, 0.1428, 0.1666, 0.2, 0.25, 0.333, 0.5, 0.6666,  
0.75, 0.8, 1.0, 1.25, 1.333, 1.5, 1.6666, 2, 3, 4, 5, 6, 7, 8, 9, 10

Domain of the original database is:  $a/c \in [0.1, 10]$ ,  $a/t \in [0.1, 0.99]$ ,  $a_1/c_1 \in [0.1, 10]$ ,  $a_1/t \in [0.1, 0.99]$  and  $R/t \in [0.1, 10]$ . The database contains  $(25 \times 11 \times 25 \times 11 \times 26) \times 4 \times 3 = 23,595,000$  beta factors. The total size of the database files is about 330MB.

The following problems have been found in the original F-A database:

*Erroneous betas:*

- Database for tension:  
No erroneous betas detected.

- Database for bending:  
The betas for  $R/t = 4, 5, 6, 7$  and  $10$  are incorrect – the betas at  $c$ - and  $c_1$ -tip are negative.
- Database for bearing:  
The betas for  $R/t=8$  and  $9$  are incorrect. They are much smaller than the betas at  $R/t=7$  and  $10$ . Many crack profiles have small negative betas at small  $R/t$  values ( $0.1 \sim 0.5$ ).

*Missing (or zero) betas:*

There are 568866 (about 2.4%) missing (or zero) betas in the database. The crack profiles with a very big crack on one side and a very small crack on the other side tend to have fewer valid betas as  $R/t$  changes. A crack profile refers to a specific combination of crack sizes ( $a/c$ ,  $a/t$ ,  $a_1/c_1$ ,  $a_1/t$ ).

### Reconstructing the F-A database

In order to correct the erroneous betas or missing (or zero) betas, we re-generate the  $\beta \sim R/t$  curve for each of the crack profiles ( $a/c$ ,  $a/t$ ,  $a_1/c_1$ , and  $a_1/t$ ). If an erroneous or missing beta is in the middle, it is replaced by the value obtained by linear interpolation for  $R/t$ . If it is at the end, it is set to the adjacent valid beta. The quality of the reconstructed  $\beta \sim R/t$  curve for a specific crack profile depends on the number of valid betas and the end  $R/t$  values with valid betas. Because some crack profiles in the original database have no valid betas at all, we have to reduce the original domain when we reconstruct a valid database. Based on the availability of the valid beta factors in the original F-A database and the needs of engineering application, NASGRO team decided to reconstruct the database in the domain:  $a/c \in [0.2, 5]$ ,  $a/t \in [0.1, 0.95]$ ,  $a_1/c_1 \in [0.2, 5]$ ,  $a_1/t \in [0.1, 0.95]$  and  $R/t \in [0.125, 10]$ . NASGRO team also extended the lower limit of  $a/t$  and  $a_1/t$  from 0.1 to 0. The beta factors at  $a/t = 0$  or  $a_1/t = 0$  are determined by the  $K_t$ -based method proposed by Yi-Der Lee.

$$\beta = \frac{F_{Kt}}{E_k} \cdot F_{ca} \quad (3.11.1)$$

where  $F_{ca}$  and  $E_k$  are two functions of the crack aspect ratio of the vanishing crack.  $F_{Kt}$  is related to the stress concentration factor ( $K_t$ ) at the corner of the vanishing crack. Suppose that the crack on the right (with crack sizes  $a$  and  $c$ ) is the vanishing crack, as shown in Figure 3.11.2.  $F_{ca} = c/a$  for  $a$ -tip, and  $F_{ca} = 1$  for  $c$ -tip.

$$E_k = \begin{cases} \sqrt{1 + 1.464 \left(\frac{c}{a}\right)^{1.65}} & \text{if } \frac{c}{a} \leq 1 \\ \frac{c}{a} \sqrt{1 + 1.464 \left(\frac{a}{c}\right)^{1.65}} & \text{if } \frac{c}{a} > 1 \end{cases} \quad (3.11.2)$$

$F_{Kt} = 1.122K_t$  for  $S_0$  and  $S_1$ , and  $F_{Kt} = 0.98175$  for  $S_3$ .  $K_t$  is the stress concentration factor at the corner of the vanishing crack, calculated by the following formula proposed by Shivakumar,

$$K_t = 1 + 2\sqrt{1 + \frac{\pi}{4} \cdot \frac{c_1}{2R} \cdot \frac{a_1}{t}} \quad (3.11.3)$$

where  $a_1$  and  $c_1$  are the crack sizes of the corner crack on the opposite side of the vanishing crack. Equation (3.11.3) agrees reasonably well with the FEA results. Here are two examples (with  $a \rightarrow 0$  and  $c \rightarrow 0$ ):

$$\begin{aligned} R/t = 0.25, \quad a_1/t = 0.65, \quad a_1/c_1 = 1.0 : \quad K_t &= 3.58 \text{ by Eq. (3.11.3);} \quad K_t = 3.27 \text{ by FEA (StressCheck)} \\ R/t = 0.125, \quad a_1/t = 0.65, \quad a_1/c_1 = 0.2 : \quad K_t &= 6.53 \text{ by Eq. (3.11.3);} \quad K_t = 6.16 \text{ by FEA (StressCheck)} \end{aligned}$$

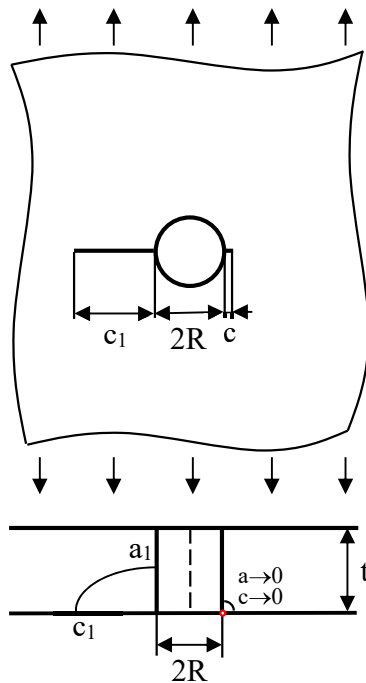


Figure 3.11.2: Two unequal corner cracks with a vanishing crack at a hole in an infinite plate

After extending the lower limit of crack sizes ( $a/t$  and  $a_1/t$ ) to 0, the domain of the new database is thus:  $a/c \in [0.2, 5]$ ,  $a/t \in [0, 0.95]$ ,  $a_1/c_1 \in [0.2, 5]$ ,  $a_1/t \in [0, 0.95]$ , and  $R/t \in [0.125, 10]$ . The new domain contains:

- The 15  $a/c$  values : 0.2, 0.25, 0.333, 0.5, 0.667, 0.75, 0.8, 1.0, 1.25, 1.333, 1.5, 2, 3, 4, 5
- The 11  $a/t$  values : 0.0, 0.1, 0.2, 0.3, 0.4, 0.5, 0.6, 0.7, 0.8, 0.9, 0.95
- The 15  $a_1/c_1$  values : 0.2, 0.25, 0.333, 0.5, 0.667, 0.75, 0.8, 1.0, 1.25, 1.333, 1.5, 2, 3, 4, 5
- The 11  $a_1/t$  values : 0.0, 0.1, 0.2, 0.3, 0.4, 0.5, 0.6, 0.7, 0.8, 0.9, 0.95
- The 24  $R/t$  values : 0.125, 0.1428, 0.1666, 0.2, 0.25, 0.3333, 0.5, 0.6666, 0.75, 0.8, 1, 1.25, 1.3333, 1.5, 1.6666, 2, 3, 4, 5, 6, 7, 8, 9, 10.

The beta factors of the reconstructed database are stored in three binary files for tension, bending and pin load. The total size of the three files is about 15MB, which is much smaller than the size of the original database (330MB) and makes the implementation possible. The following factors contribute to reduction of the database size:

- The original database contains some data we do not need. Each of the data files of the original database contains 16 columns, but only 4 columns are needed.
- The new database has smaller domain. The beta factors in the reconstructed database are given on a grid of  $15 \times 11 \times 15 \times 11 \times 24$ , compared to the grid of  $25 \times 11 \times 25 \times 11 \times 26$  of the original database.
- The new database is stored in binary files.

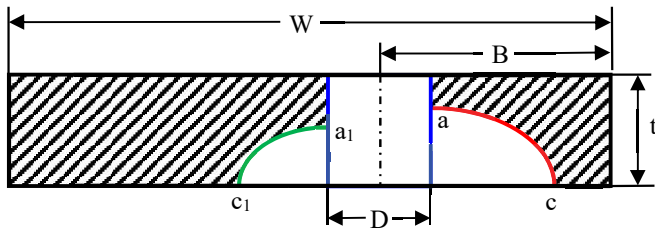
### 3.11.5.2 Calculation of stress intensity factors during crack propagation

The stress intensity factor at a specific crack tip in a finite plate during crack propagation is calculated by

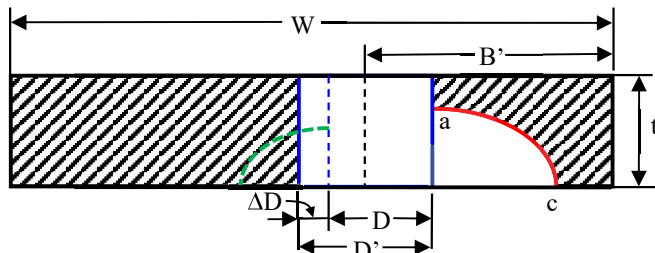
$$K = \sum_i F_{H,i} \cdot \beta_i S_i \sqrt{\pi x} \quad (3.11.4)$$

where  $i$  is stress component index ( $i = 0$  for tension, 1 for out-of-plane bending, and 3 for pin load).  $x$  is the crack size of the crack tip, i.e.,  $x = a$  for  $a$ -tip,  $x = c$  for  $c$ -tip,  $x = a_1$  for  $a_1$ -tip, and  $x = c_1$  for  $c_1$ -tip.

$\beta_i$  is the primary beta factor under stress  $S_i$ , i.e., the beta factor of the corresponding infinite plate. For a given  $R/t$  value, the beta tables are generated before crack growth analysis by interpolating off the beta factors for the  $R/t$  in the reconstructed database, where piece-wise linear interpolation is employed. During crack growth analysis, the beta factors ( $\beta_i$ ) for a given crack profile (i.e., a specific combination of  $a/c$ ,  $a/t$ ,  $a_1/c_1$  and  $a_1/t$ ) are calculated by interpolating off the beta tables for the given  $R/t$ , where four-dimensional piece-wise linear interpolation is employed.



(a) Two unequal corner cracks at an offset hole (the physical hole)  
– Right crack:  $a, c$ ; Left crack:  $a_1, c_1$   
– Geometry dimensions:  $t, W, B, D$



(b) Single corner crack with a bigger hole (the equivalent hole)  
– Right crack:  $a, c$ ; Left crack: converted into hole  
– Geometry dimensions:  $t, W, B', D'$   
where  $D' = D + \Delta D = D + 2\Delta R$ , and  $B' = B + \Delta R$

Figure 3.11.3: Schematic diagram showing the equivalent hole method (EHM) for determining the general finite width correction factors of two unequal corner cracks at an offset hole

$F_{H,i}$  is the general finite width correction factor at the crack tip under stress  $S_i$ . For tension and bending, it is determined by the equivalent hole method (EHM) developed by Guo [56]. The equivalent hole method, as shown in Figure 3.11.3, converts the opposite crack into additional hole, then uses the finite width and hole offset correction equations for a single corner crack to perform finite width correction for two unequal corner cracks. For example, if we want to determine the general finite width correction factors of the crack on the right (with crack sizes  $a$  and  $c$ ) in

Fig. 3.11.3a, we convert the crack on the left (with crack sizes  $a_1$  and  $c_1$ ) into additional hole. This way, the two-crack problem becomes a single corner crack problem with a bigger hole (i.e., the equivalent hole), as shown in Fig. 3.11.3b. The general finite width correction factors of the crack on the right is thus calculated by,

$$F_{H,i} = F'_{W,i} \cdot F'_{off,i} \quad (3.11.5)$$

where  $F'_{W,i}$  and  $F'_{off,i}$  are the finite width correction factor and hole offset correction factor of the corner crack with the equivalent hole, calculated by Eq. (3.10.5) ~ Eq. (3.10.9) for a single corner crack at a hole. The diameter of the equivalent hole is  $D'$  and the distance from the center of the equivalent hole to the plate edge is  $B'$ .  $D' = D + 2\Delta R$  and  $B' = B + \Delta R$ .  $\Delta R$  is the hole radius increment due to conversion of the opposite crack, which is calculated by the following formula derived by a semi-empirical approach,

$$\Delta R = \gamma \frac{\pi c_1}{8} \sqrt{\frac{a_1}{t}} \left( \frac{\chi^2}{\chi^2 + 0.25^2} \right)^n \quad \text{and} \quad \chi = \frac{c + R}{c_1 + R} \quad (3.11.6)$$

where the coefficient  $\gamma$  and exponent  $n$  are obtained by calibrating the FEA results of stress intensity factors.

Note that the same general finite width correction factors ( $F_{H,i}$ ) are used for both tension and bending.

It's claimed that CC17 has the following geometry limit for the corner crack in the "B" zone:

$$(D + c)/(2B - c) \leq 0.7 \quad (3.11.7)$$

The hole offset correction equation for the same corner crack at the equivalent hole is valid only if

$$(D' + c)/(2B' - c) \leq 0.7 \quad (3.11.8)$$

The above condition is inherited from the hole offset correction for a single corner crack. Examining Eq. (3.11.7) and Eq. (3.11.8), we found that the latter is more stringent and no hole offset correction is available in the range between  $(D' + c)/(2B' - c)$  and  $(D + c)/(2B - c)$ . An approximation is to use the hole offset correction factor of the physical hole to replace the hole offset correction factor for the equivalent hole. The general finite width correction factor for  $(D' + c)/(2B' - c) > 0.7$  and  $(D + c)/(2B - c) \leq 0.7$  is thus calculated by

$$F_{H,i} = F'_{W,i} \cdot F_{off,i} \quad (3.11.9)$$

where  $F_{off,i}$  is the hole offset correction factor of the physical hole.

The above same strategies are employed for calculation of  $F_{H,i}$  for the corner crack in the "W-B" zone.

The general finite width correction factor,  $F_{H,i}$ , in Eq. (3.11.4) for pin-loading differs from the tension/bend correction factor starting in version 8.1b. This version replaced the geometry correction factors for tension and bending with geometry correction factors for pin-loading that are identical to the correction factors in CC16. Consequently in all later versions of NASGRO (8.1b+), the pin-loaded solution for CC17 changes whenever the pin-loaded correction factors change in CC16, e.g., the changes in 8.2f documented in the earlier section.

Verification studies of CC17 indicated that for narrow plates, the finite width correction factors derived for tension and bend were usually non-conservative when applied to pin-loading. Instead,

CC17 now invokes the combined correction factors for a single corner crack at a pin-loaded hole. These correction factors were originally determined for CC16 (and discussed there) and have been reused in the CC17 routines. These factors correct for finite width and offset effects on the stress intensity factor solutions. Furthermore, the EHM that had been developed to improve the quality of the tension and bend solutions was found to consistently over-predict the benchmark solutions for pin loading. Therefore, the actual geometric dimensions (unmodified by the EHM) are instead used to evaluate the combined correction for pin loading.

The SIF geometry factors of CC17 in NASSIF are defined as:

$$F_i = \frac{K}{S_i \sqrt{\pi a}} \quad \text{at } a\text{-tip and } c\text{-tip} \quad (3.11.10)$$

$$F_i = \frac{K}{S_i \sqrt{\pi a_1}} \quad \text{at } a_1\text{-tip and } c_1\text{-tip} \quad (3.11.11)$$

where  $i = 0$  for remote tension, 1 for out-of-plane bending, and 3 for pin-load.

### 3.11.5.3 Geometry Limits

The geometry limits of CC17 are controlled by:

- The domain of the reconstructed F-A database, i.e.,

$$\begin{aligned} 0.25 &\leq D/t \leq 20 \\ 0.2 &\leq a/c \leq 5, \quad 0 \leq a/t \leq 0.95 \\ 0.2 &\leq a_1/c_1 \leq 5, \quad 0 \leq a_1/t \leq 0.95 \end{aligned}$$

- The geometry limits of the finite width and hole offset correction equations for a single corner crack at a hole in a finite plate, i.e.,

- For the crack in the “B” zone,

$$\begin{aligned} B/R &\geq 2, & 0.2 &\leq D/t \leq 20 \\ 0.1 &\leq a/c \leq 10, & 0 &\leq a/t \leq 0.99 \\ (D+c)/(2B-c) &\leq 0.7 \end{aligned}$$

- For the crack in the “W-B” zone,

$$\begin{aligned} (W-B)/R &\geq 2, & 0.2 &\leq D/t \leq 20 \\ 0.1 &\leq a_1/c_1 \leq 10, & 0 &\leq a_1/t \leq 0.99 \\ (D+c_1)/[2(W-B)-c_1] &\leq 0.7 \end{aligned}$$

Combining the above conditions leads to the geometry limits for CC17 as shown in Section 3.11.2.

### 3.11.6 Verification

The equivalent hole method (EHM) for the general finite width correction under tension and bending is verified by the FEA in a wide range of geometrical dimensions and crack sizes [56]. The general finite width correction factors calculated by the EHM agree well with the FEA results, as shown in Figure 3.11.4. The errors between the EHM and FEA results are usually less than 8%, and 90% of the data have errors less than 5%. Note that the verification is done for remote tension only.

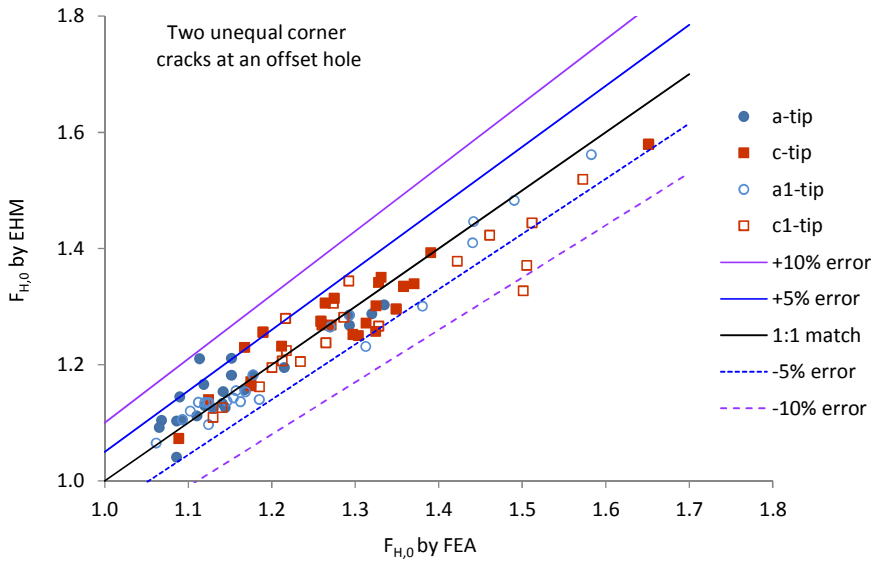


Figure 3.11.4: Verification of the equivalent hole method (EHM) under tension

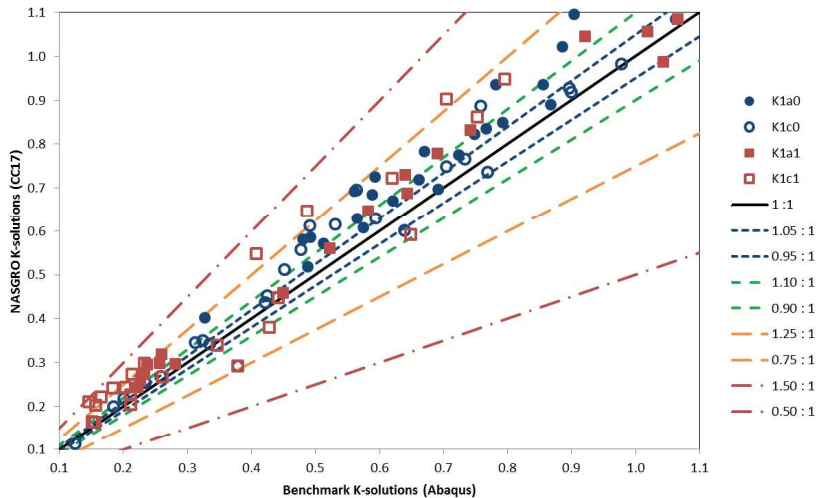


Figure 3.11.5: Verification of the CC17 correction factors for pin-loading

Figure 3.11.5 shows the comparison of CC17 stress intensity factor solutions under pin-loading against the benchmark FEA solutions. Note that a number of these test cases are for extreme geometries. The CC17 solutions generally agreed with the benchmark verification solutions within 10% for more common configurations.

References: [8, 56]

### 3.12 CC18 – Part-elliptical Corner Crack at Angled Corner – Bivariant WF

#### 3.12.1 Overview

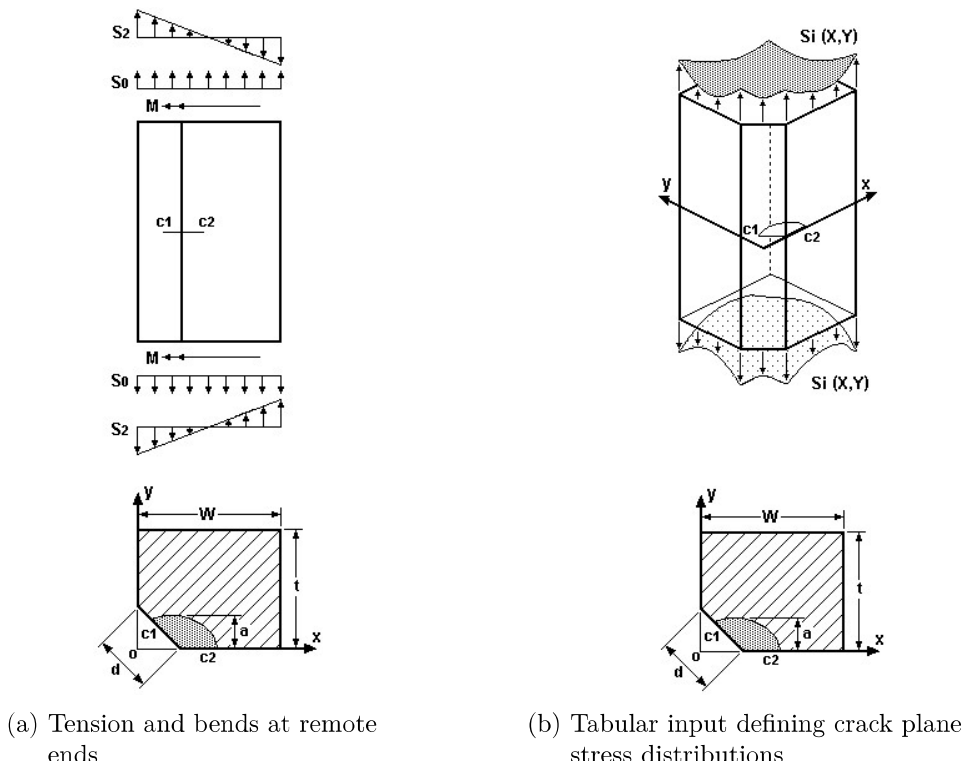


Figure 3.12.1: Configurations available for crack case CC18

This crack case addresses a partial elliptical corner crack at a  $135^\circ$  angled corner. The angled corner may be a result from  $45^\circ$  chamfering at a  $90^\circ$  corner. In contrast to CC12 crack case, the CC18 corner crack does not enclose the whole chamfer. By definition, its requirement assumes the surface crack length along the chamfer direction is less than any chamfer width. In addition, two dissimilarities should be singled out for clarification. Firstly, different length parameters relating to chamfer are designated. The chamfer length parameter with CC12 is the chamfer depth measured from the imaginary  $90^\circ$  corner of the rectangular cross section to the chamfer corner. For comparison the parameter with CC18 is the chamfer width measured between the two angled corners. Secondly, the centers of the corner crack are also designated differently. The crack center of CC12 crack model is at the imaginary  $90^\circ$  corner, while the center of CC18 crack model is always at the lower angled corner of the chamfer. Such minute differences lead to different definitions of surface crack lengths in both models. The crack growth algorithm assumes the growth at the  $c_1$ -tip, or the surface crack tip along the chamfer direction may eventually pass beyond the solution limit and this part-elliptical corner crack would transition into a CC12 corner crack.

The solution scheme for SIFs makes use of two sets of local coordinate system internally pending on the  $c_1/c_2$  ratio. For  $c_1/c_2 \leq 1$ , the local coordinate system depicted in Fig. 3.12.1 is used. The computed SIFs are with  $c_2$ - and  $a$ -tips. For  $c_1/c_2 > 1$ , a flipped local coordinate system as depicted in Fig. 3.12.2 is used and the computed SIFs are with  $c_1$ - and  $a$ -tips. The internal designation with the coordinate system is CS1 for the formal and CS2 for the latter. As noted in either coordinate

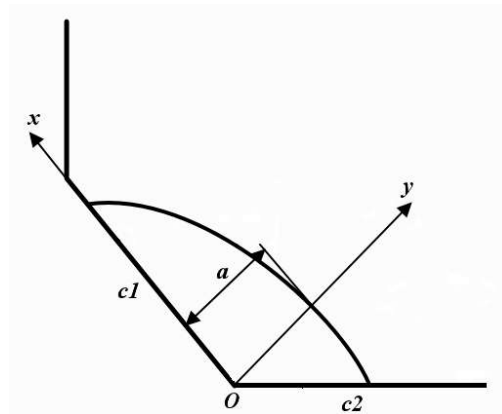


Figure 3.12.2: Alternative coordinate system used by CC18 SIF routine to compute SIFs at  $c_1$ - and  $a$ -tips when  $c_1/c_2 > 1$

system, the designation for  $c_1$ - and  $c_2$ -tips remains the same while the designation for  $a$ -tip may vary. This approach is to facilitate the crack growth computation requiring the increments in connection with two tips to be along two perpendicular axes.

### 3.12.2 Geometry

The key geometric parameters defining this crack model are:

- $W$  : plate full width
- $t$  : plate thickness
- $d$  : chamfer width
- $c_1$  : surface crack length along chamfer direction
- $c_2$  : surface crack length along plate width direction

The geometric validity bounds of the model are as follows

$$0.1 \leq c_1/c_2 \leq 10$$

$$0 \leq c_1/d \leq 0.9$$

$$\min(t, W) \geq 7.07d$$

### 3.12.3 Loading

The model supports crack plane stresses (1) derived from remote tension and bending, or (2) given as tabulated stress pairs varying as bivariate functions of normalized coordinates.

### 3.12.4 Theory

The SIF solution of CC18 is based on a weight function approach. Its point weight function (PWF) is the same as those used by SC19 and SC31 – a surface crack in a rectangular section subjected to bivariate stressing. The difference is in the way how SIF formulation accounts for the interaction between PWF and crack opening stress resulting from the reduction in effective crack area due to

Table 3.12.1: Definition of point locations indicated in PWF

Point designation	Location coordinate in elliptical system
$Q$	$(\xi, \eta)$
$Q_R$	$(\xi_0, \eta)$
$Q'$	$(\xi_0, \eta_0)$
$Q^*$	$(0, \eta)$
$\bar{Q}_x$	$(\xi, -\eta)$

the presence of a 45° chamfer. For reference, the PWF is given as follows.

$$W_{QQ'} = \frac{\sqrt{\ell_{Q_R Q^*}^2 - \ell_{QQ^*}^2}}{\pi \ell_{QQ'}^2 \sqrt{\pi \ell_{Q_R Q^*}}} \left( 1 + \frac{\ell_{QQ'}^2}{\ell_{Q_x Q'}^2} \right) \left\{ 1 + \Pi_1 \sqrt{1 - \left( \frac{\ell_{QQ^*}}{\ell_{Q_R Q^*}} \right)^2} + \Pi_2 \left( 1 - \frac{y}{y'} \right)^2 + \Pi_3 \left[ 1 - \frac{x}{\text{sign}(Q') x'} \right]^{1.5} \sqrt{1 - \frac{y}{a}} \right\} \quad (3.12.1)$$

Figure 3.12.3 is provided to facilitate identifying the point locations indicated in the above PWF equation. Their respective definitions in elliptical coordinate system: i.e., represented by elliptical radius  $\xi$  and angle  $\eta$ , can be found in Table 3.12.1. The elliptical radius corresponding to the crack tip perimeter is denoted by  $\xi_0$ . The script 1 denotes the distance between the two points indicated in its subscript; for example,  $\ell_{QQ'}$  is the distance between two points  $Q$  and  $Q'$ . The interceptions of the two axes in local  $xy$ -coordinate system with the crack tip perimeter defines two crack lengths  $a$  and  $c$ . The chord lengths  $x'$  and  $y'$  are derived by fixing  $y$  and  $x$  values with any interior point  $Q$ . The remaining unknowns in the above PWF:  $\Pi_1$ ,  $\Pi_2$ , and  $\Pi_3$ , will be determined by the reference solutions described in the later section.

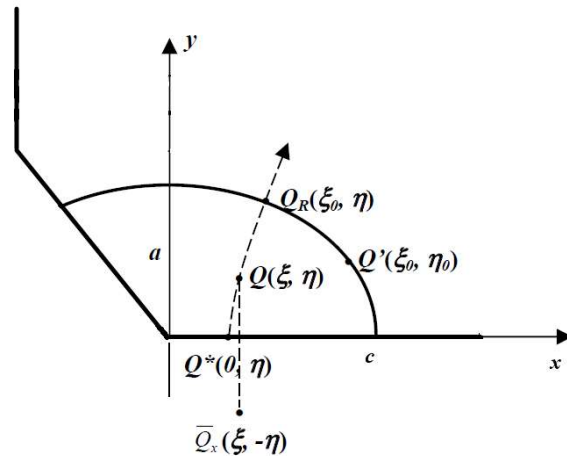


Figure 3.12.3: Geometry configuration and nomenclature for CC18 angular corner crack: point locations, crack length designation and coordinate system referenced in PWF

The CC18 SIF solution is computed by integrating the product of PWF and crack opening stress over the crack area. The formulation in equation form for SIF at the crack tip location  $Q'$  is given

by

$$K(\xi_0, \eta_0) = \int_0^{\xi_0} \int_0^{\eta_e} W_{QQ'}(\xi, \eta, \xi_0, \eta_0) \sigma(\xi, \eta) (\sin^2 \eta + \sinh^2 \xi) d\eta d\xi \quad (3.12.2)$$

where the crack opening stress applied at any point  $Q(x, y) = Q(\xi, \eta)$  on the crack surface is denoted by  $\sigma(\xi, \eta)$ . The upper limit of the internal integral  $\eta_e$  is a dependent of elliptical radius  $\xi$  and is given by

$$\eta_e = \pi - \tan^{-1} \frac{1}{\tanh \xi} \quad (3.12.3)$$

The above equation is derived with the assumption of a 45° chamfer in mind.

The reference solutions are discrete SIF results at  $c_1$ - and  $c_2$ -tips of the angular corner crack subjected to three separate sets of reference stress. In reference to the local coordinate system depicted in Fig. 3.12.3, the three sets of reference stress are given by  $\sigma_1 = 1$ ,  $\sigma_2 = 1 - y/a$ , and  $\sigma_3 = 1 - x/c$ . The geometric dimensions used for the determination of discrete SIF result are in terms of the ratios of  $c_1/c_2$  and  $c_1/d$ . The width and the thickness of the chamfered cross section have been defined large enough to minimize the side-surface effect. It is worth noting that the crack length  $c$  denoted in Fig. 3.12.3 could be associated with either  $c_1$ - or  $c_2$ -tip pending on the coordinate system being selected resulting from the relative magnitudes of  $c_1$  and  $c_2$ .

The post-transition crack model for CC18 is CC12 when the  $c_1$ -tip grows near or beyond the chamfer width. The onset of the transition is when  $c_1 \geq 0.9d$ , and the new crack depth  $a$  with the transitioned CC12 crack is given by

$$a = \begin{cases} \frac{d_s^2 \left(1 - \frac{\pi}{4}\right)}{d_s + c_2} & , c_1 \leq c_2 \\ \frac{\frac{1}{2}d_s^2 + \frac{d_s a}{\cos(\pi/4)} + \frac{1}{2}a^2 - \frac{\pi}{4}d_s(c_2 + d_s)}{\frac{\pi}{4}(c_2 + d_s)} & , c_1 > c_2 \end{cases} \quad (3.12.4)$$

Note that the crack depths with CC12 are measured from the two chamfer corners. The chamfer depth with CC12 is denoted by  $d_s$  in the above equation. The crack length  $c_2$  remains the same and is used to denote the crack length  $c$  with the transition crack model.

### 3.13 CC19 – Quarter-Elliptical Corner Crack at Hole in Lug – Univariant WF

#### 3.13.1 Overview

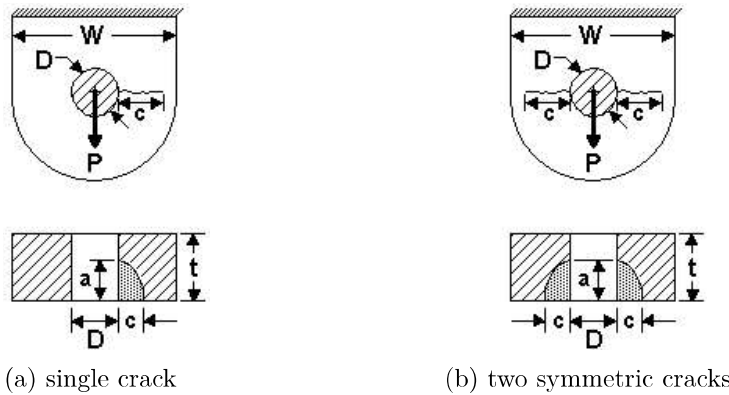


Figure 3.13.1: Configuration of the crack case CC19

The case CC19 represents a single (or two symmetric) quarter-elliptical corner-crack(s) initiated at the hole of a straight lug under pin-loading. Nominally, CC19 has the same geometry and loading as CC03. However, CC19 employs the weight function solution CC08 and the nonlinear stress variation for an uncracked lug. Consequently, CC19 represents a more powerful analysis tool, e.g. it can handle residual stresses. CC19 has a larger range of geometric parameters, e.g.  $W/D \geq 1.25$  for CC19 but  $W/D \geq 2$  for CC03. Finally, comparisons between CC03/CC19 and benchmark results demonstrate that CC19 is more accurate than CC03. See Verification section below for additional details.

#### 3.13.2 Geometry

Two available sub-configurations with a single or two symmetric crack(s) are shown in Fig. 3.13.1. Regardless of which option is picked, the following user inputs are required to define the cracked geometry:

- $t$  : lug thickness
- $W$  : lug width
- $D$  : pin hole diameter
- $a$  : initial size of the flaw along the bore surface
- $a/c$ : initial crack aspect ratio, where  $c$  is the flaw size along the lug front surface

CC19 has the same geometric validity ranges as CC08, except for the additional constraint that  $W/D \geq 1.25$ . This ratio represents a lower limit for most straight lug geometries. The overall validity ranges of this crack case are:

$$0.1 \leq D/(2t) \leq 10.0$$

$$1.25 \leq W/D \leq 10$$

$$0 \leq \frac{c}{W-D} \leq 0.45$$

$$0.1 \leq a/c$$

$$0 \leq a/t \leq 0.95$$

### 3.13.3 Loading

The crack case TC27 provides stress intensity factor solutions for loading inputs in terms of bearing stress  $S_3 = P/(Dt)$  induced by the pin load  $P$ . Individual magnitudes of the stress  $S_3$  are specified through the GUI for load block definitions.

The user has two options on treatment of the negative pin-load: (1) Compression clipping, (2) Full range. Refer to Section 13 of this Appendix for more details about each option.

### 3.13.4 Optional Features

As with many other weight function based crack cases, this case also allows incorporation of a static residual stress field along the crack plane. See Section 11.6 for more details on how the residual stresses are accounted for in NASFLA.

The cyclic stress shakedown option is available to account for local plasticity. Refer to Appendix M of the manual for more details.

### 3.13.5 Development History

This crack case was introduced to NASGRO in v8.1.

### 3.13.6 Theory

The fracture mechanics module internally estimates the local stress variations on the crack plane (in the corresponding uncracked body) along the net section and then invokes CC08. Refer to the Theory section of CC08 for additional information on integration of the weight functions.

Nonlinear stress variations along the crack plane were computed using the same assumptions as used in TC27. Refer to TC27 for additional information on the nonlinear stress variations that drive these solutions.

#### Calculation of stress intensity factors for two symmetric corner cracks

For two symmetric corner cracks, stress intensity factors may be computed based on a correction of the stress intensity factor of a single, non-symmetric crack. Verification studies of the two crack solution using finite element simulations lead to the following relationship:

$$\begin{aligned} K_{2crcks}^{a-tip} &= \frac{1}{F_{Shah}} K_{1crk}^{a-tip} \\ K_{2crcks}^{c-tip} &= \max \left( 1, \frac{1}{F_{Shah} F_{FW}} \right) K_{1rck}^{c-tip} \\ F_{Shah} &= \sqrt{\frac{D + \pi ac/4t}{D + \pi ac/2t}} \\ F_{FW} &= \sqrt{\frac{D + 0.05(W - D)}{D + c}} \end{aligned} \tag{3.13.1}$$

Here,  $F_{Shah}$  represents the Shah correction factor for a corner crack [38]. It is an appropriate correction for the stress intensity factor at the  $a$ -tip. The  $F_{FW}$  factor prevents non-conservative

stress intensity factor solutions at the  $c$ -tip for short, straight lugs when the crack is large relative to the hole diameter.

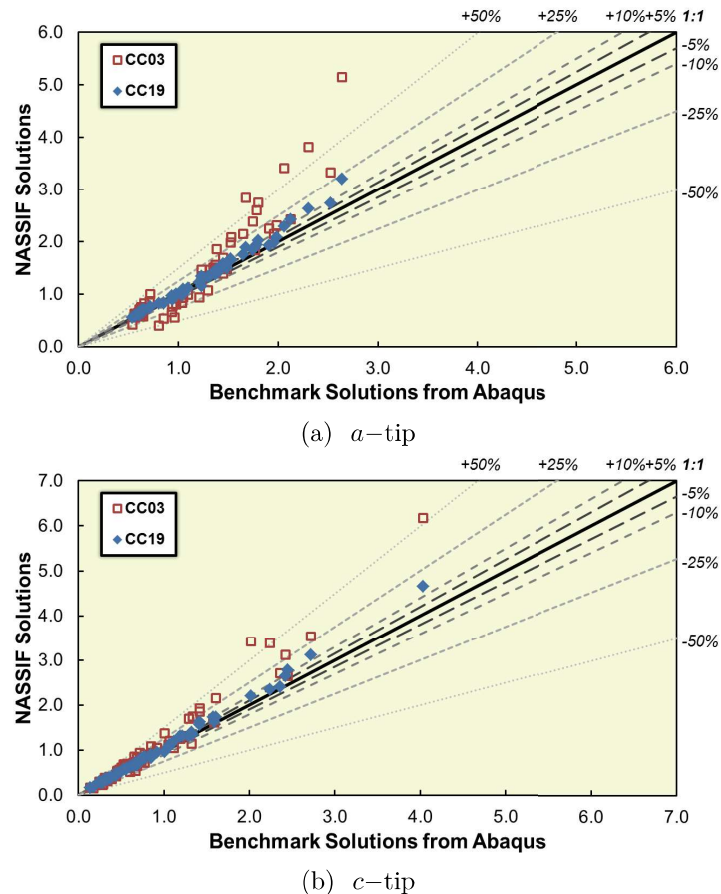


Figure 3.13.2: Verification of CC19—single crack and comparison with CC08

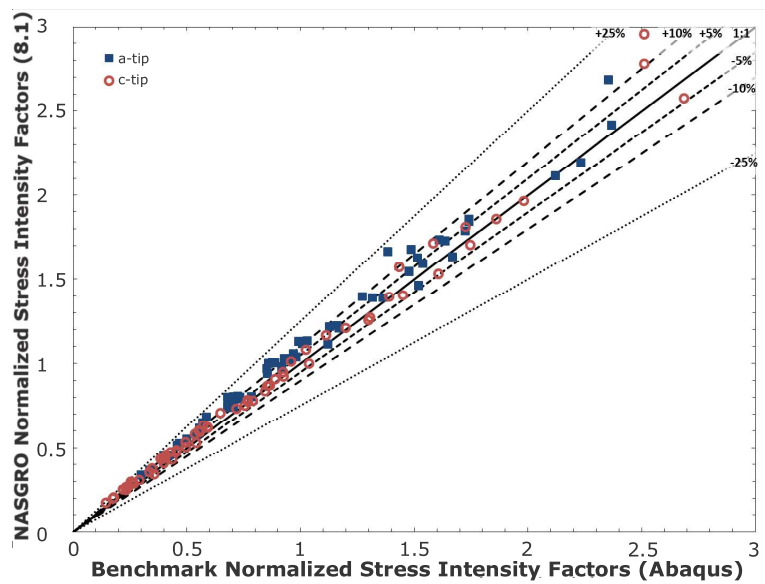


Figure 3.13.3: Comparison of stress intensity factors for symmetric cracks in lugs (CC19)

### 3.13.7 Verification

Figure 3.13.2 shows verification studies of CC19 at the  $a$ -tip and  $c$ -tip of the single corner crack. Values of stress intensity factors from detailed finite element analyses (using Abaqus 6.12-1) provide the benchmark data. Almost all stress intensity factors computed with CC19 have less than 10% error in comparison with the benchmark data. Error with CC03 may exceed 50%. For both crack cases, the error tends to be conservative (i.e., driving increased crack advance). This figure also highlights the increased range of geometries in CC19 vs. CC03; several computed values of CC19 do not have corresponding values of CC03 since the input geometry lies outside of the range of CC03 solutions.

Figure 3.13.3 highlights key results from the verification studies for the two symmetric corner cracks case. The plot compares stress intensity factors (normalized by  $S_3\sqrt{\pi a}$ ) at the  $a$ - and  $c$ -tips of the corner crack. Vertical axis is the NASGRO results, while the horizontal axis is the benchmark Abaqus model solutions with two symmetric cracks. For most cases, stress intensity factors are within 10% of the benchmark solution.

### 3.14 CC20 – Corner Crack in Plate – Displacement Control

#### 3.14.1 Overview

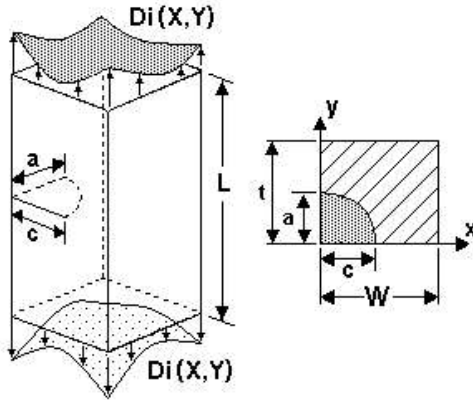


Figure 3.14.1: Configuration of crack case CC20

CC20 is similar to TC14 and TC24 in being one of the few NASGRO fracture mechanics crack models subjected to displacement-controlled load conditions. The crack model represents a quarter-elliptical corner crack at the mid-section of a rectangular bar. The plate is loaded by a combination of remotely applied uniform and linear displacements induced by tension and bending. Alternatively, generalized bivariant displacement profiles can be specified at remote ends. Besides the load type, the formulation also accounts for the constraint condition. See the Loading section below for more details.

#### 3.14.2 Geometry

The crack configuration with remote bivariant displacement condition is depicted in Fig. 3.14.1. The model requires the following geometric inputs:

- $t$  : plate thickness
- $W$  : plate width
- $L$  : plate length
- $a$  : initial size of the flaw along the plate thickness
- $a/c$ : initial crack aspect ratio, where  $c$  is the flaw size along the plate width

Since the loading is displacement controlled, this crack model also requires the material modulus of elasticity  $E$  as part of inputs in the Geometry tab.

The validity limits of the solution are given by

$$0.1 \leq a/c \leq 10$$

$$0 \leq a/t \leq 0.9$$

$$0 \leq c/W \leq 0.9$$

$$0.2 \leq L/W \leq 10$$

### 3.14.3 Loading

In the following, the applicable displacement constraint conditions are highlighted.

Remotely applied displacement can be specified in two ways:

- by displacement fields derived from remote tension  $D_0$ , in-plane bending  $D_2$ , and out-of-plane bending  $D_1$ .
- by user-specified remote displacements. The definition of the displacement variations is required to be specified by the external usage of displacement files. The format of the bivariant displacement files is the same as the historical NASGRO bivariant format as described in Section 11.1. The alternative bivariant format is not available for CC20.

Note that the loading direction is the  $z$ -direction, coinciding with the longitudinal direction of the rectangular bar, and the displacement variation at the remote ends is bivariant or in terms of two coordinate directions:  $x$  and  $y$ , with the rectangular cross section.

Two types of remote displacement constraints can be specified:

- Type I: no constraint for displacements in both  $x$ - and  $y$ -directions; displacement in  $z$ -direction is user-defined
- Type II: fixed constraint for displacements in both  $x$ - and  $y$ -directions; displacement in  $z$ -direction is user-defined

### 3.14.4 Development History

This displacement-controlled model was developed by NRL under funding by ESA and introduced to NASGRO in v8.1.

### 3.14.5 Theory

The SIF formulation of CC20 FM module is based on interpolation among reference SIF solutions determined at the two surface tips of the corner crack. The reference solutions [57] were generated using the finite element software ABAQUS by the National Aerospace Laboratory of the Netherlands (NLR). The supplemental solutions for geometrically small cracks were provided by SwRI based on the CC09 crack model with crack plane stress derived from the constrained boundary. The solution matrix was in terms of a limited number of combinations of geometric ratios, reference displacement variations and two displacement end constraints. The discrete geometric ratios are in terms of  $a/c$ ,  $a/t$ ,  $c/W$  and  $L/W$ . The reference displacement variations are the nine components of second order

bivariant functions, respectively, given by

$$\begin{aligned} & 1 \\ & 1 - x/W \\ & 1 - y/t \\ & (1 - x/W)^2 \\ & (1 - x/W)(1 - y/t) \\ & (1 - y/t)^2 \\ & (1 - x/W)^2(1 - y/t) \\ & (1 - x/W)(1 - y/t)^2 \\ & (1 - x/W)^2(1 - y/t)^2 \end{aligned}$$

To compute SIFs, the user-specified displacement variations in discrete format are first converted into bivariant polynomial form. The conversion is through a least square method for two variables and thus determines the polynomial coefficients with the nine function components. For reference, the polynomial denoting the user-specified displacement variation  $D_i$  is given by

$$\begin{aligned} D_i(x, y) = & a_i^{0,0} + a_i^{1,0} \left(1 - \frac{x}{W}\right) + a_i^{0,1} \left(1 - \frac{y}{t}\right) + a_i^{2,0} \left(1 - \frac{x}{W}\right)^2 + a_i^{1,1} \left(1 - \frac{x}{W}\right) \left(1 - \frac{y}{t}\right) \\ & + a_i^{0,2} \left(1 - \frac{y}{t}\right)^2 + a_i^{2,1} \left(1 - \frac{x}{W}\right)^2 \left(1 - \frac{y}{t}\right) + a_i^{1,2} \left(1 - \frac{x}{W}\right) \left(1 - \frac{y}{t}\right)^2 \\ & + a_i^{2,2} \left(1 - \frac{x}{W}\right)^2 \left(1 - \frac{y}{t}\right)^2 = \sum_k \sum_l a_i^{k,l} \left(1 - \frac{x}{W}\right)^k \left(1 - \frac{y}{t}\right)^l \end{aligned} \quad (3.14.1)$$

where the subscript  $i$  ranges from 1 to 4 designating the displacement variations, and the superscripts  $k$  and  $l$  denote the dual-indexed coefficient  $a_i^{k,l}$  and the exponents of the normalized functions  $(1 - x/W)$  and  $(1 - y/t)$ . The SIF is determined by simple summation of the product terms consisting of coefficients and interpolated reference solutions in connection to the reference displacement functions.

### 3.15 CC21 – Corner Crack at Edge Rectangular Cutout with Rounded Corners

#### 3.15.1 Overview

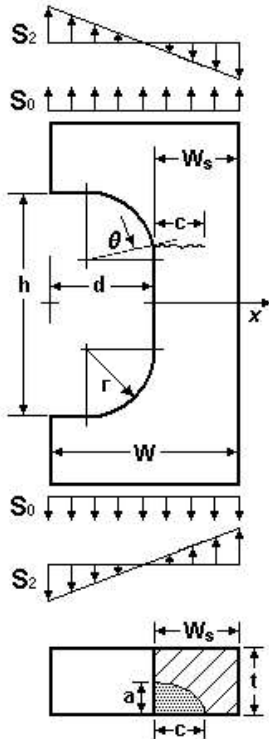


Figure 3.15.1: Configuration of case CC21

This crack model is a weight function based solution for a corner crack at an edge rectangular cutout with rounded corners. The crack is placed at the maximum stress concentration point of the rounded corner. The plate is remotely loaded by tension and/or bending stresses. A schematic describing this crack model is given in Fig. 3.15.1. For the alternative of this model with through-thickness crack, see the case TC25.

#### 3.15.2 Geometry

The key geometric parameters defining this crack model are:

- $W$  : plate full width
- $t$  : plate thickness
- $d$  : cutout depth
- $r$  : cutout radius
- $h$  : cutout height
- $a$  : initial flaw size along the thickness
- $a/c$ : initial flaw aspect ratio, where  $c$  is the surface flaw size on the front surface

The crack initiation site, in terms of the angular position  $\theta$ , is calculated by NASGRO for max stress concentration location at radius.

The geometry validity limits of this model are as follows:

$$\begin{aligned} 1 &\leq d/r \leq 11 \\ 0.05 &\leq d/W \leq 0.5 \\ 1 &\leq h/(2r) \leq 6 \\ c/W_s &\leq 0.95 \\ a/t &\leq 0.95 \\ 0.025 &\leq a/c \leq 40 \end{aligned}$$

When  $a$ -tip of the corner crack grows beyond the limit (i.e.  $a/t \geq 0.95$ ), the crack will turn into TC25 edge through-thickness crack. The crack length  $c$  along the free surface of the corner crack prior to transition is assigned to be the through-thickness crack length  $c$  of TC25.

### 3.15.3 Loading

The crack model CC21 can be subjected to remote stress variations consisting of two load types: remote tension  $S_0$  and in-plane bending stress  $S_2$ .

### 3.15.4 Optional Features

The cyclic stress shakedown option is available in the “Geometry” tab to account for stress relief near the notch tip due to local plasticity. More information is provided in Appendix M of the manual.

### 3.15.5 Development History

This crack case was first implemented in NASGRO v8.2.

### 3.15.6 Theory

CC21 utilizes the crack opening stress extracted along the crack plane and computes the stress intensity factors at both surface tips using weight function formulation. The weight function approach is the same as the one deployed in CC11 for two surface tips with univariant stress gradient along the net section direction.

The crack plane is assumed perpendicular to the load direction. The initiation site of the corner crack, designated by the  $\theta$  angle, is numerically determined in accordance with the approach deployed for TC25. Refer to the description in the section for TC25 for further details. Due to the  $\theta$  angle, the sectional width  $W_s$ , defined by  $[W - d + r(1 - \cos \theta)]$ , could be slightly larger than the net section ( $W - d$ ). The variation of crack opening stress across the crack plane is the same as the one for TC25, which is interpolated among reference solutions determined using finite element method at discrete geometric ratios with reference stresses.

### 3.16 CC22 – Corner Crack at Offset Internal Rectangular Cutout with Rounded Corners

#### 3.16.1 Overview

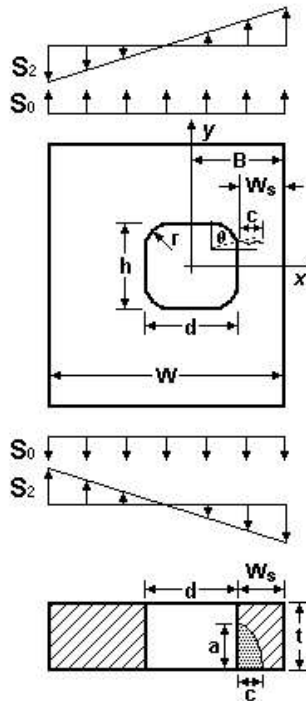


Figure 3.16.1: Configuration of case CC22

This crack model is a weight function based solution for a corner crack at the rounded corners of an offset internal rectangular cutout. A schematic is shown in Fig. 3.16.1. The crack is placed at the maximum stress concentration point of the rounded corner on the smaller net section side. The model is remotely loaded by tension and bending stresses. This is the corner crack alternative of the through crack case TC26.

#### 3.16.2 Geometry

The geometric parameters involved in defining this crack model are:

- $W$  : plate full width
- $t$  : plate thickness
- $r$  : cutout radius
- $B$  : cutout offset distance from the plate right edge
- $h$  : cutout nominal height
- $d$  : cutout nominal width
- $a$  : initial surface flaw size along the plate thickness
- $a/c$ : initial flaw aspect ratio, where  $c$  is the surface crack on the front face

The crack initiation site, in terms of angular position  $\theta$ , is calculated by NASGRO for the maximum

stress concentration location at radius.

The validity limits are expressed in terms of geometric ratios and result from reference stress limits imposed on TC26 as well as the limits on weight function solutions. The limits are as follows:

$$\begin{aligned} 1 < d/(2r) &\leq 11 \\ 0.05 \leq d/(2B) &\leq 0.5 \\ 1 < h/(2r) &\leq 6 \\ 0.1 \leq 2B/W &\leq 1 \\ 0.1 \leq d/(2t) &\leq 10 \\ 0.1 \leq a/c & \\ c/W_s &\leq 0.9 \\ a/t &\leq 0.95 \end{aligned}$$

When  $a$ -tip of this crack grows beyond 90% of the plate thickness (i.e.  $a/t \geq 0.9$ ), the crack will self-transition into TC26 edge through-thickness crack. The crack length  $c$  of the corner crack prior to transition is assigned to be the through-thickness crack length  $c$  of TC26.

### 3.16.3 Loading

The loading specification allows for a combination of remote tension ( $S_0$ ) and in-plane bending ( $S_2$ ) with their individual stress scaling factors.

### 3.16.4 Development History

This crack case was first implemented in NASGRO v8.2.

### 3.16.5 Theory

This corner crack model utilizes the crack opening stress extracted along the crack plane and computes the stress intensity factors at both surface tips using weight function formulation. The  $\theta$  angle designating the crack initiation site is determined in accordance with the approach deployed in TC26 crack model. NASGRO determines the univariant stress gradient along the crack plane direction through interpolation among reference stress solutions.

The weight function formulation adapts a hybrid approach depending on the slenderness of the internal rectangular cutout described by the  $h/d$  ratio. If this ratio is less than or equal to 1.0, the weight function result from CC08 is used. If  $h/d$  is larger than 1, an interpolative approach between the results from CC08 and CC11 is used. The approach is to account for the loss of material in the longitudinal direction in view of the assumption of a circular hole configuration with CC08 crack model.

### 3.17 CC23 – Corner Crack at Hole in Obliquely Loaded and Tapered Lug – Univariant WF

#### 3.17.1 Overview

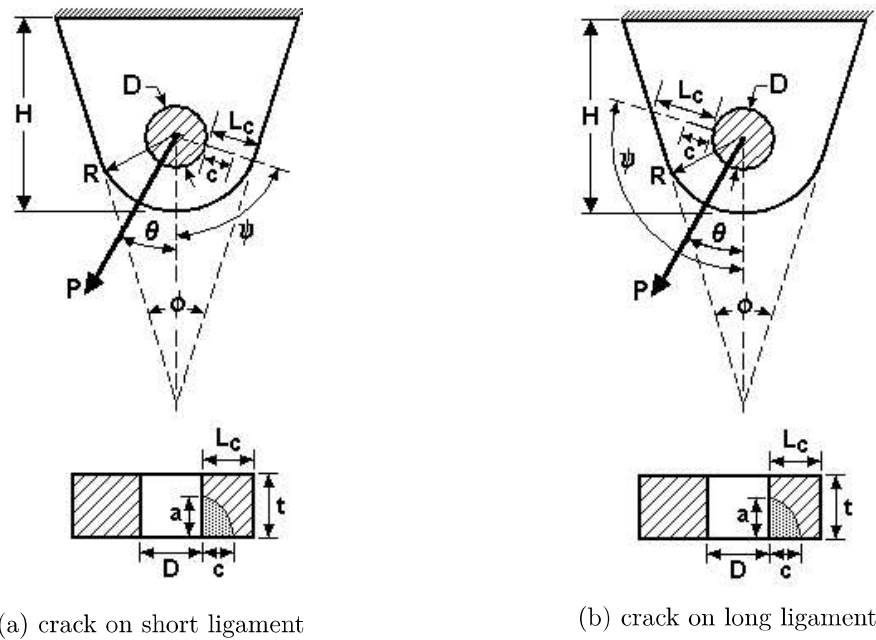


Figure 3.17.1: Configuration of crack case CC23

Crack case CC23 represents a semi-elliptical corner crack initiated at the hole of a symmetric tapered lug under oblique pin-loading. The crack is located either on a short ligament or on a long ligament side of the hole as depicted in Figs. 3.17.1a and 3.17.1b, respectively.

This solution is distinct and separate from earlier lug solutions that assumed straight, short lugs under vertical loading. Straight means that the lug geometry has no taper; short implies that these lugs have height equal to their width; vertical loading restricts loads to a constant angle.

CC23 represents a more powerful analysis tool than CC19, which is limited to straight, short lugs under normal loading. Both analyses are based on the same weight function solution, CC08. The main differences between CC19 and CC23 are the crack angle and stress gradient set. CC19 sets a constant crack angle that is perpendicular to the loading, whereas CC23 sets the crack angle based on the geometry and loading. CC19 also uses a different set of stress gradient solutions. While CC23 may be set to the same geometry as CC19 ( $W = 2R$ ;  $H = 2R$ ;  $\phi = 0^\circ$ ;  $\theta = 0^\circ$ ), CC23 is intended to span the range of tapered and obliquely-loaded lug geometries that exist on aerospace platforms. CC19 is intended as a replacement for CC03. The differing assumptions of CC19 and CC23 lead to different SIFs over the solution space. Direct comparisons between CC19 and CC23 reveal that SIF solutions from CC23 are mostly within 3% of CC19 for holes with  $2R/D \geq 2$ . The impact on fatigue crack growth lives is complicated. SIFs from CC23 may be above SIFs from CC19 for smaller cracks and below SIFs from CC19 for larger cracks. Furthermore, CC19 sets a minimum crack ligament, whereas CC23 may have a longer crack path than the minimum possible ligament.

### 3.17.2 Geometry

The required input parameters to define the cracked geometry are listed below:

- $R$  : outer radius of the lug
- $t$  : lug thickness
- $D$  : pin-hole diameter
- $H$  : heel-to-toe height of the lug
- $\phi$  : lug taper angle
- $\theta$  : pin-load angle
- $a$  : initial flaw size along the bore
- $a/c$ : initial flaw aspect ratio where  $c$  is the flaw size in the width direction

CC23 supports a much larger range of geometries and loadings relative to other available pin-loaded lug cases:

$$\begin{aligned} 0^\circ \leq \phi &\leq 90^\circ & 0.1 \leq D/(2t) &\leq 10 \\ 0^\circ \leq \theta &\leq 90^\circ & 1.25 \leq 2R/D &\leq 10 \\ 0 \leq a/t \leq 0.9 && 1 \leq H/(2R) &\leq 2 \\ 0.1 \leq a/c && & \end{aligned}$$

The crack size limit along the free surface depends on the crack location. For a crack on the long ligament, CC23 restricts the crack size based on considerations of mode mixing:

$$\begin{aligned} 0 \leq c/L_c &\leq 0.9 & \text{for crack on a short ligament} \\ c \leq \min(0.9L_c, R - D/2) && \text{for crack on a long ligament} \end{aligned}$$

The ratio  $D/(2t)$  given above establishes the hole diameter relative to the lug thickness. The ratio  $2R/D$  provides the ratio of the lug's outer radius ( $R$ ) to its pin-hole diameter ( $D$ ). The limits range from a very large hole ( $2R/D = 1.25$ ) to a very small hole ( $2R/D = 10$ ) and can cover earlier solutions for straight, short lugs under normal loading (CC19). The lug's heel-to-toe height ( $H$ ) is variable in CC23 with limits for a short lug ( $H = 2R$ ) to a much longer lug ( $H = 4R$ ). CC23 supports symmetrically tapered lugs with symmetric taper angle ( $\phi$ ) that supports straight lugs ( $\phi = 0^\circ$ ) to right-angled tapers ( $\phi = 90^\circ$ ). The oblique loading angle ( $\theta$ ) varies from perpendicular to the base ( $\theta = 0^\circ$ ) to parallel to the base ( $\theta = 90^\circ$ ).

CC23 has a large range of crack shapes controlled by the elliptical size ratio ( $a/c$ ). Limits for the crack size ( $a/t$  and  $c/L_c$ ) support most applicable geometries. Corner cracks (CC23) transition to through-thickness cracks (TC30) as  $a/t$  reaches the upper limit. Refer to the Appendix D of the NASGRO documentation for additional details on crack transitions.

CC23 in NASGRO 9.0 and onwards supports two distinct crack configurations: a crack on the short ligament (the default), and a crack on the long ligament. Cracks on the long ligament may be located at either the maximum opening stress location or the maximum Mises stress location. Refer to crack case TC30 for more information on the crack angle ( $\psi$ ), the crack path ( $L_c$ ), crack kinking, internal stress processing, and generation of benchmark finite element analyses.

### 3.17.3 Loading

Crack case CC23 provides SIF solutions for pin-loading inputs in terms of bearing stress defined as  $S_3 = P/(Dt)$ . The pin-load direction is specified by the clockwise angle  $\theta$  from vertical axis (see

Fig. 3.17.1) in the Geometry tab of the GUI along with the rest of the model input parameters. Individual magnitudes of the pin-loading are specified through the GUI for load block definitions.

### 3.17.4 Optional Features

CC23 supports residual stresses along the crack path – that is, from  $0 \leq X/L_c \leq 1$  at the angle  $\psi$ . Residual stresses will not alter the crack path. Consequently, a user may execute a NASFLA analysis to obtain  $\psi$  and then pick out the residual stress along the crack path. See section Section 11.6 of this documentation for more information about how residual stresses can be defined.

CC23 supports two negative pin-loading options: (a) compression clipping or (b) full range. Refer to Section 13 at the end of this documentation for more information.

### 3.17.5 Development History

The lug solution was first made available in v8.2. A new case with crack on long ligament side of the hole was developed and implemented in NASGRO 9.0. In v9.1, an additional option to locate the crack at the “maximum von Mises stress” location has been added for a crack in the long ligament.

### 3.17.6 Theory

The fracture mechanics module internally estimates the local stress variations on the crack plane (in the corresponding uncracked body) along the net section and then integrates these stresses with the weight function CC08 over the crack face. Refer to the Theory section of the crack case CC08 in this appendix for additional information on integration of the underlying weight function used by CC23.

### 3.17.7 Verification

Figure 3.17.2 summarizes verification studies of CC23 done for a crack on the short ligament. Values of SIFs from detailed finite element analyses (using Abaqus 6.12-1) provide the benchmark SIFs from crack geometries. Most SIFs computed with CC23 have less than 10% error in comparison with the benchmark data. Excessive error tends to be conservative (i.e., driving increased crack advance), though there are a few outliers where the error is non-conservative. These outliers represent geometries that have crack tips intersecting the straight taper edge at an angle.

Figure 3.17.3 summarizes verification studies of CC23 with a crack on the long ligament using the maximum opening stress criteria. Values of SIFs from detailed finite element analyses (using Abaqus 6.14-3) provide the benchmark SIFs from crack geometries. Most SIFs computed with CC23 have less than 10% error in comparison with the benchmark data. Excessive error tends to be conservative (i.e., driving increased crack advance), though there are a few outliers where the error is non-conservative. These outliers represent geometries that have longer crack tips, where mixed mode loading is important.

Figure 3.17.4 summarizes verification studies of CC23 with a crack on the long ligament using the maximum Mises stress criteria. Values of SIFs from detailed finite element analyses (using Abaqus 6.14-3) provide the benchmark SIFs from crack geometries. Most SIFs computed with CC23 have less than 10% error in comparison with the benchmark data. Excessive error tends to

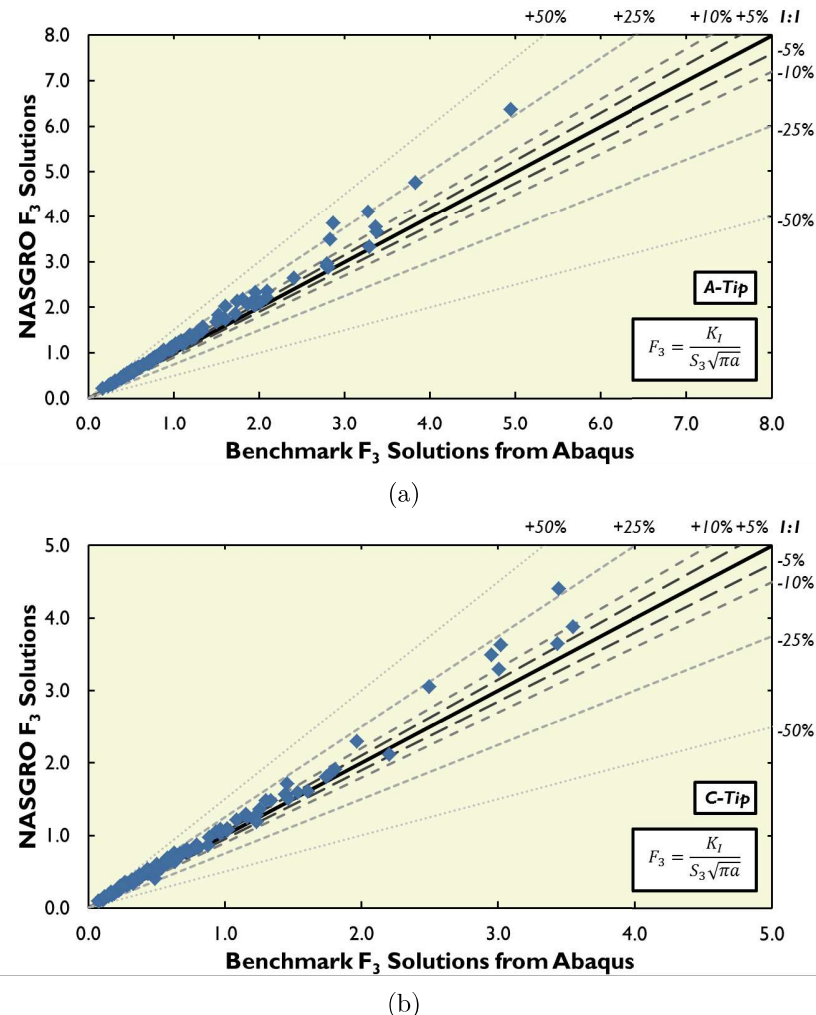


Figure 3.17.2: Verification of CC23 with Abaqus benchmark solutions at the (a) a-tip and (b) c-tip with the crack on the short ligament

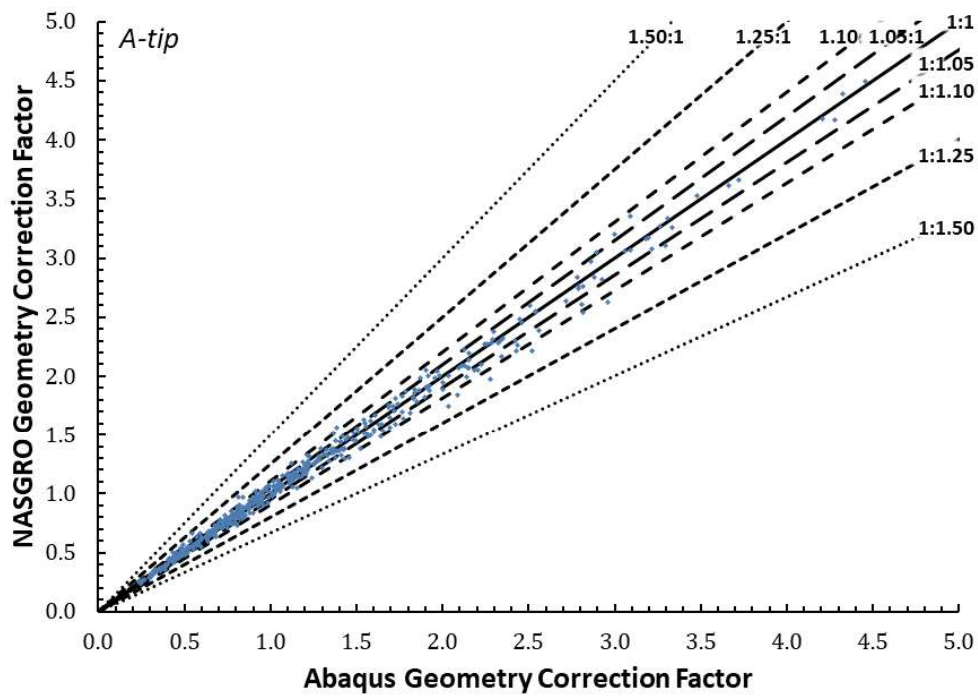


Figure 3.17.3: Verification of CC23 with Abaqus benchmark solutions at the *a*-tip, with crack on the long ligament using the maximum opening stress criteria

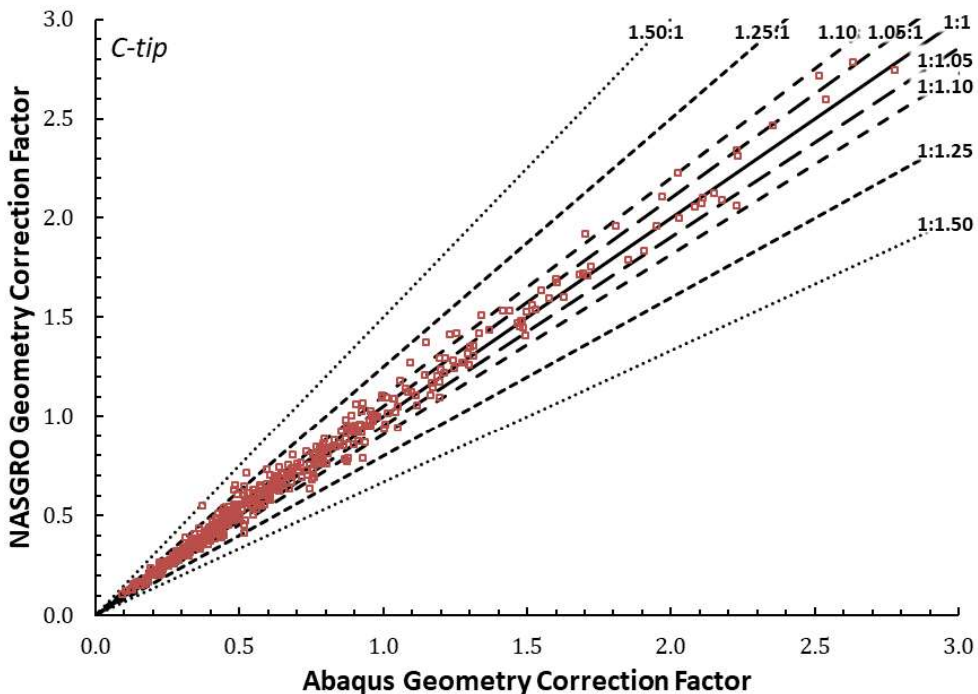


Figure 3.17.4: Verification of CC23 with Abaqus benchmark solutions at the *c*-tip, with crack on the long ligament using the maximum opening stress criteria

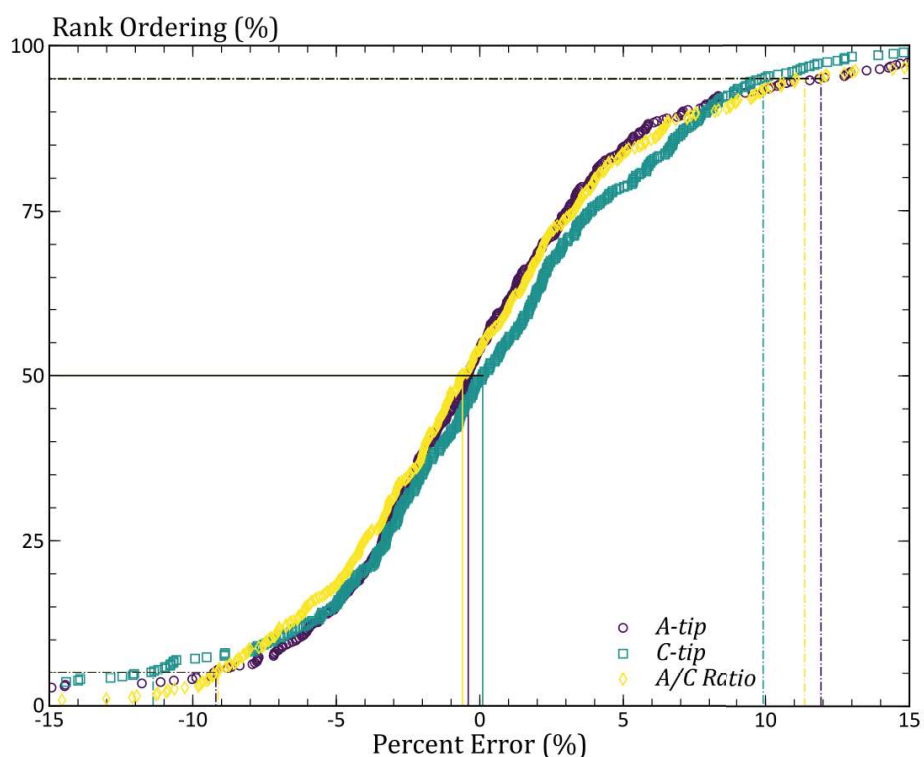


Figure 3.17.5: Verification of CC23 with Abaqus benchmark solutions at the c-tip, with crack on the long ligament using the maximum Mises stress criteria

be conservative (i.e., driving increased crack advance), though there are a few outliers where the error is non-conservative.

## 4 Embedded Cracks

### 4.1 EC04 – Elliptical Embedded Crack (Offset) in a Plate – Bivariant WF

#### 4.1.1 Overview

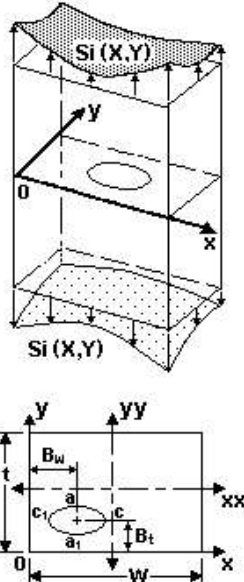


Figure 4.1.1: Configuration of case EC04

The crack case EC04 is a bivariant weight function solution for an embedded elliptical crack in a plate with rectangular cross-section. The crack plane bivariant stressing is defined in terms of either tension/bending combinations, 2D polynomial equations, or tabular inputs. The crack can be located offset from the center of the plate's cross-section.

For an alternative of this crack case with univariant stressing, see the next case EC05. The superceded case EC02 is also a univariant alternative of this case. However, EC04 has wider solution limits relative to EC02. EC04 is also based on a new set of highly accurate reference solutions generated by the advanced hybrid finite/boundary element computer program FADD3D for determining SIF variation along the crack perimeter. EC04 will give results in agreement with EC05 when the prescribed stress field is univariant in nature.

#### 4.1.2 Geometry

The cracked geometry is depicted in Fig. 4.1.1. The geometric input parameters are:

- $t$  : plate thickness
- $W$  : plate full width
- $B_w$  : offset distance of the crack center from the plate left surface
- $B_t$  : offset distance of the crack center from the plate front surface
- $a$  : half the initial elliptical flaw size along the plate thickness direction
- $a/c$  : initial flaw aspect ratio, where  $c$  is half the crack size in the plate width direction

The solution limits in terms of dimensionless geometric parameters are given by:

$$0 \leq \min\left(\frac{a}{B_t}, \frac{a}{t - B_t}\right) \leq 0.99$$

$$0 \leq \min\left(\frac{c}{B_w}, \frac{c}{W - B_w}\right) \leq 0.99$$

$$0.1 \leq a/c \leq 10$$

Once the crack size reaches 99% of the shortest crack ligament, this case will self-transitions to either SC31, CC09, TC11, or TC12 depending on which case best represents the transitioning crack geometry. Appendix D of the NASGRO documentation provides more details of the transition process and the program logic employed to select the post-transition model.

#### 4.1.3 Loading

Three input methods are available for users to specify bivariant stress fields. Respectively, the stress fields can be represented by (1) remote tension/bends (default option), (2) bivariant polynomial functions, or (3) user-specified gradients in a tabular format. In all cases, the normalized coordinates  $X$  and  $Y$  are used. The normalized coordinates  $(X, Y)$  are in reference to the thickness  $t$  and the width  $W$  of the plate and defined by  $X = x/W$  and  $Y = y/t$ , where the  $xy$ -coordinate system is the same as the one depicted in Fig. 4.1.1.

##### Remote Tension/Bends

If the simple load type in terms of remote tension and bends is selected, the first three stress quantities are internally generated assuming the stress variations are in terms of unit tension ( $S_0$ ), unit out-of-plane bending ( $S_1$ ), and unit in-plane bending ( $S_2$ ). In equation form, their variations are given by

- Unit tension:  $S_0(X, Y) = 1$
- Unit out-of-plane bending:  $S_1(X, Y) = 1 - 2Y$
- Unit in-plane bending:  $S_2(X, Y) = 1 - 2X$

The stress inputs  $S_1$  and  $S_2$  can be related to the remote out-of-plane and in-plane moments  $M_1$  and  $M_2$  as follows:

$$\begin{aligned} S_1 &= \frac{6M_1}{Wt^2} && M_1 : \text{out-of-plane moment} \\ S_2 &= \frac{6M_2}{W^2t} && M_2 : \text{in-plane moment} \end{aligned} \tag{4.1.1}$$

##### Bivariant Polynomial Function

If bivariant polynomial functions option is selected, the coefficients for the 2D polynomial functions are required on the GUI screen. The bivariant polynomial function is represented in terms of normalized coordinates  $X$  and  $Y$  and is given by

$$\begin{aligned} S_i^{poly} = \sum C_i^{m,n} X^m Y^n &= C_i^{0,0} + C_i^{1,0}X + C_i^{0,1}Y + C_i^{2,0}X^2 + C_i^{1,1}XY + C_i^{0,2}Y^2 + \\ &\quad C_i^{3,0}X^3 + C_i^{2,1}X^2Y + C_i^{1,2}XY^2 + C_i^{0,3}Y^3 + C_i^{3,1}X^3Y + \\ &\quad C_i^{2,2}X^2Y^2 + C_i^{1,3}XY^3 + C_i^{3,2}X^3Y^2 + C_i^{2,3}X^2Y^3 + \\ &\quad C_i^{3,3}X^3Y^3 \end{aligned} \tag{4.1.2}$$

where the subscript  $i$  of the polynomial coefficients  $C_i^{m,n}$  denotes the index of applied stress quantity, and the superscripts  $m$  and  $n$  designates the exponents of the normalized dimensions  $X$  and  $Y$ , respectively. Up to a total of four independent polynomials can be defined (i.e.  $i = 1$  to 4).

### Tabular Input

If the stress distributions can not be described by either remote tension/bending or bivariant polynomial functions, the stress variations on a crack plane of an uncracked geometry can be organized in a tabular form and stored in text file format. The GUI is then used to specify the file locations and names for analysis. The stress file format is of generic NASGRO format for bivariant stresses used by bivariant SIF solution modules. For more details, refer to Section 11.1 – Stress Gradient Input Formats of this appendix.

#### 4.1.4 Optional Features

The tabular stress input option of this case allows incorporation of a static residual stress field along the crack plane. See Section 11.6 for more details on how the residual stresses are accounted for in NASFLA.

NASFLA also allows separate definitions of tension/compression or t1/t2 stress gradients for this case when stresses are defined via tabular input. Refer to Sections 11.2 and 11.3 for further details about this capability.

#### 4.1.5 Development History

This SIF solution was introduced to NASGRO in v6.0.

#### 4.1.6 Theory

The EC04 solution is based on a new weight function formulation similar to the formulation used in CC09 and SC19 and has its own independent set of reference solutions. Its basic weight function (Fig. 4.1.2) is identical to the point weight function proposed by Orynyak [48, 49] and the basic weight functions used in CC09 and SC19. To account for the effects of free surfaces, three correction terms were used and the approximate weight function for the formulation is given by:

$$W = W_{basic} + W_{correction} \\ = \frac{\sqrt{R^2 - r^2}}{\pi \sqrt{\pi R l_{QQ'}^2}} \left\{ 1 + \Pi_1 \sqrt{1 - \frac{r}{R}} + \Pi_2 \left[ 1 - \frac{y}{\text{sign}(Q', y)y'} \right] + \Pi_3 \left[ 1 - \frac{x}{\text{sign}(Q', x)x'} \right] \right\} \quad (4.1.3)$$

where  $W_{correction}$  represents the correction terms with coefficients  $\Pi_1$ ,  $\Pi_2$ , and  $\Pi_3$ , and  $Q(x, y)$  denotes the location where the point load is applied. The chordal lengths  $x'$  and  $y'$  can be determined by

$$x' = c \sqrt{1 - \frac{y^2}{a^2}}, \quad y' = a \sqrt{1 - \frac{x^2}{c^2}} \quad (4.1.4)$$

$\text{sign}(Q', y)$  denotes the sign of  $x$ -coordinate of  $Q'$  and  $\text{sign}(Q', x)$  the sign of  $y$ -coordinate of  $Q'$ . The stress intensity factor for any location  $Q'$  along the crack perimeter can thus be written as

$$K^{Q'} = \int_A W \sigma(x, y) dA \quad (4.1.5)$$

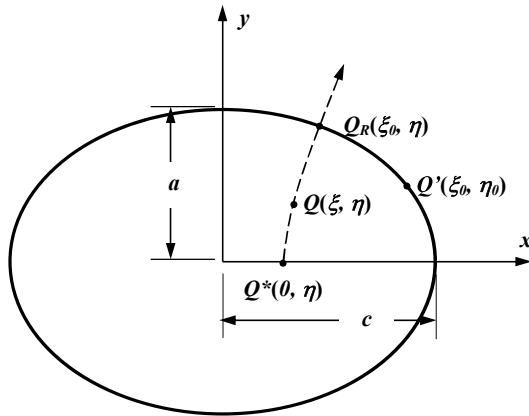


Figure 4.1.2: Embedded crack in an infinite domain

where the integration is carried out over the whole embedded crack surface.

The surface integral can be transformed to be in reference to an elliptical coordinate system with its origin at the crack center to facilitate further mathematical manipulations. In that case,  $Q^*$ ,  $Q$  and  $Q_R$  are defined to share the same elliptical angle  $\eta$ , and  $Q'$  and  $Q_R$  have the same elliptical “radius”  $\xi_0$ . The value of  $\xi_0$  depends on the crack aspect ratio  $\alpha = a/c$ . For  $a/c < 1$  and  $b = \sqrt{c^2 - a^2}$ .

$$x = b \cosh \xi \cos \eta \quad , \quad y = b \sinh \xi \sin \eta$$

$$\xi_0 = \ln \left( \frac{1 + \alpha}{1 - \alpha} \right)$$

$$R = b \sqrt{(\cosh \xi_0 \cos \eta - \cos \eta)^2 + \sinh^2 \xi_0 \sin^2 \eta}$$

$$r = b \sqrt{(\cosh \xi \cos \eta - \cos \eta)^2 + \sinh^2 \xi \sin^2 \eta} \quad (4.1.6)$$

$$l_{QQ'} = b \sqrt{(\cosh \xi \cos \eta - \cos \xi_0 \cos \eta_0)^2 + (\sinh \xi \sin \eta - \sinh \xi_0 \sin \eta_0)^2}$$

$$\frac{y}{y'} = \frac{\sinh \xi \sin \eta}{\alpha \sqrt{\cosh^2 \xi_0 - \cosh^2 \xi \cos^2 \eta}} \quad , \quad \frac{x}{x'} = \frac{\alpha \cosh \xi \cos \eta}{\sqrt{\sinh^2 \xi_0 - \sinh^2 \xi \sin^2 \eta}}$$

$$dA = b^2 (\sin^2 \eta + \sinh^2 \xi) d\xi d\eta$$

and the integral becomes

$$K^{Q'} = \int_0^{\xi_0} \int_0^{2\pi} (W_{basic} + W_{correction}) \sigma(\xi, \eta) c^2 (\sin^2 \eta + \sinh^2 \xi) d\eta d\xi \quad (4.1.7)$$

The coefficients  $\Pi_1$ ,  $\Pi_2$ , and  $\Pi_3$  are determined by three sets of reference solutions at the preferred crack tip locations. The surface integral is determined by the Gauss-Chebyshev numerical integration scheme.

#### 4.1.7 Verification

Verification of EC04 follows the verification procedure outlined in [52]. Full details of the verification effort can be found in that document. Fig. 4.1.3 presents the key verification plot for EC04.

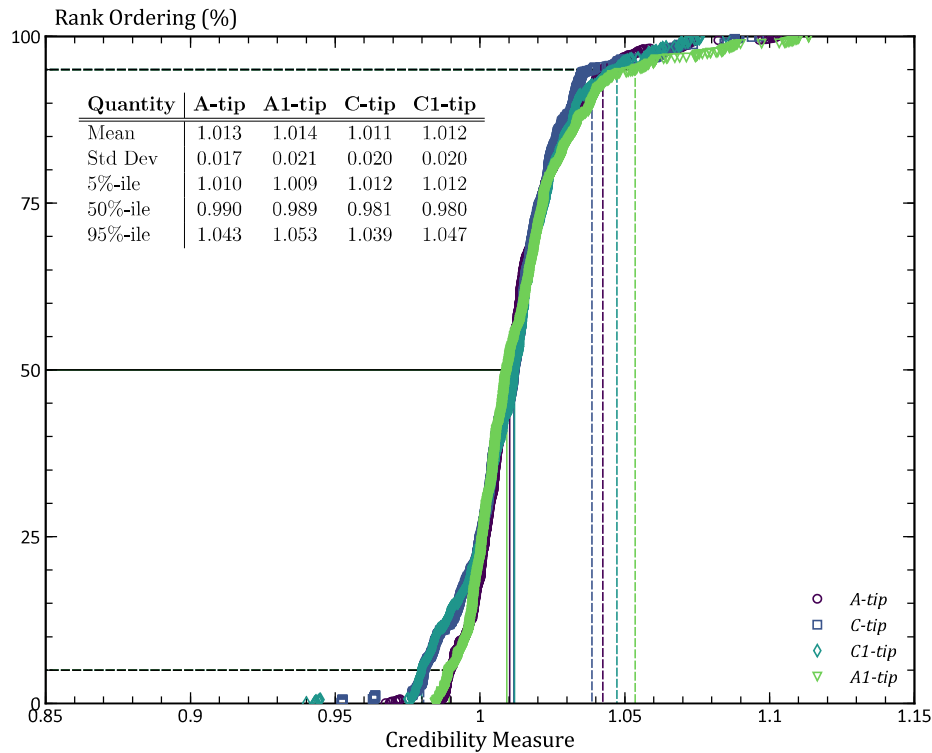


Figure 4.1.3: Verification plot for EC04 showing the cumulative distribution of discrepancies. The credibility measure is the ratio of the NASGRO SIF solution to the FEA SIF solution. This figure rank orders the credibility matrix and provides statistical quantity measures.

These results employ 205 geometries semi-randomly generated by Latin Hypercube methods. These geometries are independent on the calibration matrix. For this bivariant solution, Fig. 4.1.3 employs 12 stress gradients. The credibility measure is the ratio of the NASGRO SIF solution to the FEA SIF solution for the same solution.

As shown in Fig. 4.1.3, most ( $> 90\%$ ) of the SIF's values computed by NASGRO are within 5% of the value computed by high-fidelity FEA. Results shown here censor crack tips if their crack growth rate is less than  $10 \times$  the maximum growth rate at any other tip of the crack. Here, we assume that  $da/dN \propto \Delta K^3$ . For example, if  $F_I = 0.1$  at the  $a$ -tip and  $F_I = 1$  at the  $c$ -tip, then the  $a$ -tip would be removed from Fig. 4.1.3. These slow-growing crack tips do not support continued crack advance but produce long tails in the cumulative distributions that unnecessarily bias the result. NASGRO SIF solutions are generally conservative relative to the FEA SIF solutions.

## 4.2 EC05 – Elliptical Embedded Crack (Offset) in a Plate – Univariant WF

### 4.2.1 Overview

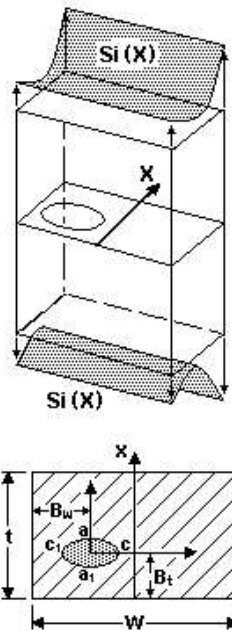


Figure 4.2.1: Configuration of case EC05

Crack case EC05 is a univariant weight function solution for an embedded crack in a plate with rectangular cross-section subjected to remote stressing. Both EC02 and EC05 are for a plate subjected to unvariant stressing. The differences are as follows: (1) EC05 makes use of a subset of the more accurate reference solutions generated for the EC04 crack case, (2) EC05 has wider solution limits, and (3) EC05 makes use of the point weight function similar to Glinka's derivation for surface cracks as detailed in the Theory section below.

### 4.2.2 Geometry

The geometric inputs used to define the crack geometry depicted in Fig. 4.2.1 are listed below:

- $t$  : plate thickness
- $W$  : plate full width
- $B_w$  : offset distance of the crack center from the plate left surface
- $B_t$  : offset distance of the crack center from the plate front surface
- $a$  : half the initial elliptical flaw size along the plate thickness direction
- $a/c$ : initial flaw aspect ratio, where  $c$  is half the crack size in the plate width direction

The solution limits in terms of dimensionless geometric parameters are given by:

$$\begin{aligned} 0 \leq \min\left(\frac{a}{B_t}, \frac{a}{t - B_t}\right) &\leq 0.99 \\ 0 \leq \min\left(\frac{c}{B_w}, \frac{c}{W - B_w}\right) &\leq 0.99 \\ 0.01 \leq a/c &\leq 10 \end{aligned}$$

Once the crack size reaches 99% of the shortest crack ligament, this case will self-transitions to either SC30, CC11, TC11, or TC12 depending on which case best represents the transitioning crack geometry. Appendix D of the NASGRO documentation provides more details of the transition process and the program logic employed to select the post-transition model.

#### 4.2.3 Loading

Stress loading can be defined in three different ways:

1. The user can apply a uniform tension ( $S_0$ ) and/or bending ( $S_1$ ) stresses at the remote ends of the plate. This is the default option in the GUI. The bending stress  $S_1$  is related to the applied moment  $M$  as:

$$S_1 = \frac{6M}{Wt^2} \quad (4.2.1)$$

2. The stress gradients can be defined via sixth-order polynomials along the normalized  $x$ -direction:

$$X = x/t \quad (4.2.2)$$

where  $x$  is the axis in the through-thickness direction of the plate. Up to four polynomials may be entered ( $S_0$  through  $S_3$ ).

3. The weight function solution also permits direct input of the principal normal stresses on the crack plane as pairs of ( $X_i$ ,  $S_i$ ). Here, the  $X$ -axis is the normalized coordinate defined in Eq. (4.2.2) above. The range of  $X$  for stress definition must be:  $0 \leq X \leq 1$ . Up to four separate tabular stress distributions ( $S_0$  to  $S_3$ ) can be defined by direct input in Geometry tab.

#### 4.2.4 Optional Features

The tension/bending and tabular stress input options of this case allow incorporation of a static residual stress field along the crack plane. See Section 11.6 for more details on how the residual stresses are accounted for in NASFLA.

The cyclic stress shakedown option is available to account for local plasticity. Refer to Appendix M of the manual for more details.

NASFLA allows separate definitions of tension/compression or t1/t2 stress gradients for this case when entered via tabular input. Refer to Sections 11.2 and 11.3 for further details about this capability.

#### 4.2.5 Development History

This SIF solution was introduced to NASGRO in v6.0. Geometry limits of this model were expanded to be consistent with EC02 in v8.1.

#### 4.2.6 Theory

This case assumes the stress variation is univariant and varying along the local  $x$ -axis. The 1D basic weight function varying along  $x$ -axis for  $a$ -,  $c$ -,  $a_1$ - and  $c_1$ -tips can be determined by integrating the point weight function for a penny-shape embedded crack in an infinite domain with a unit load along the chordal length intersected by a fixed  $x$ -value. By preserving the singular terms in the basic weight functions and on account of two sets of reference solution, the approximate 1D weight functions for an embedded crack with elliptical crack perimeter can thus be postulated as

$$\begin{aligned} W^a(x) &= \frac{2}{\sqrt{2\pi(a-x)}} \left[ 1 + M_1^a \sqrt{1 - \frac{x}{a}} + M_2^a \left( 1 - \frac{x}{a} \right) + M_3^a \left( 1 - \frac{x}{a} \right)^{3/2} \right] \\ W^{a_1}(x) &= \frac{2}{\sqrt{2\pi(a+x)}} \left[ 1 + M_1^{a_1} \sqrt{1 + \frac{x}{a}} + M_2^{a_1} \left( 1 + \frac{x}{a} \right) + M_3^{a_1} \left( 1 + \frac{x}{a} \right)^{3/2} \right] \\ W^c(x) = W^{c_1}(x) &= \begin{cases} \frac{1}{\sqrt{\pi x}} \left[ 1 + M_1^c \sqrt{\frac{x}{a}} + M_2^c \frac{x}{a} \right] & \text{if } x \geq 0 \\ \frac{1}{\sqrt{\pi(-x)}} \left[ 1 + M_1^c \sqrt{\frac{-x}{a}} + M_2^c \frac{x}{a} \right] & \text{if } x < 0 \end{cases} \end{aligned} \quad (4.2.3)$$

The coefficient  $M$ 's in the above equations are for correction terms, and the weight function solutions for  $a$ -,  $a_1$ - and  $c$ -tips (or  $c_1$ -tip) are given by

$$\begin{aligned} K^a &= \int_{-a}^a \frac{2\sigma(x)}{\sqrt{2\pi(a-x)}} \left[ 1 + M_1^a \sqrt{1 - \frac{x}{a}} + M_2^a \left( 1 - \frac{x}{a} \right) + M_3^a \left( 1 - \frac{x}{a} \right)^{3/2} \right] dx \\ K^{a_1} &= \int_{-a}^a \frac{2\sigma(x)}{\sqrt{2\pi(a+x)}} \left[ 1 + M_1^{a_1} \sqrt{1 + \frac{x}{a}} + M_2^{a_1} \left( 1 + \frac{x}{a} \right) + M_3^{a_1} \left( 1 + \frac{x}{a} \right)^{3/2} \right] dx \\ &= \int_{-a}^a \frac{2\sigma(-x)}{\sqrt{2\pi(a-x)}} \left[ 1 + M_1^{a_1} \sqrt{1 - \frac{x}{a}} + M_2^{a_1} \left( 1 - \frac{x}{a} \right) + M_3^{a_1} \left( 1 - \frac{x}{a} \right)^{3/2} \right] dx \\ K^c = K^{c_1} &= \int_0^a \frac{\sigma(x) + \sigma(-x)}{\sqrt{\pi x}} \left[ 1 + M_1^c \sqrt{\frac{x}{a}} + M_2^c \frac{x}{a} \right] dx \end{aligned} \quad (4.2.4)$$

These coefficients can be determined by boundary conditions and reference solutions. Details are described in the following

- At  $x = -a$ ,  $W^a(-a) = 0$  which leads to

$$1 + \sqrt{2}M_1^a + 2M_2^a + 2^{3/2}M_3^a = 0 \quad (4.2.5)$$

- Using the reference solutions at  $a$ -tip for reference stress  $\sigma(x) = 1$ ,  $K_u^a$  gives

$$K_u^a = \int_{-a}^a \frac{2}{\sqrt{2\pi(a-x)}} \left[ 1 + M_1^a \sqrt{1 - \frac{x}{a}} + M_2^a \left( 1 - \frac{x}{a} \right) + M_3^a \left( 1 - \frac{x}{a} \right)^{3/2} \right] dx \quad (4.2.6)$$

3. Using the other reference solutions at  $a$ -tip for reference stress  $\sigma(x) = x/a$ ;  $K_b^a$  gives

$$K_b^a = \int_{-a}^a \frac{2x/a}{\sqrt{2\pi(a-x)}} \left[ 1 + M_1^a \sqrt{1 - \frac{x}{a}} + M_2^a \left( 1 - \frac{x}{a} \right) + M_3^a \left( 1 - \frac{x}{a} \right)^{3/2} \right] dx \quad (4.2.7)$$

The above three conditions uniquely determine the coefficients for  $a$ -tip:  $M_1^a$ ,  $M_2^a$ , and  $M_3^a$ . Respectively, they are given by

$$\begin{aligned} M_1^a &= -4\sqrt{2} - \frac{3}{2} \frac{\pi}{\sqrt{2Q}} \tilde{K}_u^a + \frac{15}{2} \frac{\pi}{\sqrt{2Q}} \tilde{K}_b^a \\ M_2^a &= \frac{15}{2} + \frac{15}{4} \frac{\pi}{\sqrt{Q}} \tilde{K}_u^a - \frac{45}{4} \frac{\pi}{\sqrt{Q}} \tilde{K}_b^a \\ M_3^a &= -2\sqrt{2} - 3 \frac{\pi}{\sqrt{2Q}} \tilde{K}_u^a + \frac{15}{2} \frac{\pi}{\sqrt{2Q}} \tilde{K}_b^a \end{aligned} \quad (4.2.8)$$

where  $\tilde{K}_u^a$  and  $\tilde{K}_b^a$  are the normalized reference solutions of  $K_u^a$  and  $K_b^a$  by  $\sqrt{\pi a/Q}$  and  $Q$  is the shape factor for an ellipse. Using a similar approach, the other coefficients can be determined and listed as follows.

$$\begin{aligned} M_1^{a_1} &= -4\sqrt{2} - \frac{3}{2} \frac{\pi}{\sqrt{2Q}} \tilde{K}_u^{a_1} - \frac{15}{2} \frac{\pi}{\sqrt{2Q}} \tilde{K}_b^{a_1} \\ M_2^{a_1} &= \frac{15}{2} + \frac{15}{4} \frac{\pi}{\sqrt{Q}} \tilde{K}_u^{a_1} + \frac{45}{4} \frac{\pi}{\sqrt{Q}} \tilde{K}_b^{a_1} \\ M_3^{a_1} &= -2\sqrt{2} - 3 \frac{\pi}{\sqrt{2Q}} \tilde{K}_u^{a_1} - \frac{15}{2} \frac{\pi}{\sqrt{2Q}} \tilde{K}_b^{a_1} \\ M_1^c &= -4 + \frac{3}{2} \frac{\pi}{\sqrt{Q}} \tilde{K}_u^c \\ M_2^c &= 3 - \frac{3}{2} \frac{\pi}{\sqrt{Q}} \tilde{K}_u^c \end{aligned} \quad (4.2.9)$$

The normalized reference solutions are based on the same two reference stresses: unit tension and unit bending along the local  $x$ -axis.

#### 4.2.7 Verification

Verification of EC05 follows the verification procedure outlined in [52]. Full details of the verification effort can be found in that document. Fig. 4.2.2 presents the key verification plot for EC05. These results employ 205 geometries semi-randomly generated by Latin Hypercube methods. These geometries are independent on the calibration matrix. For this univariant solution, Fig. 4.2.2 employs 5 stress gradients. The credibility measure is the ratio of the NASGRO SIF solution to the FEA SIF solution for the same solution.

As shown in Fig. 4.2.2, most ( $> 90\%$ ) of the SIF's values computed by NASGRO are within 5% of the value computed by high-fidelity FEA. Results shown here censor crack tips if their crack growth rate is less than  $10\times$  the maximum growth rate at any other tip of the crack. Here, we assume that  $da/dN \propto \Delta K^3$ . For example, if  $F_I = 0.1$  at the  $a$ -tip and  $F_I = 1$  at the  $c$ -tip, then the  $a$ -tip

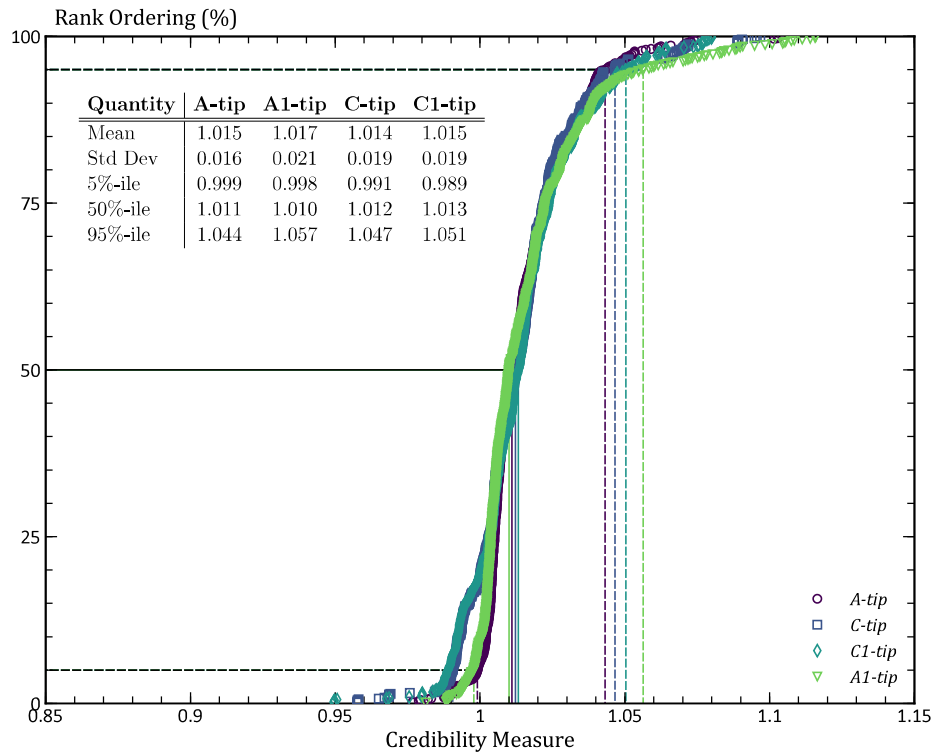


Figure 4.2.2: Verification plot for EC05 showing the cumulative distribution of discrepancies. The credibility measure is the ratio of the NASGRO SIF solution to the FEA SIF solution. This figure rank orders the credibility matrix and provides statistical quantity measures.

would be removed from Fig. 4.2.2. These slow-growing crack tips do not support continued crack advance but produce long tails in the cumulative distributions that unnecessarily bias the result. NASGRO SIF solutions are generally conservative relative to the FEA SIF solutions.

## 5 Surface Cracks

### 5.1 SC01 – Semi-elliptical Surface Crack in Plate – Tension and Bending

#### 5.1.1 Overview

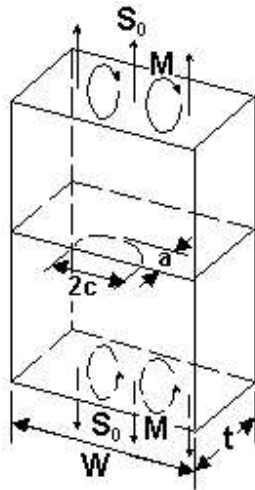


Figure 5.1.1: Configuration of the crack case SC01

SC01 is for surface cracks of semi-elliptical shape in a finite plate. The crack is located at the center of the plate surface.

Note that newer crack cases (SC30 and SC31) with much broader geometry ranges have been developed for this crack geometry. Both SC30 and SC31 support symmetric and offset crack positions. SC01 and its companion SC02 are legacy solutions that have good accuracy and will generally give similar answers to SC30 and SC31.

#### 5.1.2 Geometry

The crack configuration is depicted in Fig. 5.1.1. The cracked plate geometry is defined by four input parameters:

- $W$  : plate full width
- $t$  : plate thickness
- $a$  : crack depth
- $a/c$ : crack aspect ratio

The crack size and aspect ratio are bounded by:

$$0 < \frac{2c}{W} \leq 1$$

$$0.1 \leq \frac{a}{c} \leq 1.2$$

### 5.1.3 Loading

SC01 supports remote uniform tension stress  $S_0$  and remote out-of-plane bending stress  $S_1$ . The peak bending stress across the plate thickness  $S_1$  is related to the applied moment  $M$  shown in Fig. 5.1.1 by:

$$S_1 = \frac{6M}{Wt^2} \quad (5.1.1)$$

Note that the newer cases SC30 (univariant) and SC31 (bivariant) are weight function solutions that allow arbitrary crack plane stress gradients. SC30 also allows convenient specification of remote tension and bend stresses.

### 5.1.4 Theory

SIFs are computed by direct tabular interpolation of the finite element solutions given in Tables 5.1.1 and 5.1.2. The SIFs were computed using nodal forces ahead of the crack tip. More details and additional results may be found in [58] for certain types of nonuniform loads. The values listed in Tables 5.1.1 and 5.1.2 are factors  $F\sqrt{Q}$  defined as

$$\begin{aligned} F_0\sqrt{Q} &= \frac{K_I}{S_0\sqrt{\pi a/Q}} && \text{for tension} \\ F_1\sqrt{Q} &= \frac{K_I}{S_1\sqrt{\pi a/Q}} && \text{for bending} \end{aligned} \quad (5.1.2)$$

where,  $S_0$  and  $S_1$  are the applied tension and peak bending stresses,  $Q$  is given by:

$$Q = \begin{cases} 1 + 1.464(a/c)^{1.65} & \text{for } a/c \leq 1 \\ 1 + 1.464(c/a)^{1.65} & \text{for } a/c > 1 \end{cases} \quad (5.1.3)$$

NASSIF outputs the geometry factors in two forms for this case:  $F_0$ ,  $F_1$  and  $F_0\sqrt{Q}$ ,  $F_1\sqrt{Q}$ .

References: [58]

Table 5.1.1: Stress intensity correction factors due to tension ( $F_0\sqrt{Q}$ ) for the case SC01.

		At the $c$ -tip: Tensile Loading				
$2c/W$	$a/c$	$a/t$				
		0.0	0.2	0.5	0.8	1.0
0.0	0.2	0.5622	0.6110	0.7802	1.1155	1.4436
0.0	0.4	0.6856	0.7817	0.9402	1.1583	1.3383
0.0	1.0	1.1365	1.1595	1.2328	1.3772	1.5145
0.1	0.2	0.5685	0.6133	0.7900	1.1477	1.5014
0.1	0.4	0.6974	0.7824	0.9456	1.2008	1.4256
0.1	1.0	1.1291	1.1544	1.2389	1.3892	1.5273
0.4	0.2	0.5849	0.6265	0.8438	1.3154	1.7999
0.4	0.4	0.7278	0.8029	1.0127	1.4012	1.7739
0.4	1.0	1.1366	1.1969	1.3475	1.5539	1.7238
0.6	0.2	0.5939	0.6415	0.9045	1.5056	2.1422
0.6	0.4	0.7385	0.8351	1.1106	1.6159	2.1036
0.6	1.0	1.1720	1.2855	1.5215	1.8229	2.0621
0.8	0.2	0.6155	0.6739	1.0240	1.8964	2.8650
0.8	0.4	0.7778	0.9036	1.3151	2.1102	2.9068
0.8	1.0	1.2630	1.4957	1.9284	2.4905	2.9440
1.0	0.2	0.6565	0.7237	1.2056	2.6060	4.2705
1.0	0.4	0.8375	1.0093	1.6395	2.9652	4.3596
1.0	1.0	1.3956	1.8446	2.6292	3.6964	4.5865

		At the $a$ -tip: Tensile Loading				
$2c/W$	$a/c$	$a/t$				
		0.0	0.2	0.5	0.8	1.0
0.0	0.2	1.1120	1.1445	1.4504	1.7620	1.9729
0.0	0.4	1.0900	1.0945	1.2409	1.3672	1.4404
0.0	1.0	1.0400	1.0400	1.0672	1.0883	1.0800
0.1	0.2	1.1120	1.1452	1.4595	1.7744	1.9847
0.1	0.4	1.0900	1.0950	1.2442	1.3699	1.4409
0.1	1.0	1.0400	1.0260	1.0579	1.0846	1.0820
0.4	0.2	1.1120	1.1577	1.5126	1.8662	2.1012
0.4	0.4	1.0900	1.1140	1.2915	1.4254	1.4912
0.4	1.0	1.0400	1.0525	1.1046	1.1093	1.0863
0.6	0.2	1.1120	1.1764	1.5742	1.9849	2.2659
0.6	0.4	1.0900	1.1442	1.3617	1.5117	1.5761
0.6	1.0	1.0400	1.1023	1.1816	1.1623	1.0955
0.8	0.2	1.1120	1.2047	1.6720	2.2010	2.5895
0.8	0.4	1.0900	1.1885	1.4825	1.6849	1.7727
0.8	1.0	1.0400	1.1685	1.3089	1.2767	1.1638
1.0	0.2	1.1120	1.2426	1.8071	2.5259	3.0993
1.0	0.4	1.0900	1.2500	1.6564	1.9534	2.0947
1.0	1.0	1.0400	1.2613	1.4890	1.4558	1.3010

Table 5.1.2: Stress intensity correction factors due to bending ( $F_1\sqrt{Q}$ ) for the case SC01.

		At the $c$ -tip: Bending Loading				
$2c/W$	$a/c$	$a/t$				
		0.0	0.2	0.5	0.8	1.0
0.0	0.2	0.5622	0.5772	0.6464	0.7431	0.8230
0.0	0.4	0.6856	0.7301	0.7694	0.7358	0.6729
0.0	1.0	1.1365	1.0778	1.0184	0.9716	0.9474
0.1	0.2	0.5685	0.5809	0.6524	0.7646	0.8624
0.1	0.4	0.6974	0.7315	0.7856	0.8008	0.7895
0.1	1.0	1.1291	1.0740	1.0114	0.9652	0.9435
0.4	0.2	0.5849	0.5981	0.6934	0.8654	1.0249
0.4	0.4	0.7278	0.7519	0.8327	0.9312	1.0068
0.4	1.0	1.1366	1.1079	1.0634	1.0358	1.0268
0.6	0.2	0.5939	0.6158	0.7438	0.9704	1.1802
0.6	0.4	0.7385	0.7816	0.8906	1.0215	1.1211
0.6	1.0	1.1720	1.1769	1.1759	1.1820	1.1900
0.8	0.2	0.6155	0.6446	0.8320	1.1794	1.5113
0.8	0.4	0.7778	0.8386	1.0150	1.2791	1.5073
0.8	1.0	1.2630	1.3633	1.4785	1.5360	1.5431
1.0	0.2	0.6565	0.6848	0.9593	1.5053	2.0518
1.0	0.4	0.8375	0.9232	1.2285	1.7607	2.2637
1.0	1.0	1.3956	1.6821	2.0140	2.1482	2.1446

		At the $a$ -tip: Bending Loading				
$2c/W$	$a/c$	$a/t$				
		0.0	0.2	0.5	0.8	1.0
0.0	0.2	1.1120	0.8825	0.6793	0.3063	-0.0497
0.0	0.4	1.0900	0.8292	0.5291	0.1070	-0.2489
0.0	1.0	1.0400	0.7411	0.3348	-0.1149	-0.4396
0.1	0.2	1.1120	0.8727	0.6697	0.3071	-0.0348
0.1	0.4	1.0900	0.8243	0.5170	0.1047	-0.2336
0.1	1.0	1.0400	0.7398	0.3322	-0.1172	-0.4408
0.4	0.2	1.1120	0.8683	0.6794	0.3439	0.0291
0.4	0.4	1.0900	0.8330	0.5270	0.1257	-0.1989
0.4	1.0	1.0400	0.7602	0.3572	-0.1080	-0.4543
0.6	0.2	1.1120	0.8904	0.7248	0.4033	0.0915
0.6	0.4	1.0900	0.8625	0.5803	0.1678	-0.1874
0.6	1.0	1.0400	0.7982	0.4072	-0.0856	-0.4750
0.8	0.2	1.1120	0.9191	0.7925	0.5102	0.2254
0.8	0.4	1.0900	0.8987	0.6619	0.2524	-0.1300
0.8	1.0	1.0400	0.8556	0.4981	-0.0329	-0.4960
1.0	0.2	1.1120	0.9545	0.8827	0.6666	0.4351
1.0	0.4	1.0900	0.9417	0.7723	0.3810	-0.0250
1.0	1.0	1.0400	0.9323	0.6312	0.0505	-0.5249

## 5.2 SC02 – Semi-elliptical Surface Crack in Plate – Univariant WF

### 5.2.1 Overview

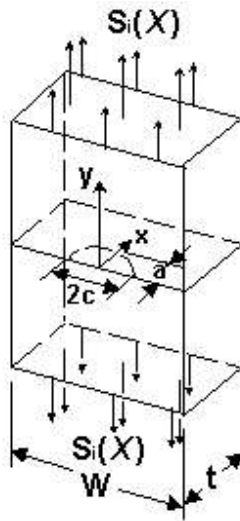


Figure 5.2.1: Configuration of the crack case SC02

This is a more general version of the case SC01, where the loading may include nonlinear stresses across the plate thickness. The semi-elliptical crack is symmetrically located at the center of the front face of the finite-width plate.

Note that newer crack cases (SC30 and SC31) with much broader geometry ranges have been developed for this crack geometry. Both SC30 and SC31 support symmetric and offset crack positions. SC01 and its companion SC02 are legacy solutions that have good accuracy and will generally give similar answers to SC30 and SC31.

### 5.2.2 Geometry

The cracked plate geometry is shown in Fig. 5.2.1. It requires four geometric input parameters:

- $W$  : plate full width
- $t$  : plate thickness
- $a$  : crack depth
- $a/c$ : crack aspect ratio

The crack size and aspect ratio are bounded by:

$$0 < \frac{2c}{W} \leq 1$$

$$0.1 \leq \frac{a}{c} \leq 1.2$$

### 5.2.3 Loading

The stress variation across the thickness of a plate is input in a discrete form as pairs of  $(X_i, S_i)$ , where  $X_i = x_i/t$ . The  $x$ -axis starts at the center of the crack mouth and points toward the

deepest point  $a$  along the crack front as shown in Fig. 5.2.1. The normalized axis  $X$  is bounded by  $0 \leq X \leq 1$ . Up to four such nonlinear stress distributions ( $S_0$  through  $S_3$ ) may be input. Once the discretized gradients are entered, a plot of the data and a smooth curve through them may be obtained in the “Geometry” tab of the GUI.

Note that the newer univariant and bivariant weight function based crack cases (SC30 and SC31) provide additional capabilities such as 2D crack plane stress gradients, residual stresses and stress shakedown.

#### 5.2.4 Theory

A weight function method developed to obtain the stress intensity factors of this crack case is detailed in [58]. The approach is summarized below.

For univariant stress distributions varying along the  $x$ -axis of the potential crack plane (see Fig. 5.2.1), the stress intensity factor can be obtained from the weight function formulation given by

$$K_r = \int_0^a \sigma_r(x) m(x, a) dx \quad (5.2.1)$$

where,  $\sigma_r(x)$  is the stress distribution on the crack plane and  $m(x, a)$  is the weight function that depends on the crack depth  $a$  and the position along the crack face  $x$ . Glinka and Shen [59] have developed following approximate weight functions for semi-elliptical surface cracks:

- for the deepest point ( $a$ -tip)

$$m_a(x, a) = \frac{2}{\sqrt{2\pi(a-x)}} \left( 1 + M_{1a} \left( 1 - \frac{x}{a} \right)^{1/2} + M_{2a} \left( 1 - \frac{x}{a} \right) + M_{3a} \left( 1 - \frac{x}{a} \right)^{3/2} \right) \quad (5.2.2)$$

- for the surface point ( $c$ -tip)

$$m_c(x, a) = \frac{2}{\sqrt{2\pi x}} \left( 1 + M_{1c} \left( \frac{x}{a} \right)^{1/2} + M_{2c} \left( \frac{x}{a} \right) + M_{3c} \left( \frac{x}{a} \right)^{3/2} \right) \quad (5.2.3)$$

where,  $M_1$ ,  $M_2$  and  $M_3$  are the constants that can be determined from two reference solutions and a condition imposed on the weight function as explained in [59].

The two reference solutions used for this case are uniform tension and linearly decreasing stress fields as shown in Fig. 5.2.2a and Fig. 5.2.2b, respectively.

The stress intensity factor for the uniform tension is expressed as

$$K_{r1} = F_{r1} \sigma_0 \sqrt{\pi a / Q} \quad \text{for } \sigma_{r1}(x) = \sigma_0 \quad (5.2.4)$$

and for the tapered stress distribution, it is

$$K_{r2} = F_{r2} \sigma_0 \sqrt{\pi a / Q} \quad \text{for } \sigma_{r2}(x) = \sigma_0 \left( 1 - \frac{x}{a} \right) \quad (5.2.5)$$

where,  $Q$  is defined in Eq. (5.1.3). For the given crack size and plate dimensions, the reference geometry factors  $F_{r1}$  and  $F_{r2}$  can be looked up from Tables 5.1.1 and 5.1.2 using the following relations

$$F_{r1} = F_0^{SC01} \sqrt{Q} \quad (5.2.6)$$

$$F_{r2} = \left( 1 - \frac{1}{2a/t} \right) F_0^{SC01} \sqrt{Q} - \frac{F_1^{SC01} \sqrt{Q}}{2a/t} \quad (5.2.7)$$

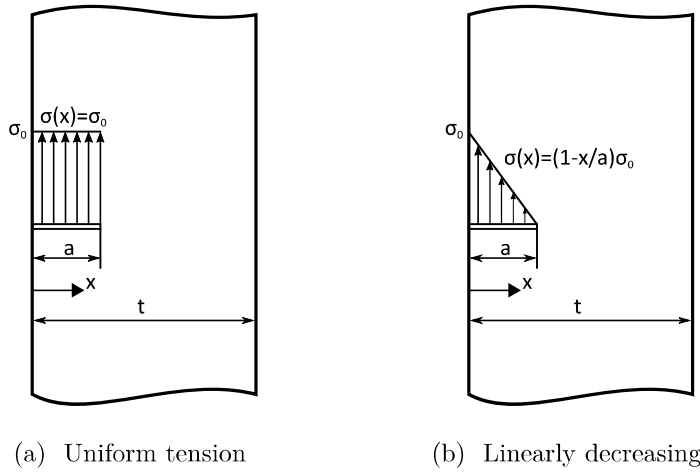


Figure 5.2.2: Two reference solutions used in the weight function method.

### Coefficients $M_i$ for the $a$ -tip

The weight function condition for the  $a$ -tip is that the second derivative of  $m(x, a)$  must equal to zero at  $x = 0$  [59]

$$\frac{\partial m_a(x, a)}{\partial x^2} \Big|_{x=0} = 0 \quad (5.2.8)$$

This condition leads to

$$M_{2a} = 3 \quad (5.2.9)$$

The other two constants can be solved for by plugging the Eq. (5.2.2) to Eq. (5.2.1) for the two reference conditions given in Eqs. (5.2.4) and (5.2.5), which will give

$$M_{1a} = \frac{\pi}{\sqrt{2Q}}(4F_{r1} - 6F_{r2}) - \frac{24}{5} \quad (5.2.10)$$

$$M_{3a} = 2 \left( \frac{\pi}{\sqrt{2Q}}F_{r1} - M_{1a} - 4 \right) \quad (5.2.11)$$

### Coefficients $M_i$ for the $c$ -tip

The weight function condition for the  $c$ -tip is that it vanishes  $x = a$  which gives [59]

$$1 + M_{1c} + M_{2c} + M_{3c} = 0 \quad (5.2.12)$$

The next two equations are obtained by plugging in the Eq. (5.2.3) to Eq. (5.2.1) for the two reference solutions given in Eqs. (5.2.4) and (5.2.5). Solving these three equations for three coefficients will give

$$M_{1c} = \frac{\pi}{\sqrt{4Q}}(30F_{r2} - 18F_{r1}) - 8 \quad (5.2.13)$$

$$M_{2c} = \frac{\pi}{\sqrt{4Q}}(60F_{r1} - 90F_{r2}) + 15 \quad (5.2.14)$$

$$M_{3c} = -(1 + M_{1c} + M_{2c}) \quad (5.2.15)$$

Once the coefficients ( $M_i$ ) of the weight function are determined for the given crack size, aspect ratio and plate dimensions, the Eq. (5.2.1) can be numerically integrated to determine the stress intensity factors for any stress distributions along the plane of the crack. Additional details can be found in [60] including quadratic and cubic loadings that were used to verify the weight function method.

References: [58, 59, 60]

### 5.3 SC03 – Semi-elliptical Surface Crack in Pressurized Sphere

#### 5.3.1 Overview

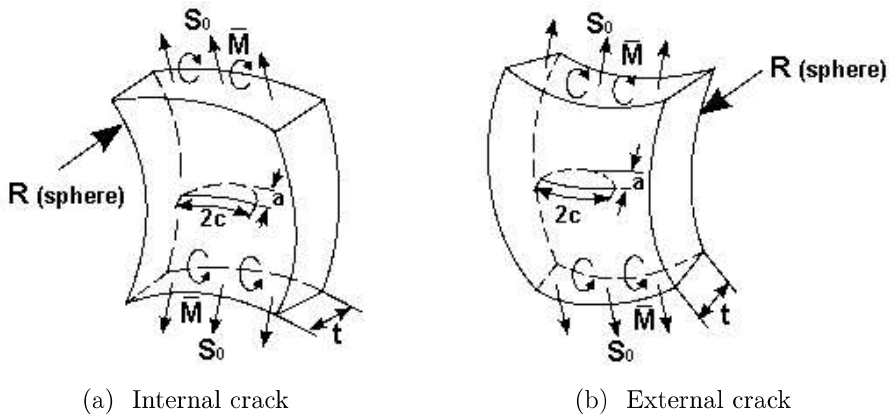


Figure 5.3.1: Configuration of the crack case SC03

This case is for a semi-elliptical surface crack in a pressurized sphere. The crack is located either on the exterior or interior surface as shown in Figs. 5.3.1a and 5.3.1b, respectively.

#### 5.3.2 Geometry

Four input parameters are used to define the geometry of this crack configuration:

- $R$  : inner radius of the sphere
- $t$  : wall thickness of the sphere
- $a$  : crack depth
- $a/c$ : crack aspect ratio

This model has following validity ranges:

$$1 \leq R/t$$

$$0.1 \leq a/c \leq 1.2$$

If the bending stress  $S_1$  is absent, this case will self-transition to a through crack (TC06) of length “ $2c$ ” when the crack depth reaches the wall thickness, i.e.  $a/t \geq 1$ . The effect of crack face pressure exerting on internal crack of SC03, if applied, is neglected after transition. Refer to Appendix D of the NASGRO manual for further details about case transitions.

### 5.3.3 Loading

SC03 supports uniform tension ( $S_0$ ) and bending ( $S_1$ ) stresses. Crack face pressure loading is also available via  $S_4$  for internal cracks only. Note that if stresses are input via a long block format in NASFLA,  $S_4$  values must use columns 6 and 7, the data fields normally reserved for  $S_2$  (which is not used for this case).

The maximum bending stress across the wall thickness ( $S_1$ ) is related to the uniform moment per unit length ( $\bar{M}$ ) shown in Fig. 5.3.1 as:

$$S_1 = \frac{6\bar{M}}{t^2} \quad (5.3.1)$$

### 5.3.4 Theory

The solution for this crack case is made up of a combination of the flat plate solution (SC01) assuming a wide plate and applying the corrections due to the curvature from crack cases SC04 and SC05 for cylinders. This procedure was applied only for tensile loading. The solution for bending stress is assumed to be the same as that of a flat plate.

$$F_0 = F_{01} \left( \frac{F_{04}}{F_{01}} \right) \left( \frac{F_{05}}{F_{01}} \right) \quad (5.3.2)$$

$$F_1 = F_{11}$$

The geometry factors  $F_{01}$ ,  $F_{11}$  are obtained from Tables 5.1.1 and 5.1.2 for wide plates using  $2c/W = 0.05$  for tension and bending, respectively. The factor  $F_{04}$  is obtained from Tables 5.4.1 and 5.4.2 for the crack case SC04 under uniform tension. The factor  $F_{05}$  is obtained from Tables 5.5.1 and 5.5.2 for the crack case SC05 for tension.

By the principle of superposition, the geometry factor  $F_4$  due to the crack face pressure  $S_4$  comes out to be the same as  $F_0$  for remote tension:

$$F_4 = F_0 \quad (5.3.3)$$

References: [61]

## 5.4 SC04 – Semi-elliptical Surface Crack (Axial) in a Hollow Cylinder – Univariant WF

### 5.4.1 Overview

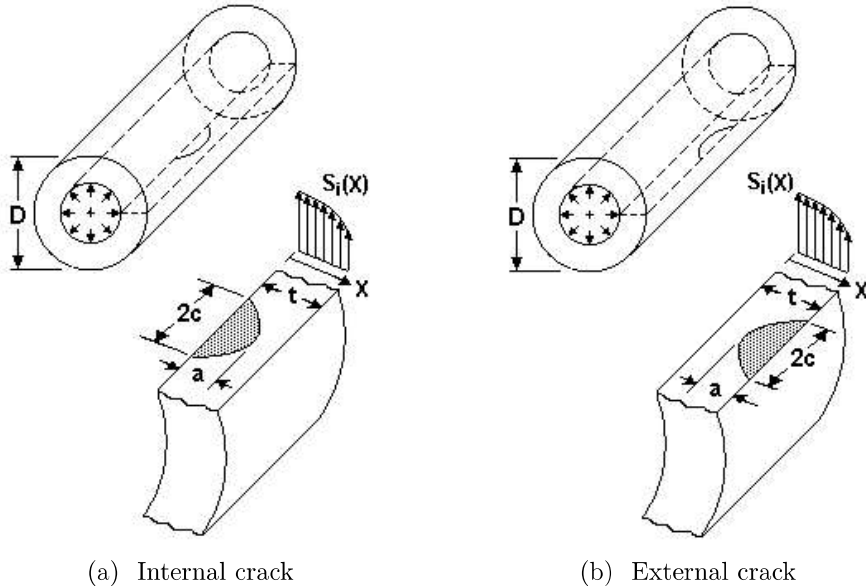


Figure 5.4.1: Configuration of the crack case SC04

This crack configuration represents an axial part-through crack of semi-elliptical shape in a hollow cylinder. The crack can be defined either on the interior or on the exterior surface of the cylinder. The model can be loaded by a combination of non-linear hoop stress across the cylinder wall and internal pressure.

For circumferentially oriented cracks in hollow cylinders, see the cases SC05 and SC06. Refer to SC10 for surface cracks in threaded hollow cylinders.

### 5.4.2 Geometry

The geometry of this configuration is shown in Fig. 5.4.1 for the internal and external cracks. The cracked hollow cylinder is defined by four geometric parameters:

- $D$  : cylinder outer diameter
- $t$  : cylinder wall thickness
- $a$  : crack depth
- $a/c$ : crack aspect ratio

The model validity ranges of the geometry, crack size and aspect ratio are:

$$4 \leq D/t$$

$$0 \leq a/t \leq 1$$

$$0.1 \leq a/c \leq 1.2$$

When the crack depth reaches the cylinder wall thickness, i.e.  $a/t \geq 1$ , this case will transition to

a through crack case TC07 with the crack length set to  $2c$ . Refer to Appendix D of the NASGRO manual for further details about case transitions.

### 5.4.3 Loading

The stress variation across the cylinder wall is defined in a discrete form as pairs of  $(X_i, S_i)$ , where  $X_i = x_i/t$ . The  $x$ -axis starts at the inner wall. The normalized axis  $X$  is bounded by  $0 \leq X \leq 1$ . Regardless of whether the crack is on the inside or outside, the stress distribution must be defined beginning on the inside surface ( $X = 0$ ) to the outside surface ( $X = 1$ ). Up to four such nonlinear stress distributions ( $S_0$  through  $S_3$ ) may be input. Once the discretized gradient is entered, a plot of the data and a smooth curve through it may be obtained in the “Geometry” tab of the GUI.

Provision is also made in the program to allow the user to specify internal pressure in the cylinder, for which hoop stresses are calculated by the program. This loading option can be activated by checking the box next to “S0 from unit internal pressure” in the “Geometry” tab. In the case of an internal crack, the operative stresses (in the weight function calculation of  $K_I$ ) are the sum of the hoop stresses and the crack-face pressure, while for an external crack, hoop stresses alone are present.

### 5.4.4 Theory

This model makes use of a weight function method similar to the case SC02, the theory of which is summarized in Section 5.2.4. The weight function for an axial surface crack in a hollow cylinder is assumed to be of the same form as in flat plates. The effects of curvature are introduced by the reference solution. Additional details of the background work can be found in [60, 61], including quadratic and cubic loadings that were used to verify the weight function method.

Two reference solutions were obtained using the finite element method with applied stressing of a form  $\sigma_0(x/a)^n$ . The normalized stress intensity factors  $F_{ref}\sqrt{Q}$  for the uniform ( $n = 0$ ) and linear stresses ( $n = 1$ ) are provided in Tables 5.4.1 and 5.4.2, respectively. Normalization on  $K$  is done as follows:

$$F_{ref}\sqrt{Q} = \frac{K_I}{\sigma_0 \sqrt{\pi a/Q}} \quad (5.4.1)$$

where,  $Q$  is defined by

$$Q = \begin{cases} 1 + 1.464(a/c)^{1.65} & \text{for } a/c \leq 1 \\ 1 + 1.464(c/a)^{1.65} & \text{for } a/c > 1 \end{cases} \quad (5.4.2)$$

The term  $R$  in these tables denotes the inner radius, i.e.  $R = D/2 - t$ . These reference solutions are used to determine the coefficients of the weight function for the given crack size and cylinder dimensions. Then, the  $K$  solutions for arbitrary nonlinear stresses are obtained by numerical integration.

NASSIF outputs the geometry factors in two forms for this case:  $F$  and  $F\sqrt{Q}$ .

Reference: [60, 61]

Table 5.4.1: Reference SIF Correction Factors for SC04 – Internal Longitudinal Cracks,  $F_{ref}$ 

$R/t$	$a/t =$	$a/c = 0.2$					$a/c = 0.4$					$a/c = 1.0$				
		0	.2	.5	.8	1.0	0	.2	.5	.8	1.0	0	.2	.5	.8	1.0
<i>c-tip, Uniform Loading (n=0)</i>																
1	0.608	0.615	0.871	1.554	2.277	0.740	0.745	0.916	1.334	1.752	1.044	1.080	1.116	1.217	1.315	
2	0.600	0.614	0.817	1.300	1.783	0.730	0.760	0.919	1.231	1.519	1.132	1.113	1.155	1.286	1.416	
4	0.577	0.606	0.797	1.201	1.586	0.737	0.770	0.924	1.219	1.487	1.119	1.128	1.191	1.316	1.428	
10	0.579	0.607	0.791	1.179	1.548	0.733	0.777	0.936	1.219	1.469	1.114	1.140	1.219	1.348	1.456	
50	0.582	0.613	0.790	1.148	1.482	0.721	0.782	0.946	1.201	1.413	1.133	1.154	1.239	1.389	1.520	
<i>c-tip, Linear Loading (n=1.0)</i>																
1	0.083	0.085	0.171	0.363	0.544	0.112	0.119	0.181	0.307	0.421	0.169	0.182	0.200	0.218	0.229	
2	0.078	0.083	0.150	0.291	0.421	0.072	0.122	0.197	0.271	0.317	0.192	0.190	0.207	0.247	0.285	
4	0.070	0.079	0.141	0.262	0.370	0.110	0.123	0.174	0.263	0.339	0.188	0.194	0.214	0.248	0.277	
10	0.070	0.079	0.138	0.253	0.356	0.109	0.125	0.176	0.259	0.328	0.187	0.197	0.221	0.255	0.282	
50	0.068	0.081	0.138	0.239	0.328	0.103	0.127	0.180	0.253	0.310	0.189	0.201	0.227	0.265	0.294	
<i>a-tip, Uniform Loading (n=0)</i>																
1	1.076	1.056	1.395	2.530	3.846	1.051	1.011	1.149	1.600	2.087	0.992	0.987	1.010	1.155	1.314	
2	1.049	1.091	1.384	2.059	2.739	1.075	1.045	1.160	1.510	1.876	1.037	1.003	1.023	1.129	1.242	
4	1.003	1.097	1.405	1.959	2.461	1.024	1.057	1.193	1.443	1.665	1.005	1.009	1.041	1.105	1.162	
10	0.973	1.115	1.427	1.872	2.230	0.992	1.072	1.217	1.393	1.521	0.994	1.015	1.050	1.090	1.118	
50	0.936	1.145	1.459	1.774	1.974	0.982	1.095	1.244	1.370	1.438	1.002	1.026	1.058	1.085	1.099	
<i>a-tip, Linear Loading (n=1.0)</i>																
1	0.693	0.647	0.767	1.174	1.615	0.689	0.646	0.694	0.889	1.093	0.704	0.701	0.709	0.730	0.750	
2	0.673	0.661	0.764	1.033	1.301	0.674	0.659	0.710	0.854	0.995	0.732	0.707	0.714	0.774	0.840	
4	0.649	0.666	0.776	0.996	1.197	0.668	0.666	0.715	0.828	0.934	0.720	0.713	0.726	0.768	0.810	
10	0.635	0.673	0.783	0.960	1.108	0.656	0.672	0.723	0.806	0.875	0.715	0.715	0.729	0.760	0.788	
50	0.620	0.681	0.790	0.917	1.008	0.651	0.677	0.727	0.791	0.838	0.716	0.715	0.726	0.751	0.775	

Note:  $R$  is the inner radius of the cylinder

Table 5.4.2: Reference SIF Correction Factors for SC04 – External Longitudinal Cracks,  $F_{ref}$ 

$R/t$	$a/t =$	$a/c = 0.2$					$a/c = 0.4$					$a/c = 1.0$				
		0	.2	.5	.8	1.0	0	.2	.5	.8	1.0	0	.2	.5	.8	1.0
<i>c</i> -tip, Uniform Loading (n=0)																
1	0.755	0.594	0.648	1.293	2.129	0.889	0.809	0.934	1.492	2.143	1.148	1.202	1.354	1.594	1.796	
2	0.720	0.611	0.693	1.207	1.826	0.817	0.796	0.959	1.425	1.915	1.152	1.185	1.318	1.560	1.775	
4	0.589	0.612	0.786	1.160	1.517	0.754	0.793	0.994	1.400	1.781	1.127	1.163	1.286	1.498	1.681	
10	0.598	0.612	0.806	1.262	1.715	0.750	0.788	0.984	1.378	1.747	1.123	1.156	1.266	1.453	1.613	
50	0.582	0.613	0.790	1.148	1.482	0.721	0.782	0.946	1.201	1.413	1.133	1.154	1.239	1.389	1.520	
<i>c</i> -tip, Linear Loading (n=1.0)																
1	0.153	0.076	0.089	0.271	0.481	0.170	0.132	0.170	0.329	0.497	0.202	0.214	0.256	0.327	0.387	
2	0.121	0.079	0.105	0.245	0.395	0.140	0.130	0.182	0.315	0.443	0.196	0.209	0.250	0.315	0.370	
4	0.073	0.080	0.134	0.242	0.339	0.118	0.130	0.195	0.318	0.427	0.189	0.204	0.243	0.302	0.350	
10	0.078	0.080	0.142	0.277	0.402	0.114	0.128	0.192	0.309	0.411	0.188	0.202	0.236	0.286	0.326	
50	0.068	0.081	0.138	0.239	0.328	0.103	0.127	0.180	0.253	0.310	0.189	0.201	0.227	0.265	0.294	
<i>a</i> -tip, Uniform Loading (n=0)																
1	1.244	1.237	1.641	2.965	4.498	1.146	1.175	1.452	2.119	2.800	1.030	1.054	1.146	1.305	1.442	
2	1.111	1.193	1.655	2.732	3.842	1.077	1.136	1.403	1.942	2.454	1.020	1.044	1.117	1.236	1.335	
4	1.009	1.162	1.640	2.510	3.313	1.000	1.109	1.360	1.727	2.025	0.986	1.030	1.094	1.156	1.194	
10	0.981	1.147	1.584	2.298	2.921	0.975	1.096	1.310	1.565	1.749	0.982	1.025	1.078	1.118	1.137	
50	0.936	1.145	1.459	1.774	1.974	0.982	1.095	1.244	1.370	1.438	1.002	1.026	1.058	1.085	1.099	
<i>a</i> -tip, Linear Loading (n=1.0)																
1	0.754	0.719	0.867	1.336	1.839	0.716	0.709	0.806	1.046	1.279	0.715	0.725	0.760	0.817	0.866	
2	0.688	0.700	0.868	1.255	1.634	0.685	0.692	0.785	0.984	1.168	0.720	0.722	0.746	0.797	0.844	
4	0.650	0.691	0.861	1.178	1.464	0.655	0.685	0.773	0.914	1.032	0.711	0.720	0.743	0.777	0.804	
10	0.636	0.685	0.839	1.099	1.323	0.645	0.680	0.755	0.858	0.938	0.709	0.718	0.738	0.765	0.786	
50	0.620	0.681	0.790	0.917	1.008	0.651	0.677	0.727	0.791	0.838	0.716	0.715	0.726	0.751	0.775	

Note:  $R$  is the inner radius of the cylinder

## 5.5 SC05 – Semi-elliptical Surface Crack (Circumferential) in Hollow Cylinder

### 5.5.1 Overview

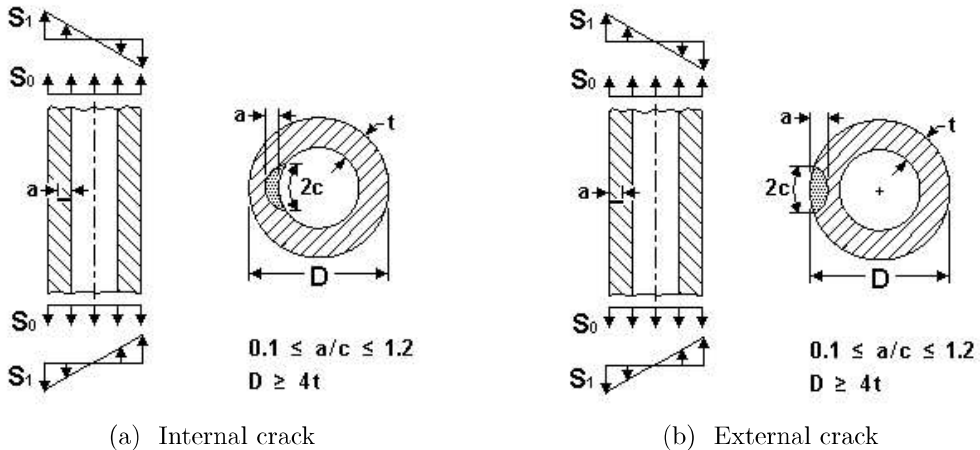


Figure 5.5.1: Configuration of the crack case SC05

This case is for a semi-elliptical surface crack in a hollow cylinder. The crack is circumferentially oriented, and it can be defined on either the interior or exterior surface of the hollow cylinder. The model is loaded by a combination of remote tension stress and bending stress.

For an axially oriented crack in a hollow cylinder, refer to the case SC04. See the next case (SC06) for a constant-depth circumferential crack in a hollow cylinder.

### 5.5.2 Geometry

The case geometries for both internal and external cracks are shown in Fig. 5.5.1. The cracked cylinder is defined by four geometric parameters:

- $D$  : cylinder outer diameter
  - $t$  : cylinder wall thickness
  - $a$  : crack depth
  - $a/c$ : crack aspect ratio

The model validity ranges of the geometry, crack size and aspect ratio are:

$$4 \leq D/t$$

$$0 \leq a/t \leq 1$$

$$0.1 \leq a/c \leq 1.2$$

When the crack depth reaches the cylinder wall thickness, i.e.  $a/t \geq 1$ , this case will transition to a through crack case TC08 with the crack length set to  $2c$ . Refer to Appendix D of the NASGRO manual for further details about case transitions.

### 5.5.3 Loading

SC05 allows two types of external loading: (a) remote tension stress  $S_0$  and (b) remote bending stress  $S_1$ . The bending moment is applied in such a way so that the resulting stress magnitude is maximized at the center of the crack mouth.

### 5.5.4 Theory

The solution is based on direct tabular interpolation of the finite element results given in Tables 5.5.1 and 5.5.2. The values listed are factors  $F_0$  for tension and  $F_1$  for bending. The term  $R$  in these tables denotes the inner radius, i.e.  $R = D/2 - t$ .

The geometry factors are normalized as follows:

$$\begin{aligned} F_0 &= \frac{K_I}{S_0\sqrt{\pi a}} && \text{for tension} \\ F_1 &= \frac{K_I}{S_1\sqrt{\pi a}} && \text{for bending} \end{aligned} \quad (5.5.1)$$

Extrapolated values are used for cases where, as the crack grows, the  $a/c$  value may become greater than 1.0, up to 1.2. At the lower end,  $a/c$  values down to 0.1 are now allowed, the values below 0.2 representing an extrapolation of finite element results.

Note that Poisson's ratio  $\nu$  is one of the required material input parameters even though it is not used in  $K$  computation of SC05. However,  $\nu$  appears in the  $K$  formulation of the TC08, to which this case self-transitions if the crack penetrates through the cylinder wall. See the Theory section of the case TC08 for additional details of where  $\nu$  is used.

NASSIF outputs the geometry factors in two forms for this case:  $F$  and  $F\sqrt{Q} = K_I/(S\sqrt{\pi a/Q})$ , where  $Q$  is defined as

$$Q = \begin{cases} 1 + 1.464(a/c)^{1.65} & \text{for } a/c \leq 1 \\ 1 + 1.464(c/a)^{1.65} & \text{for } a/c > 1 \end{cases} \quad (5.5.2)$$

Reference: [60]

Table 5.5.1: SIF Correction Factors for Internal Cracks of Case SC05

$a/t =$	0	.2	.5	.8	1.0	0	.2	.5	.8	1.0	0	.2	.5	.8	1.0										
$R/t$	$a/c = 0.2$				$a/c = 0.4$				$a/c = 0.6$				$a/c = 0.8$												
$c\text{-tip, Uniform Loading} - F_0$																									
1	0.580	0.593	0.610	0.846	1.117	0.630	0.650	0.665	0.841	1.041	0.670	0.688	0.702	0.831	0.976	0.695	0.709	0.722	0.817	0.919	0.700	0.713	0.726	0.796	0.872
2	0.600	0.617	0.671	0.824	0.975	0.660	0.669	0.714	0.837	0.956	0.695	0.703	0.741	0.838	0.930	0.715	0.721	0.752	0.828	0.898	0.710	0.722	0.747	0.806	0.860
4	0.613	0.633	0.726	0.898	1.049	0.664	0.681	0.756	0.894	1.014	0.698	0.712	0.772	0.880	0.974	0.716	0.727	0.774	0.858	0.930	0.718	0.727	0.762	0.827	0.883
10	0.591	0.644	0.785	1.000	1.178	0.651	0.689	0.797	0.967	1.108	0.692	0.718	0.799	0.930	1.041	0.714	0.732	0.791	0.891	0.975	0.717	0.730	0.774	0.849	0.913
300	0.538	0.583	0.747	1.075	1.398	0.601	0.679	0.818	1.023	1.199	0.668	0.722	0.829	0.969	1.074	0.700	0.739	0.817	0.919	0.996	0.726	0.736	0.785	0.878	0.960
$c\text{-tip, Bending Loading} - F_1$																									
1	0.337	0.265	0.111	0.080	0.050	0.358	0.308	0.216	0.150	0.120	0.370	0.338	0.293	0.253	0.230	0.375	0.355	0.340	0.343	0.354	0.371	0.360	0.359	0.378	0.400
2	0.400	0.403	0.410	0.420	0.430	0.430	0.443	0.450	0.465	0.493	0.460	0.470	0.482	0.520	0.559	0.480	0.485	0.503	0.548	0.590	0.482	0.486	0.505	0.547	0.587
4	0.498	0.510	0.569	0.678	0.775	0.539	0.550	0.602	0.698	0.782	0.567	0.577	0.622	0.704	0.775	0.581	0.590	0.628	0.696	0.756	0.583	0.590	0.620	0.675	0.723
10	0.544	0.595	0.722	0.915	1.072	0.605	0.637	0.732	0.888	1.019	0.646	0.664	0.734	0.858	0.965	0.668	0.677	0.728	0.824	0.909	0.670	0.675	0.713	0.786	0.851
300	0.538	0.583	0.747	1.075	1.398	0.601	0.679	0.818	1.023	1.199	0.668	0.722	0.829	0.969	1.074	0.700	0.739	0.817	0.919	0.996	0.726	0.736	0.785	0.878	0.960
$a\text{-tip, Uniform Loading} - F_0$																									
1	0.960	0.987	1.064	1.065	2.406	0.875	0.888	0.944	1.360	1.857	0.795	0.799	0.841	1.119	1.437	0.720	0.721	0.754	0.941	1.146	0.650	0.653	0.684	0.823	0.969
2	0.990	1.022	1.093	1.380	1.685	0.900	0.911	0.961	1.163	1.377	0.800	0.813	0.847	0.985	1.130	0.710	0.726	0.751	0.846	0.943	0.620	0.652	0.674	0.745	0.815
4	1.031	1.045	1.141	1.332	1.504	0.920	0.926	0.991	1.123	1.243	0.819	0.821	0.862	0.951	1.031	0.729	0.729	0.756	0.814	0.868	0.650	0.652	0.672	0.713	0.751
10	0.983	1.059	1.189	1.337	1.440	0.888	0.936	1.020	1.120	1.192	0.800	0.827	0.878	0.941	0.989	0.718	0.732	0.761	0.801	0.831	0.642	0.651	0.671	0.697	0.717
300	1.059	1.090	1.384	1.682	1.881	0.948	0.951	1.079	1.188	1.251	0.792	0.832	0.888	0.940	0.971	0.720	0.733	0.754	0.777	0.792	0.642	0.656	0.675	0.691	0.700
$a\text{-tip, Bending Loading} - F_1$																									
1	0.520	0.545	0.659	1.074	1.523	0.470	0.493	0.597	0.919	1.254	0.430	0.446	0.542	0.792	1.039	0.385	0.405	0.494	0.693	0.879	0.350	0.368	0.454	0.621	0.771
2	0.700	0.719	0.821	1.088	1.352	0.630	0.643	0.728	0.935	1.135	0.560	0.575	0.648	0.808	0.957	0.503	0.515	0.579	0.706	0.819	0.448	0.463	0.523	0.629	0.720
4	0.839	0.865	0.974	1.173	1.347	0.748	0.767	0.849	0.997	1.126	0.666	0.681	0.743	0.852	0.946	0.592	0.606	0.651	0.735	0.805	0.528	0.542	0.583	0.648	0.702
10	0.902	0.985	1.120	1.267	1.366	0.822	0.871	0.959	1.064	1.141	0.744	0.770	0.824	0.897	0.954	0.669	0.682	0.715	0.765	0.806	0.597	0.607	0.631	0.667	0.695
300	1.059	1.090	1.384	1.682	1.881	0.948	0.951	1.079	1.188	1.251	0.792	0.832	0.888	0.940	0.971	0.720	0.733	0.754	0.777	0.792	0.642	0.656	0.675	0.691	0.700

Note:  $R$  is the inner radius of the cylinder

Table 5.5.2: SIF Correction Factors for External Cracks of Case SC05

$a/t =$	0	.2	.5	.8	1.0	0	.2	.5	.8	1.0	0	.2	.5	.8	1.0										
$R/t$	$a/c = 0.2$							$a/c = 0.4$							$a/c = 0.6$										
<i>c</i> -tip, Uniform Loading – $F_0$																									
1	0.590	0.672	0.893	1.249	1.552	0.664	0.713	0.871	1.138	1.368	0.712	0.739	0.846	1.039	1.209	0.734	0.747	0.818	0.954	1.075	0.731	0.739	0.788	0.882	0.966
2	0.560	0.660	0.876	1.177	1.416	0.643	0.706	0.859	1.086	1.271	0.699	0.734	0.838	1.006	1.148	0.727	0.744	0.876	0.915	1.046	0.728	0.737	0.787	0.881	0.964
4	0.540	0.653	0.873	1.162	1.383	0.630	0.701	0.858	1.081	1.257	0.691	0.731	0.839	1.006	1.145	0.722	0.742	0.815	0.940	1.046	0.725	0.735	0.786	0.880	0.962
10	0.542	0.646	0.867	1.172	1.414	0.630	0.697	0.855	1.087	1.275	0.689	0.728	0.838	1.010	1.153	0.720	0.741	0.815	0.941	1.049	0.722	0.734	0.785	0.879	0.961
300	0.538	0.583	0.747	1.075	1.398	0.601	0.679	0.818	1.023	1.199	0.668	0.722	0.829	0.969	1.074	0.700	0.739	0.817	0.919	0.996	0.726	0.736	0.785	0.878	0.960
<i>c</i> -tip, Bending Loading – $F_1$																									
1	0.592	0.643	0.742	0.870	0.967	0.659	0.690	0.761	0.861	0.940	0.704	0.720	0.768	0.844	0.908	0.727	0.731	0.760	0.819	0.871	0.729	0.724	0.740	0.785	0.829
2	0.552	0.645	0.798	0.972	1.092	0.632	0.691	0.801	0.939	1.040	0.687	0.720	0.795	0.902	0.987	0.716	0.731	0.780	0.863	0.932	0.720	0.724	0.757	0.820	0.876
4	0.545	0.645	0.835	1.075	1.254	0.624	0.690	0.827	1.014	1.158	0.678	0.717	0.814	0.956	1.069	0.706	0.728	0.794	0.899	0.987	0.710	0.722	0.767	0.845	0.912
10	0.524	0.633	0.850	1.136	1.357	0.612	0.684	0.840	1.057	1.229	0.672	0.715	0.823	0.984	1.115	0.703	0.727	0.801	0.918	1.016	0.705	0.721	0.772	0.859	0.932
300	0.538	0.583	0.747	1.075	1.398	0.601	0.679	0.818	1.023	1.199	0.668	0.722	0.829	0.969	1.074	0.700	0.739	0.817	0.919	0.996	0.726	0.736	0.785	0.878	0.960
<i>a</i> -tip, Uniform Loading – $F_0$																									
1	1.140	1.189	1.469	2.179	2.898	1.000	1.019	1.188	1.583	1.969	0.860	0.872	0.960	1.140	1.303	0.737	0.748	0.785	0.847	0.899	0.644	0.647	0.660	0.685	0.708
2	1.126	1.167	1.370	1.759	2.112	0.975	1.005	1.132	1.362	1.564	0.844	0.865	0.935	1.051	1.149	0.733	0.746	0.780	0.827	0.866	0.640	0.648	0.663	0.683	0.698
4	1.099	1.157	1.320	1.576	1.790	0.959	0.999	1.103	1.260	1.388	0.835	0.862	0.923	1.006	1.072	0.728	0.746	0.777	0.815	0.843	0.637	0.649	0.666	0.683	0.693
10	1.079	1.146	1.284	1.470	1.615	0.945	0.993	1.083	1.198	1.284	0.827	0.859	0.914	0.977	1.020	0.724	0.745	0.776	0.806	0.825	0.636	0.650	0.668	0.684	0.693
300	1.059	1.090	1.384	1.682	1.881	0.948	0.951	1.079	1.188	1.251	0.792	0.832	0.888	0.940	0.971	0.720	0.733	0.754	0.777	0.792	0.642	0.656	0.675	0.691	0.700
<i>a</i> -tip, Bending Loading – $F_1$																									
1	1.110	1.124	1.252	1.676	2.120	0.945	0.958	1.008	1.207	1.419	0.850	0.816	0.810	0.857	0.914	0.729	0.697	0.656	0.624	0.608	0.641	0.601	0.545	0.495	0.466
2	1.115	1.121	1.236	1.487	1.721	0.966	0.964	1.018	1.144	1.263	0.836	0.827	0.837	0.876	0.915	0.726	0.711	0.694	0.681	0.675	0.635	0.615	0.585	0.554	0.534
4	1.097	1.124	1.242	1.429	1.586	0.949	0.969	1.035	1.138	1.223	0.822	0.834	0.863	0.905	0.937	0.716	0.720	0.725	0.728	0.730	0.630	0.625	0.619	0.605	0.593
10	1.042	1.117	1.248	1.403	1.514	0.918	0.969	1.051	1.142	1.205	0.808	0.839	0.885	0.930	0.959	0.709	0.727	0.750	0.767	0.775	0.623	0.634	0.645	0.649	0.649
300	1.059	1.090	1.384	1.682	1.881	0.948	0.951	1.079	1.188	1.251	0.792	0.832	0.888	0.940	0.971	0.720	0.733	0.754	0.777	0.792	0.642	0.656	0.675	0.691	0.700

Note:  $R$  is the inner radius of the cylinder

## 5.6 SC06 – Constant-Depth Surface Crack (Circumferential) in Hollow Cylinder – Univariant WF

### 5.6.1 Overview

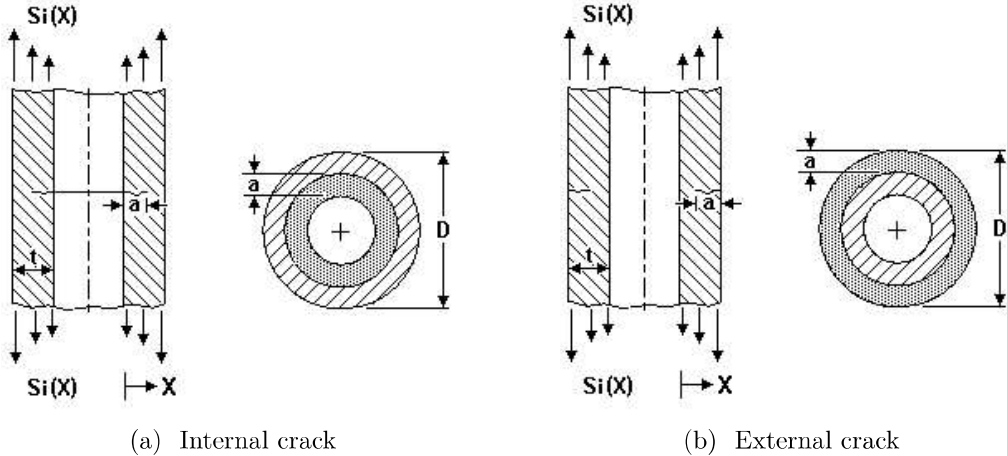


Figure 5.6.1: Configuration of the crack case SC06

This case is for circumferential cracks in hollow cylinders, which are often used as idealizations of flaws in weldments caused by lack of penetration. The crack can be defined as either internal or external as shown in Figs. 5.6.1a and 5.6.1b, respectively. The hollow cylinder wall is remotely loaded by univariant stress distribution.

### 5.6.2 Geometry

Three key geometric input parameters of this case are:

- $D$  : cylinder outer diameter
- $t$  : cylinder wall-thickness
- $a$  : crack depth

The allowed limit on diameter to cylinder wall thickness ratio is:

$$2.2 \leq D/t \leq 2000$$

Also, the maximum crack depth  $a$  permitted by this SIF model is 0.95 $t$ :

$$a/t \leq 0.95$$

### 5.6.3 Loading

Up to four separate univariant stress distributions can be defined in discretized (tabular) form along the wall thickness. These distributions are denoted as  $S_0$ ,  $S_1$ ,  $S_2$  and  $S_3$  (i.e.  $S_i$ ;  $i \subseteq \{0, 1, 2, 3\}$ ). Each one of these discrete distributions are defined as a function of normalized distance  $X = x/t$  from the cylinder inner wall towards the outer wall as depicted in Fig. 5.6.1. Regardless of whether the crack is on the inside or outside, the stress distribution must be defined beginning on the inside surface ( $x/t = 0$ ) to the outside surface ( $x/t = 1$ ). Note the limit on  $X$ :